3-21-2013

Finite Element Analysis of a Highly Flexible Flapping Wing

Justin K. Mason

FINITE ELEMENT ANALYSIS OF A HIGHLY FLEXIBLE FLAPPING WING

THESIS

Justin K. Mason, First Lieutenant, USAF

AFIT-ENY-13-M-22

DEPARTMENT OF THE AIR FORCE
AIR UNIVERSITY

AIR FORCE INSTITUTE OF TECHNOLOGY

Wright-Patterson Air Force Base, Ohio

AFIT-ENY-13-M-22

FINITE ELEMENT ANALYSIS OF A HIGHLY FLEXIBLE FLAPPING WING

THESIS

Presented to the Faculty

Department of Aeronautics and Astronautics

Graduate School of Engineering and Management

Air Force Institute of Technology

Air University

Air Education and Training Command

In Partial Fulfillment of the Requirements for the

Degree of Master of Science in Aeronautical Engineering

Justin K. Mason, BS

First Lieutenant, USAF

March 2013

AFIT-ENY-13-M-22

FINITE ELEMENT ANALYSIS OF A HIGHLY FLEXIBLE FLAPPING WING

Justin K. Mason, BS
First Lieutenant, USAF

Approved:

_____	_____
Black, Jonathan T., PhD AFIT/ENY (Chairman)	Date
_____	_____
Blandino, Joseph R., PhD VMI (Member)	Date
_____	_____
Jennings, Alan L., PhD AFT/ENY (Member)	Date

Abstract

Small unmanned aerial systems are being designed to emulate the flapping kinematics of insects and birds which show superior control in slow speed regimes compared to fixed wing or rotorcraft aircraft. The flight of flapping wing vehicles is characterized by aeroelastic effects. Wing membranes are highly flexible with large deformations during the stroke. Predicting the aeroelastic response of a flapping wing is an essential step towards predicting performance characteristics of different designs. Most research has been dedicated towards understanding the aerodynamic side of the aeroelastic response with minimal effort spent towards validating the structural response. A finite element model of a wing from a commercial flapping wing vehicle was created to validate the structural response. Vacuum testing allowed the isolation of the inertial response for a direct comparison to the finite element model. Model tuning was accomplished through modal testing. The finite element model was run through a nonlinear dynamic simulation to match the test article flapping motion. Wing tip displacement amplitude was matched to within 8%. The membrane kinematics of the finite element model were similar to the vacuum test article but overall membrane deflections predicted by the finite element solver were less than observed deflections seen in the vacuum. Modeling the wing membrane dynamics proved to be difficult because of the nonlinearities associated with the flexible membrane. This research shows that significant focus must be placed on validating the structural side of a flexible structure in order to correctly model the complete aeroelastic response.

Acknowledgments

I would like to thank my thesis advisor Dr. Black for his guidance on this thesis over the past 18 months. I would also like to thank Dr. Jennings for helping me with all the laboratory experiments and answering all my questions along the way. I would like to thank my other committee member from VMI, Dr. Blandino for taking time to review my work. Thank you to Dr. Cobb and Dr. Palazotto for their advice and insight into my project.

Justin K. Mason

Table of Contents

Page

List of Figures

List of Tables

FINITE ELEMENT ANALYSIS OF A HIGHLY FLEXIBLE FLAPPING WING

I. Introduction

1.1 Why Small Unmanned Aerial Systems

When manned flight first became possible, researchers focused on ways to travel higher, faster, and with larger payloads. Now that technology has allowed the miniaturization of payloads, research agencies are shifting their focus to develop smaller, slower aircraft to accomplish complicated missions. In 1996 the Defense Advance Research Projects Agency (DARPA) established goals of a Small Unmanned Aerial System (SUAS) program listed in Table 1 [1]. The Air Force Research Laboratory (AFRL) set out to build an operational bird size SUAS by 2015 and an insect size SUAS by 2030. The problem is this reduction in size creates new challenges for aircraft designers.

Table 1: SUAS Goals set by DARPA [1]

Parameter	**SUAS Value**
Size	<15 cm
Weight	10-100 grams
Useful Payload	1-18 grams
Endurance	20-60 minutes
Air Speed	30-65 km/hr cruise, hover is tradeoff with endurance/range
Range	1-10 km

Since 1996, the Department of Defense (DoD) goals for SUASs have evolved with the progress of technology and feasibility but the same design challenges remain. Most current operational SUASs are based on conventional aircraft design. Conventional

aircraft generate lift by speeding air flow over rigid airfoil shaped surfaces. To achieve the required air speed over the lifting surfaces, conventional aircraft must physically move forward through the air with the aid of a propulsion system. As such, conventional aircraft operate in the high Reynolds number region and are generally unable to perform well in slow operating regions within a confined space. The difference in Reynolds number regimes is graphically displayed in Figure 1 with the weight of the vehicle. Miniaturization of conventional aircraft designs to meet the future requirements of agencies like the DoD and AFRL is not feasible because of the low Reynolds numbers and unsteady flow involved in the envisioned operating region [1, 2]. Figure 2 shows select current operational Unmanned Aerial Vehicles (UAVs) sizes compared to their payload; the projected SUAS region has yet to be broached by operation aircraft [3]. To solve these design challenges, research has focused on the flapping motion of natural flyers (birds and insects) to discover features that allow them control in low Reynolds numbers and unsteady flow regimes with the ultimate goal of incorporating those features into future systems.

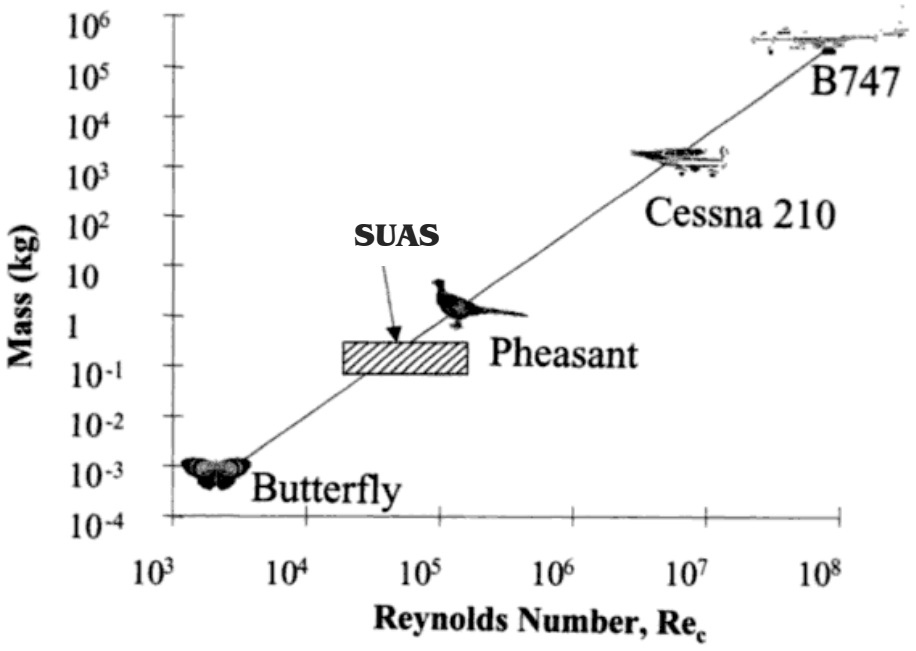

Figure 1. Reynolds number range for flight vehicles [4].

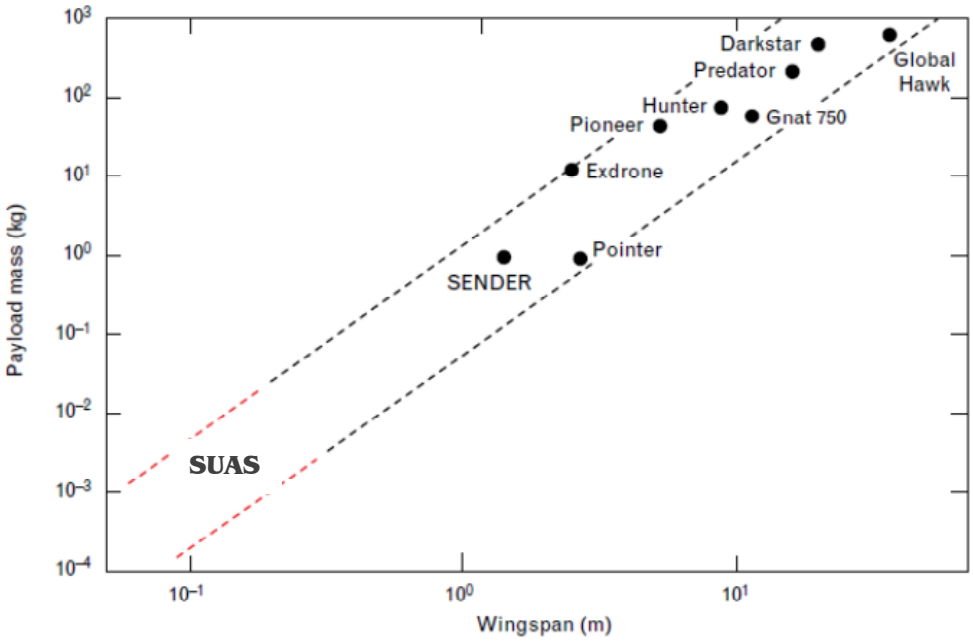

Figure 2: Payload versus wingspan for existing UAVs and proposed SUASs. Predicted capabilities fall within the trends extrapolated from larger vehicles [3].

Flapping wing flight offers many advantages over conventional aircraft for small, slow traveling vehicles. As stated earlier, conventional aircraft must physically travel forward through the air to generate lift and as such conventional aircraft can never hover. For flapping wing vehicles, the ability to hover offers a huge operational advantage for a myriad of different tasks. Flapping wings also have an aerodynamic advantage over conventional design. Birds and insects demonstrate an amazing ability to maneuver through the air, and although this feat is not obtainable by current flapping wing test vehicles, the potential maneuverability is far beyond the best a conventional aircraft could ever achieve at slow speeds.

Rotorcraft are another category of aircraft that could potentially fill this small, slow vehicle requirement. Rotorcraft offer the ability to hover and can achieve decent aerodynamic performance characteristics. However, rotorcraft are loud and would not be an ideal choice where stealth is a must like surveillance and reconnaissance. Even when not performing stealth missions, the noise pollution generated from a rotorcraft can be damaging to a local community. Flapping wing offers two advantages here in the stealth category: they can be quiet and inconspicuous. Flapping wings vehicles can be very quiet especially in nature. Some insects, like butterflies, cannot be heard unless they are quite literally on top of a person. Because flapping wing vehicles mimic natural flyers, they have the potential to blend in with the environment. No astute person will mistake a rotorcraft for a bird or insect. All the advantages flapping wing vehicles exhibit over conventional aircraft and rotorcraft makes them an ideal platform for future SUAS.

The flapping wing motion of natural flyers is a recent area of extensive study because of its potential application to SUASs and has given rise to the production of flapping wing small unmanned aerial systems. Before the mid 1990s, virtually no serious research was conducted on the flapping wing aspect of flight. Therefore, replicating a natural flyer's wing motion and dynamic response is an area of on-going practice [5, 1]. Since flapping wing effects are not fully understood, researchers, including biologists and engineers alike, turn to nature for the answers. While biologist have extensively studied the flying mechanics behind birds and insects for quite some time, the reasons why these mechanics work are not yet fully known [4].

Natural flyers such as birds and insects operate in the unsteady low Reynolds number region and do so with precise control and agility. By studying these natural flyers, researchers aim to understand what allows birds and insects to operate in low Reynolds numbers regimes successfully and then apply those characteristics to SUASs. While birds and insects both use flapping to maneuver through the air, birds have complex wings with muscles and joints which allow them to actively change the shape of their wing throughout different flight regimes. Insect wings do not have muscles and joints so the shape of their wing in flight is caused by a combination of inertial and aerodynamic loads acting on the surface [5]. This study will also focus on passively controlled wings (like insects) that contain no mechanism to actively control the wing shape in flight.

1.2 Research Focus

Why is modeling the motion of a flapping wing important to aircraft designers and future flapping wing SUASs? To answer this question, it is important to know an overview of how operational aircraft are designed. Somewhere in the field, someone or some agency has a mission that needs to be accomplished. Mission requirements crucial to mission success are formulated based upon these needs. Mission requirements can be very specific such as detailing a range and payload capacity or they can be broad description of a task to be accomplished. System engineers take these mission requirements and translate them into performance characteristics. Performance characteristics are usually more quantitative measures like aircraft weight, max speed, etc. that have meaning to an aircraft designer. Conventional aircraft designers know how to incorporate design features into an aircraft to meet the performance characteristics. Here, design features refer to specific details of the aircraft like wingspan, aspect ratio, camber, and a myriad of other quantities. The problem with flapping wing SUASs is that it is not understood how design features affect the performance of the vehicle. Without this information designers cannot build optimal designs to meet specific performance characteristics. SUASs can be successfully built and flown through trial and error even though why they fly is not understood. Current research is aimed at figuring out how design features translate into performance characteristics. By modeling a flapping wing, researchers will be able to predict performance characteristics for any wing design, and aircraft designers will be able to truly optimize designs for operational use.

Simply put, the focus of this research was to successfully model the deformations of a flapping small unmanned aerial system wing with a finite element (FE) analysis. Solely

using a FE solver would greatly simplify the modeling process; however, FE only predicts the structural deformations. Computational Fluid Dynamics (CFD) is a very powerful but computationally intensive way to model the aerodynamic effects of a flapping wing. While other research has successfully used CFD and FE analysis to model a flapping wing, the application is still limited due to the complexity of the simulation and computational effort [6]. Most SUAS researched is focused on studying the flapping wings of insects such as the dragonfly, hawkmoth, butterfly, etc. but this research will focus on a commercially built SUAS. Most research shows that insect wings behave aeroelastically, but their wings are still fairly stiff. This research will focus on a wing with a stiff leading edge beam attached to a highly flexible membrane. As such, the relative deformations observed will be greater than previous studies of biological inspired SUASs.

Modeling the aeroelastic response of a flexible flapping wing is very complicated so the FE model was first verified by testing in a vacuum chamber. In the absence of air, the deformations observed result from the inertial forces of the wing and are directly related to the structure and material properties. The deformations recorded in the vacuum were compared to the deformations recorded in the air. The only difference between the two setups was the presence or lack of aerodynamic forces. This difference allowed for an assessment of the dominance of inertial versus aeroelastic forces.

1.3 Modeling Efforts

Most modeling efforts have attempted to validate biological flapping wings of various insects. Many researchers focus solely on the aerodynamic side of the aeroelastic

response and little effort has gone into validating the structural models. The research efforts that have focused on structural modeling have either used static analysis efforts or analyzed relatively stiff wings. This research will focus on the wings of a test article characterized by billow during the flap cycle. All the methods proposed for this research have been used in previous studies but none have been put together to model the dynamic deformations of a flexible flapping wing in this manner.

1.4 Chapter Overview

Chapter II, the literary review section, will cover the background behind flapping wing motion and review many research efforts to model the structural and aerodynamic response. Chapter III details the test article used for testing, laboratory setup, the methodology used in the research, and the structural model. Chapter IV provides the results and analysis of all tests. Chapter V draws the final conclusions on the research and provides recommendations for future work.

1.5 Preview of the Results

Correctly modeling all the intricacies of flapping wing motion proved to be a difficult task. The dynamic nature of the flapping motion coupled with the nonlinearity of the wing membrane meant precise modeling of the problem was required. The FE wing tip displacement amplitude was matched to within 8%. The membrane kinematics of the finite element model were similar to the vacuum test article but overall membrane deflections predicted by the finite element solver was less than observed deflections seen in the vacuum. Modal tuning brought the leading edge beam of the wing to within 1% of

the test article. Wing modal testing showed that the addition of the membrane to the beam reduced the first beam bending mode by 32% and the flapping motion was dominated by the first membrane mode not the first beam mode.

II. Literary Review

2.1 Low Reynolds Number and Unsteady Flow

As stated earlier, the small scale and low Reynolds number regime of SUASs coupled with the unsteady aerodynamics associated with the flapping motion make the flapping wing SUASs aerodynamics different from conventional aircraft control. Viscous forces become dominant for small scale vehicles and drag is very sensitive to small changes in lift [7]. In conventional aircraft aerodynamics, aerodynamic coefficients are generally calculated or measured for an aircraft in steady level flight. Flapping wing are never in steady level flight—they are in a constant state of motion in order to maintain flight and as such classical methods for calculating lift and drag fail to add up to measured values. The quasi-steady assumption can help simplify flapping wing aerodynamic calculations at the expense of accuracy. By assuming that aerodynamic coefficients can be calculated for the wing under a series of static conditions, the net aerodynamic forces can be calculated over the entire flapping cycle to get net average values. This assumption is not perfect and does not take into account unsteady phenomenon. As the velocity of the vehicle increases the quasi-steady contributions to net forces will dominate but conversely as the forward velocity decreases the unsteady effects are greater [7, p. 7]. The advance ratio is a non-dimensional parameter of the forward velocity relative to the flapping speed as shown in Equation (0.1) [8, 7, 9]:

$$J = \frac{V_\infty}{2\Phi\omega R} \tag{0.1}$$

where V_∞ is the freestream velocity of the vehicle, Φ is the wing stroke amplitude in radians measured peak-to-peak, ω is the flapping frequency in Hz, and R is the wing length. A general rule of thumb states that for $J > 10$ quasi-steady terms dominate while unsteady terms are the bigger players for $J < 10$.

In 2006 Ansari et al. overviewed the most common ways in literature to model aerodynamics of insect flight [10]. They categorized them into the following methods: steady-state, quasi-steady, semi-empirical, and fully unsteady. First, they detailed the main aerodynamic phenomena associated with unsteady effects. These aerodynamic phenomena are the Wagner effect, wake capture, apparent mass effect, Kramer effects, and the leading edge vortex. These effects are crucial to insect aerodynamics because the flapping wings would stall at the high angles of attack seen in flight under steady-state conditions. This allows flapping wing vehicles to attain higher forces than those predicted by quasi-steady methods.

The Wagner effect is an unsteady phenomenon that actually reduces the effective lift from quasi-steady methods. This effect, first studied in 1931, arises from the wing's acceleration and deceleration throughout the flapping cycle [11]. When the wing accelerates, the circulation around it slowly rises to the steady-state equivalent. During this acceleration, a vortex is generated and shed. These vortices rotate in the opposite direction of contributory circulation and reduce the effective lift. However, Sane remarked that the Wagner effect may be negligible at the Reynolds number associated with insect flight [11]. He did acknowledge that the isolation of the Wagner effect from other unsteady phenomena is difficult but cites several recent studies that have ignored the Wagner effect.

The second effect, wake capture, is also known as wake passage and wing-wake interaction. This very significant effect was first observed by Dickinson in 1994 [11]. During flight, a flapping wing generates strong vortices and often travels through its own wake especially during hover. Strong vortices generated from stroke reversal create pockets of high energy flow. When the wing reverses direction it interacts with these high areas of high energy flow and results in a higher force on the wing. Figure 3 below pictorially shows this process. In 2002 Sun and Tang performed a CFD analysis of flapping wing kinematics and concluded that the high accelerations associated with stroke reversal is the cause of large lift forces seen at the beginning and end of a stroke [12]. These results contradict the experiments of Dickinson in the 1990s and shows that while the spikes in forces seen at stroke reversal are an important part of the flap cycle, different researchers attribute the cause for such peaks to different phenomenon.

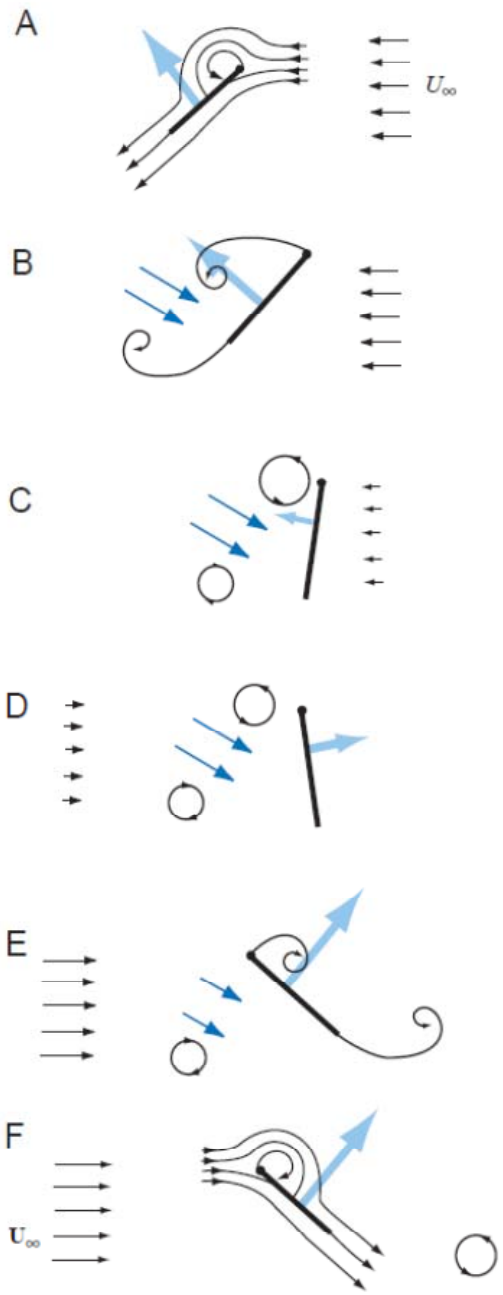

Figure 3. A hypothesis for wing-wake interaction from Sane: Parts A-F depicts a wing section as it reverses stroke. As the wing transitions from a steady translation (A) phase and rotates around a chordwise axis in preparation for stroke reversal, it generates vorticity at both the leading and trailing edges (B). These vortices induce a strong velocity field (dark blue arrows) in the intervening region (C,D). As the wing comes to a halt and then reverses stroke (D,E), it encounters this jet. As the wing interacts with its wake, a peak is registered in the aerodynamic force record (light blue arrows), which is sometimes called wake capture or wing-wake interaction.

The third effect is the apparent or added mass effect. If an object were to move at a constant velocity through an inviscid fluid, kinetic energy would be conserved through the separation of the fluid in front of the object to that of it closing behind it. If that same object where to accelerate in an inviscid fluid, energy is not conserved. To account for the extra energy needed to accelerate the fluid surrounding the object, a reaction force is added called the apparent or added mass force. Since flapping wings are constantly accelerating and decelerating this is an important term. Sunada and Ellington later showed that for wings with symmetrical half-strokes the net apparent mass force is zero, however not all insects for flying vehicles flap with symmetrical half-strokes [13].

Sane calls the fourth effect the single greatest feature of insect wing aerodynamics: leading edge vortex. The existence of leading edge vortices delaying stall on conventional aircraft at high angles of attack has been studied, but direct evidence of their role in insect flight did not come until Ellington et al. in 1996 [10, 11]. They built a 3-D scaled version of the *Manduca sexta* (hawkmoth) and seeded the flow field with smoke. A leading edge vortex was observed through each half-stroke and was responsible for delaying stall at high angles of attack. This augmentation on lift has been described as the same phenomenon seen on delta wings. Insects typically operate at high angles of attack and this effect is the main contributor. Since its realization, numerous studies have been done on the leading edge vortex for different insects. Many theories exist as to why the leading edge vortex is stable and attached to the wing. Some studies have shown that a high spanwise flow may create this condition whereas others have concluded that the reason for its formulation changes with Reynolds number [11]. Although identified as a

critical player in flapping wing aerodynamics predicting leading edge vortices is very difficult as they are not fully understood.

The Kramer effect is present when a flapping wing rotates about a span-wise axis (change in angle of attack) while translating through the freestream flow. When this occurs the Kutta condition breaks down and additional circulation must be generated to reestablish the Kutta condition. Basically, rotational circulation is generated to counteract the change in angle of attack of the wing. Depending on the direction of rotation the extra circulation generated can either supplement or detract from the lift of the wing. The Kramer effect is most prominent during stroke reversal when the wing rotates rapidly.

Another aerodynamic phenomena detailed by Sane [11] is the clap and fling effect. The clap and fling effect refers to when an insect's or any vehicle's wings touch or clap at the top of the stroke then fling apart. Theory behind the clap and fling effect is that as the two wings clap together the leading edges of the wings meet before the trailing edge. As the wings close together, the opposing circulations cancel each other out. The vortices shed by the trailing edge are much smaller and as a result the Wagner effect is reduced. When the two wings fling apart they create a low pressure zone which surrounding air rushes to fill. This provides a quicker build up of circulation or helps in the development of a leading edge vortex. The actual significance of the clap and fling effect is still debated. Many insects do not use the clap and fling mechanism yet achieve high lift values. Sane argues that in most flapping insects and birds larger flapping amplitude will produce more lift. Clap and fling, as seen in nature, could simply be a

result of the insect trying to achieve the highest possible amplitude mechanically possible and there is no added benefit to it.

These unsteady phenomena are important for a comprehensive model of a flapping wing. Full realization is important to SUAS designers in order to optimize the design for specific mission capabilities. The problem is that these phenomena are extremely complicated and relatively recently discovered with most observations coming in the 1990s. As such, the actual implications of these models are not known but researchers have attempted to generate models to predict physical results. These models can be quite simple or more complicated methods like CFD code that accounts for the attached flow to the wing as well as the separated flow to incorporate unsteady phenomena like the wake capture effect.

Steady-state methods, as labeled by Ansari [10], are based upon momentum theory. The wings of the insects are modeled as a partial actuator disc based upon parameters such as the vehicle weight, wing length or area. Ansari notes that this is a very limited method because it actually fails to take into account flapping kinematics or wing geometry but instead transforms the flapping wing vehicle into a representative partial actuator disk.

Quasi-steady methods are a fairly common way to model aerodynamic effects on a flapping wing. Osborne is generally cited as the first contributor to quasi-steady methods [14, 9, 10]. One of the most common ways to model the quasi-steady effects is through the use of blade element theory (BET). This method is appealing because of the relatively simple computational effort involved. Because of the simplifications of BET, it generally under predicts lift forces because it does not take into account unsteady

phenomena. This method could be used as a conservative estimate for SUAS designers early in the design process. One example of why quasi-steady methods over simplify the problem is the small angle assumption. Most methods use thin airfoil theory to predict the lift coefficient on the wing. For thin airfoils at low angles of attack, it was been shown that the lift coefficient can be approximated by $C_L = 2\pi\alpha$. This assumption is usually made for faster modeling purposes because it is common for insect wings to operate at angles of attack of 35° [10] which falls outside the low angle of attack region. However, quasi-steady methods tend to be more accurate for flapping wing fliers at higher speeds. As the speed increases, the unsteady effects become less significant compared to the quasi-steady terms.

Semi-empirical methods attempt to correct for the simplification of quasi-steady methods by supplementing them with corrections based on experimental results. These methods can involve supplementing aerodynamic coefficients to try to incorporate the unsteady effects. Walker and Westneat [15] attempted to added skin friction drag into their model based by computing a skin friction coefficient based on Reynolds number. Others attempt to match lift and drag coefficients developing a unique equation for them based upon empirically measured data. The success of empirical methods is mixed. Empirical methods do build upon quasi-steady methods—increasing their accuracy—yet the method relies on experimental data rather than modeling the flow physics. As such, the models are very specific to individual vehicles. This method is not entirely useful to the aircraft designer early in the design process as some experimental results must be attained to design a vehicle. Since these methods are based upon quasi-steady

assumption, they are not computationally intensive so if the data is already available then the modeling can be accomplished relatively easily.

Unsteady methods are analytical methods that rely purely on unsteady aerodynamics. The main features of these methods are that they model the flow attached to the wing as well as the wake from shedding leading and trailing edge vortices. These methods are fairly new and as a result a plethora of different approaches exist in literature. Some methods can be less computationally intense at the sacrifice of accuracy while others involve complex coding that can be computationally intensive.

BET was originally developed in the late 19th and early 20th century to calculate the aerodynamic forces on helicopter blades and is the foundation for most helicopter aerodynamics [16, p. 46]. The theory is based upon a lifting-line theory applied to a helicopter blade (modeled as an airfoil) as it rotates through the air. By looking at the cross-section of the blade as shown in Figure 4, aerodynamic coefficients can be calculated based on the orientation and speed. For helicopter blades the total aerodynamic forces can be calculated by integrating the forces over the entire blade. The basics of this approach have been adapted to predict flapping wing aerodynamic forces as shown in Figure 5.

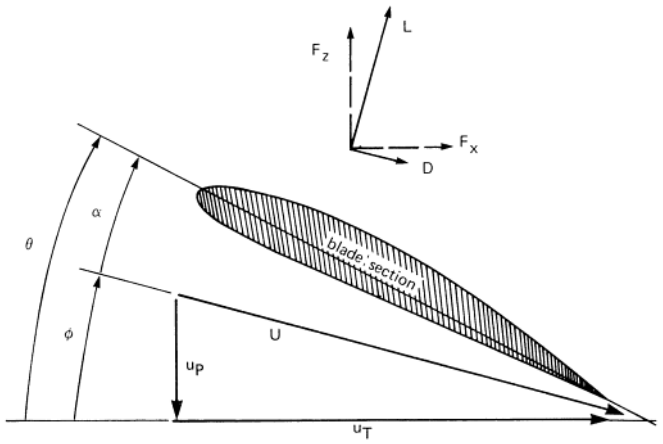

Figure 4. Example of original blade element theory problem.

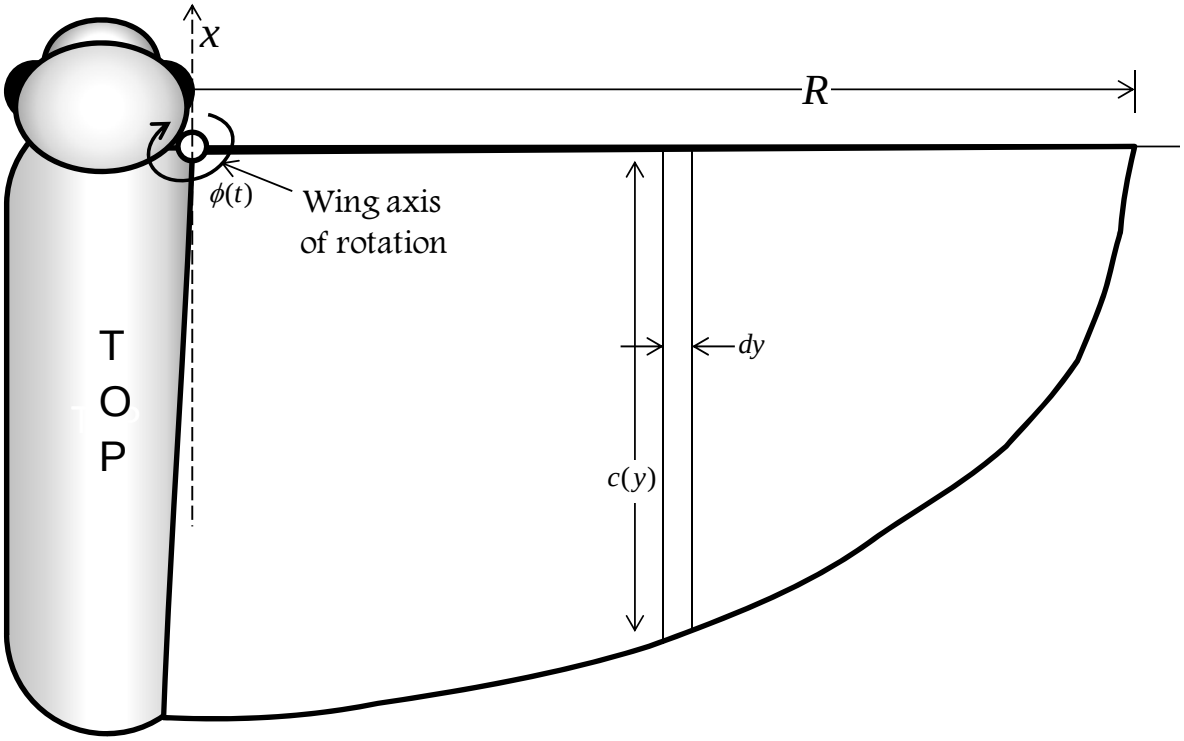

Figure 5. Blade element theory parameters definitions.

Here $\phi(t)$ is the wing stroke angle, R is the wing length, $c(y)$ is the chord length, and dy is the differential width of the blade element. In this figure $\phi(t)$ is the rotation about

the z-axis going into the page. The lift on the differential strip is derived from the generic lift equation:

$$L = \frac{1}{2}\rho C_L V_\infty^2 S \tag{0.2}$$

$$dL = \frac{1}{2}\rho C_L\left(\alpha(t)\right)\dot{\phi}^2(t)\, y^2 c(y)\, dy \tag{0.3}$$

where L is lift, ρ is air density, C_L is lift coefficient, V_∞ is the freestream velocity, and S is the wing planform area. In Equation (0.3) it is assumed that the only velocity is from the stroke angular velocity, $\dot{\phi}(t)$, and *dL* represents the instantaneous differential lift on the blade element section. The total lift is found by integrating over the wing so that the instantaneous lift can be found and similarly drag can be derived the same way:

$$L = \int_0^R dL = \int_0^R \frac{1}{2}\rho C_L\left(\alpha(t)\right)\dot{\phi}^2(t)\, y^2 c(y)\, dy \tag{0.4}$$

$$D = \int_0^R dD = \int_0^R \frac{1}{2}\rho C_D\left(\alpha(t)\right)\dot{\phi}^2(t)\, y^2 c(y)\, dy \tag{0.5}$$

where *D* is the instantaneous, and C_D is the coefficient of drag. This is a very basic formulation of BET. In 2011 Yan et al. developed and extended BET that includes a more comprehensive model with more parameters and unsteady aerodynamic methods [17].

Yan et al. wanted to create a BET model that captured the strong peak in aerodynamic forces seen at the start of each stroke. They theorized that the added mass effect and wake capture were the two unsteady mechanisms responsible for this peak; however, since wake capture is difficult to model they developed an extended unsteady blade

element model that incorporates the added mass effect. They set up their coordinate system as shown in Figure 8. Here, ***XYZ*** is the earth coordinate system while ***X'Y'Z'*** is the wing-fixed coordinate system. T represents the period of a full stroke so $0.5T$ is one half-stroke. As before, $\phi(t)$ is the stroke angle and ϕ_m is the stroke amplitude. C_{Le} and C_{Tr} are defined as the upper and lower limitations of the wing chord. Instead of using along the span, Yan et al. used a differential area on the wing as a blade element so c is the distance from the axis of rotation (***Y'***), r is the distance from ***Z'*** and $\Delta c, \Delta r$ are the differential widths of the element. R_b and R_T are the upper and lower limitation functions of spanwise length and are a function of c (note that R_t in Figure 8 should be R_T). With these parameters defined their blade element model is similar to the one listed above incorporates more kinematics as seen below in Equation (0.6) and (0.7).

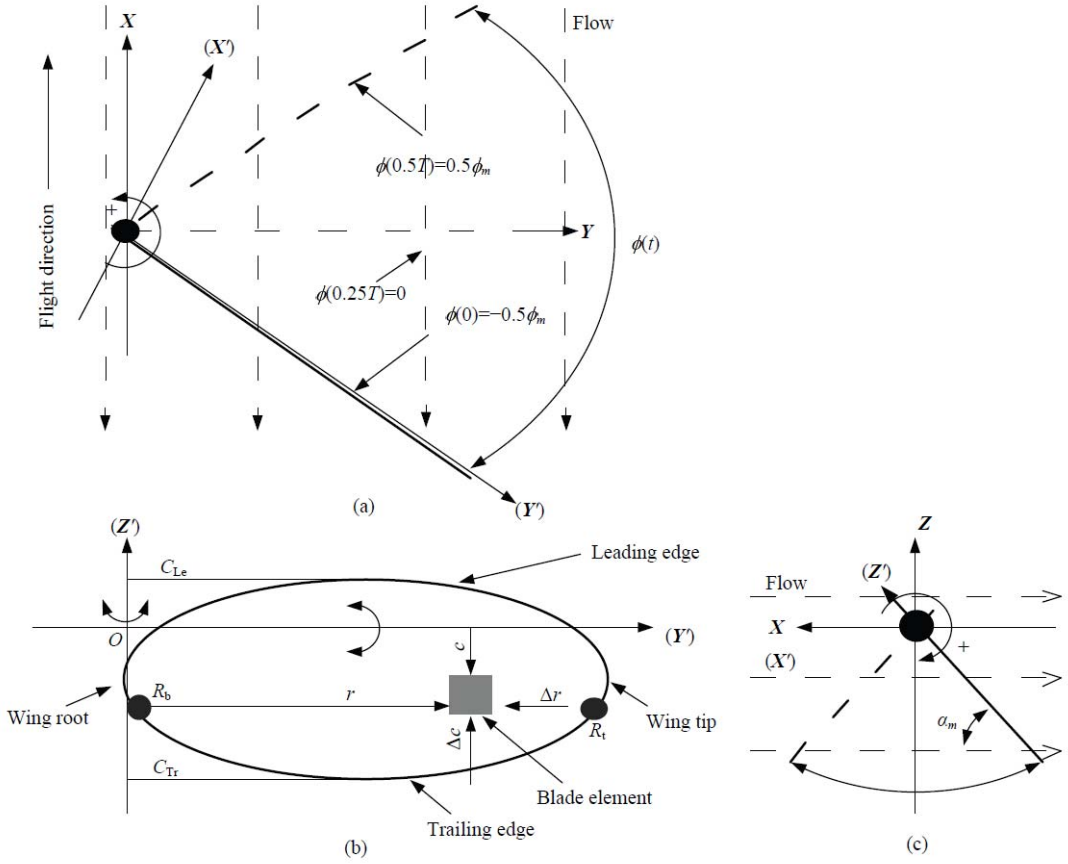

Figure 6. Schematic from Yan et al. [17] detailing their formulation of extended blade element theory model.

$$F^{D}_{tran,rot} = 0.5\rho \int_{C_{Le}}^{C_{Tr}} \int_{R_b(c)}^{R_T(c)} C_D \left[U\left(\phi, \dot{\phi}, \alpha, \dot{\alpha}, r, c\right) \right]^2 drdc \tag{0.6}$$

$$F^{L}_{tran,rot} = 0.5\rho \int_{C_{Le}}^{C_{Tr}} \int_{R_b(c)}^{R_T(c)} C_L \left[U\left(\phi, \dot{\phi}, \alpha, \dot{\alpha}, r, c\right) \right]^2 drdc \tag{0.7}$$

In these equations $F^{D}_{tran,rot}$ and $F^{L}_{tran,rot}$ are drag and lift forces respectively associated with translation and rotation. The previous BET model did not take into account any

translation of the body. The model by Yan et al. incorporates this and more through the velocity term U. The velocity term represents three different parameters:

$$U = C_{rot}U_{rot}\left(\dot{\alpha},c\right)+U_{trans}\left(\dot{\phi},r\right)+U_{bod,str}\left(\phi,\alpha\right) \tag{0.8}$$

$$U_{rot}\left(\dot{\alpha},c\right)=c\dot{\alpha} \tag{0.9}$$

$$U_{trans}\left(\dot{\phi},r\right)=r\dot{\phi} \tag{0.10}$$

$$U_{bod,str}\left(\phi,\alpha\right)=U_{body}\cos\left(\phi\right)\sin\left(\alpha\right) \tag{0.11}$$

where U_{rot} is the instantaneous linear component of rotational velocity of the blade element, U_{trans} is the instantaneous linear component of stroke velocity of the element, $U_{bod,str}$ is the instantaneous flight velocity component in the wing stroke direction, and U_{body} is the flight velocity of the insect. In the above equations $\alpha,\dot{\alpha}$ are the angle of attack and angular velocity of angle of attack respectively, $\phi,\dot{\phi}$ are the wing stroke angle, and angular velocity of wing stroke angle, *c* is the chordwise distance from the axis of rotation, and *r* is the spanwise distance from the axis of rotation. The model is more comprehensive because it allows for further discretization of the wing and incorporates body translational velocity as well as the velocity associated with a change in angle of attack.

Vanneste et al. [18] performed a similar approach on a bio-inspired robotic insect. This flapping wing flyer was electro-magnetic actuated with a wingspan in the 3-5 cm range. The wings were micromachined to mimic insect wings with a high degree of repeatability. Vanneste et al. set out to predict aerodynamic forces on the wing throughout the flapping cycle through the use of FE and an aerodynamic model. A

combination of 2 node beam elements and 8 node shell elements where used in Ansys. A quasi-steady approach was chosen for the aerodynamic model because the speed and ease of implementation. Vanneste et al. actually developed their model after Sane et al. [19] which is a semi-empirical model. The lift and drag coefficients were experimentally measured from a scaled fruit fly wing on a biomimicking flapper immersed in an oil tank. Vanneste et al. successfully coupled their aerodynamic and structural models, however, the accuracy of their results cannot be determined as they had no experimental results to validate their model.

The work of Seshadri et al. [20] provided good insight into the comparison of classical steady methods versus unsteady methods. They took a rigid rectangular wing and hooked it up to a four-bar flapping mechanism. To separate the aerodynamic forces from the inertial forces the flapping mechanism was placed in a vacuum and forces were measured throughout the flap cycle. These forces were subtracted from the forces measured by the same flapping mechanism flapped in air. Seshadi et al. makes a point to mention that the method of subtracting forces measured in a vacuum from the forces measured in air is only valid for a rigid wing. This makes sense since a rigid wing will roughly hold the same shape as it flaps in a vacuum as it does in air so the instantaneous inertial forces will be the same in both cases. For a non-rigid wing, the aerodynamic forces will deform the wing so that the inertial forces measured in a vacuum will be different from the inertial forces measured at the same point in the flap cycle in air.

After isolating the aerodynamic forces the same rigid wing was placed in a wind tunnel. Wind speed was varied to match the range of Reynolds numbers seen during the flapping tests and the angle of attack was varied to find the max possible lift coefficient.

The results from Seshadri are shown in Figure 7. The wind tunnel test represents the steady state method for measuring lift and drag coefficients based a conventional aircraft. The flapping wing tests contain all the unsteady effects not present in conventional aircraft. Unsteady lift coefficients were up to six times higher than those measured by steady state methods. This shows two important points. One, flapping wing flyers have a huge advantage over conventional aircraft designs in the low Reynolds number regime. Two, the unsteady terms are very important to aerodynamic models to predict the proper aerodynamic coefficients.

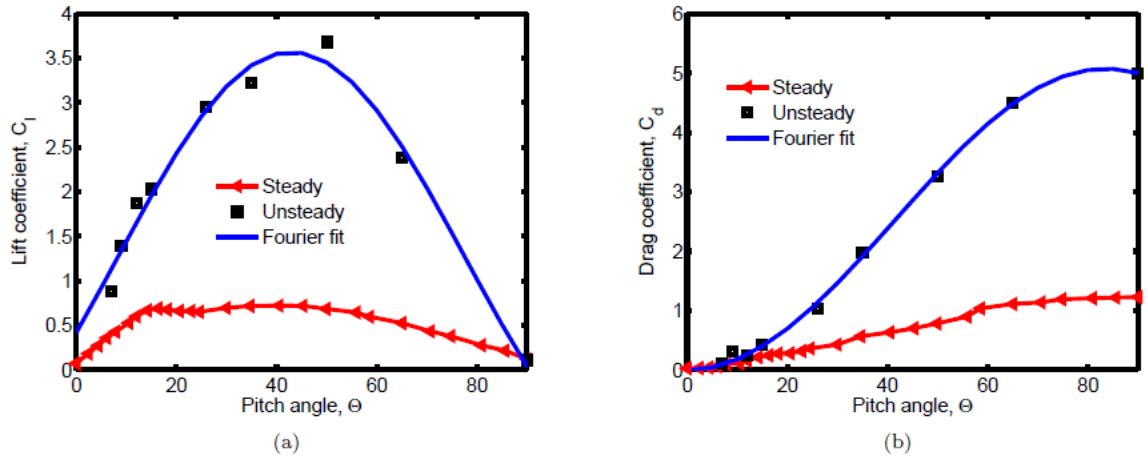

Figure 7. Experimental results from Seshadri et al. comparing measured lift coefficients of a rigid rectangular wing in a wind tunnel (steady) to those measured on the same wing placed in a flapping mechanism (unsteady)[20].

Seshadri et al. also developed an analytical model to compare with the experimental results. They used a semi-empirical BET model with aerodynamic coefficients based upon a curve fit of the unsteady data measured in the lab. While their BET theory model does use the unsteady aerodynamic coefficients measured in the lab it does not directly model any unsteady phenomena discussed above and instead tries to incorporate this

effects through the use of empirical data. Their BET model over predicted the lift forces actually measured as seen in Figure 8. Furthermore, BET was only able to capture two of the three peaks in lift over the flap cycle. Seshadri et al. measured a spike in lift during stroke reversal at the end of the first half-stroke but BET could not predict it. The lack of this third peak was attributed unsteady effects such as rotational circulation and wake capture. As for the over prediction in lift force, they hypothesized that it was due to a premature shedding of a leading edge vortex but had no conclusive data to back up their hypothesis. Unfortunately Sehadri et al. did not perform a BET model with the steady state coefficients measured in the wind tunnel. It would be expected that this model would under predict the lift, but to what degree would have been of some interest.

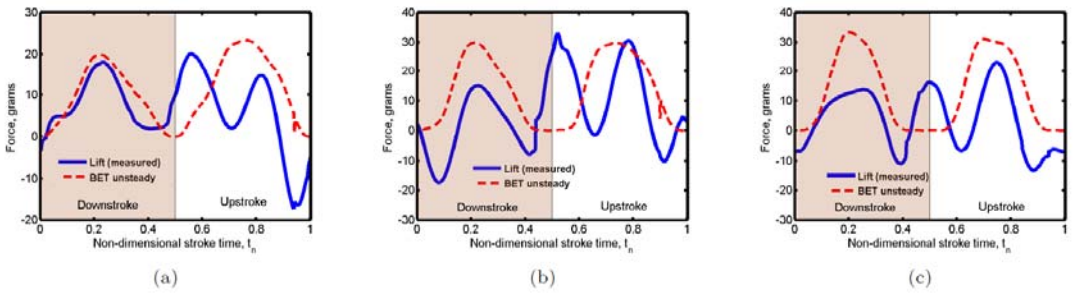

Figure 37. Lift variation for (a) $\psi = 40^o$ (b) $\psi = 60^o$ (c) $\psi = 80^o$

Figure 8. Results from Seshadri et al. displaying their empirical BET model versus experimentally measured results for stroke amplitude of (a) 110° (b) 100° (c) 87.3° [20].

In 2011, Thielicke el al.[21] created a unique BET model incorporating the work on delta wings into their aerodynamic coefficients. Leading edge vortices are a major source of lift in unsteady flapping wing aerodynamics, likewise conventional delta wings also rely on these same vortices for lift especially at slow speeds during high angles of attack. Thielicke et al. theorizes that although the stabilization mechanisms for the leading edge

vortices may be different from delta wings to flapping wings the flow phenomena and aerodynamic effects are similar. Delta wings can have lift coefficients as high as 6 [22] which is comparable to the increased lift coefficients measured on flapping wings. They use a concept developed by Polhamus of NASA back in 1966 [23] to predict lift coefficients of sharp edge delta wings. His theory, based on potential flow and vortex lift, had a trigonometric relationship between aerodynamic coefficients and angle of attack. Thielicke et al. would then use this relationship for lift and drag coefficients within their BET based model. The trigonometric relationship from Polhamus can be found in Equation (0.12) below:

$$C_L = K_p \sin\alpha \cos^2\alpha + K_v \cos\alpha \sin^2\alpha * \frac{\alpha}{|\alpha|} + C_{L_o} \tag{0.12}$$

where C_L is lift coefficient, α is angle of attack, C_{L_o} is the lift coefficient at zero angle of attack, and K_p and K_v are the constants of proportionality in potential flow lift and vortex lift respectively. Drag coefficient is found by the following relationship in Equation (0.13):

$$C_D = \Delta C_D + C_{D_o}, \quad \Delta C_D = C_L \tan\alpha \tag{0.13}$$

where C_D is the drag coefficient, ΔC_D is the drag coefficient due to lift, and C_{D_o} is the drag coefficient of the wing at zero angle of attack. This model would be classified as a semi-empirical method since the values of lift coefficients were based on the research done by Polhamus and the values of C_{L_o} and C_{D_o} must be experimentally determined. However, this is a very innovative method compared to the direction in recent literature and the Thielicke et al. produced excellent results to back up this approach. Figure 9

shows an example of the results they obtained using their method. The dashed line represents force balance measurements, the triangles represent the BET model using the aerodynamic coefficients from Polhamus, and the circles represent aerodynamic coefficients using classical steady methods. Their model matched the experimental results reasonably well for a semi-empirical approach. Figure 10 shows the summery of their results. The model predicted the experimental values better than the classical methods, but for the horizontal force the method was just as accurate and tended to over predict as the freestream velocity increased. Thielicke et al. also noted that as the flapping frequency increased the delta wing method over predicted the forces generated on the wing. This finding is a cause of some concern because the fastest frequency tested was 10 Hz. Insects such of the fruit fly have a flapping frequency of 200 Hz [24] so if the delta wing method continues to over predict forces generated as the frequency increases then it would be nearly useless for fast flapping insect sized vehicles.

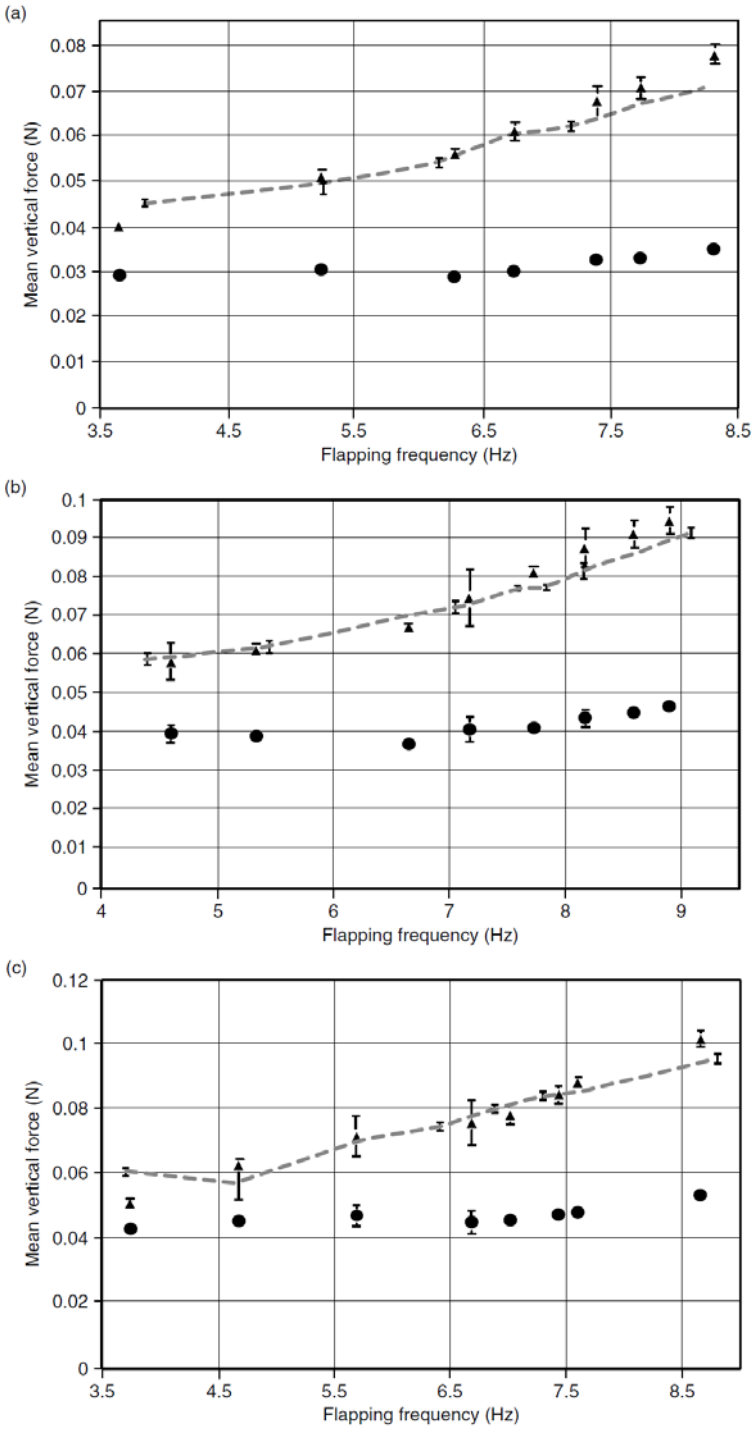

Figure 9. Results from Thielicke et al. showing the good predictability of their "vortex-lift" BET approach. The graphs show the steady state coefficients (circles) and "vortex-lift" method (triangles) compared to force balance measurements (dashed line). The different figures are for different freestream velocity (a) 2.28 m/s (b) 2.57 m/s (c) 2.84 m/s. [21]

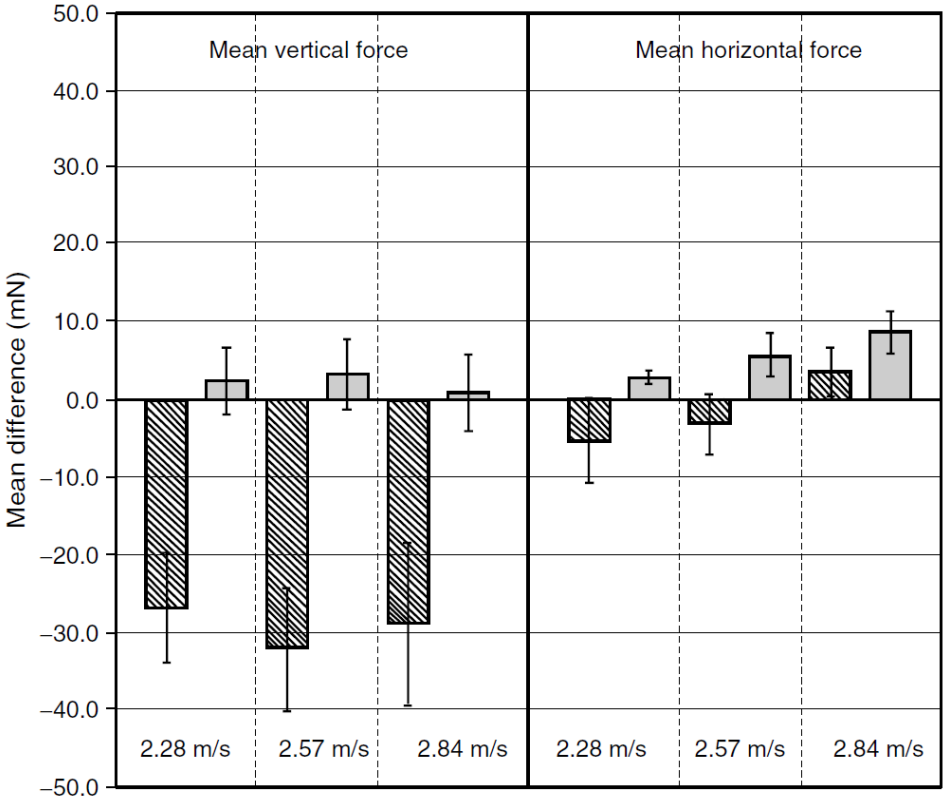

Figure 10. Summary results from Thielicke et al. comparing the averaged difference of the steady state coefficient model (dark shade) and "vortex-lift" method (light shade) from the experimental results at different freestream velocities. The "vortex-lift" method outperformed the classical method for the vertical force but tended to over predict the horizontal force as the freestream velocity increased. [21]

The aerodynamic forces associated with flapping wing flight are complex in nature and not yet fully understood since most research in the field began in the 1990s. Many models try to capture these complex aerodynamic interactions. Some models use simple BET to achieve a fast approximation while others use a combination of empirical terms and unsteady corrections. The highly unsteady and nonlinear nature makes the

aerodynamic forces difficult to predict but models are getting more accurate as researchers gain better understanding of the flapping wing effects.

2.2 Aeroelastic Response

Understanding, predicting, and controlling the flapping motion of passively controlled wings is being approached from many ways with most of the research focused on the areas of the aeroelastic response, flapping dynamics, and the structural qualities intrinsic to wings [5, 25]. The aeroelastic response involves the interaction between the wing structure and the fluid medium through which it moves through. A passively controlled wing deforms only by a combination of the inertial forces of the wing and the aeroelastic response so knowing and predicting the aeroelastic response is needed to predict the behavior of a flapping wing small unmanned aerial system.

Combes and Daniel , biologists from the University of Washington, performed numerous experiments with hawkmoth wings, *Manduca Sexta*, in 2003. They realized that if the aeroelastic contribution to wing deformation was small compared to the deformation caused by wing inertia alone then it would be much simpler to model insect flight [26]. In order to determine the importance of inertial loading versus the fluid structure interaction, they sought to compare deformations of a hawkmoth wing flapping in air with that in a vacuum. Since no fluid exists in a vacuum, any deformation present in the wing will be from inertial loading only. By comparing the deformations in a vacuum to those in air, Combes and Daniel would be able to determine the dominance of aeroelastic forces in hawkmoth flight. Since they did not have access to a vacuum chamber, they created a helium chamber to reduce the air density by 85% [26]. They saw

slightly more pronounced deformations in the helium chamber yet very similar to the air tested wings, leading to their conclusion that the inertial loading is more significant in predicting wing deformation in hawkmoths. To predict this deformation Combes and Daniel used a simple finite element (FE) model of the wing and adjusted the mass damping to match the observed deformations in air and helium. However, Combes and Daniel only picked three points on the wing (wing tip, leading edge, and trailing edge) to match measure and match to their FE model.

Norris, Palazotto, and Cobb set out to corroborate the results of Combes and Daniel that the hawkmoth's flapping wings are ultimately dominated by inertial-elastic response, but eventually came to the conclusion that the wing behaves more aeroelastically [5]. Their approach differed from Combes and Daniel in two important ways: vacuum testing and deformation modeling [5]. Where Combes and Daniel were only able to test in a helium chamber, Norris et al tested the hawkmoth wing in a vacuum chamber at pressure of 300 mTorr. This test was more representative of removing the surrounding fluid from the wing and isolating the inertial deformations of the flapping wing. Secondly, Combes and Daniel only modeled three points on the hawkmoth wing but Norris et al used stroboscopic photogrammetry to record nearly the entire deformation throughout the stroke. Understanding this aeroelastic response is important to predicting how the passively controlled wing will behave.

As Combes and Daniels previously noted [26], predicting the inertial forces is much simpler than modeling the fluid structure interaction between the air and the structure. Unlike conventional rigid aircraft wings, passively control flapping wings are strongly coupled with the aerodynamic forces produced throughout the flapping motion. CFD is a

numerical method to calculate the aerodynamic forces experienced by an aircraft structure in flight commonly used nowadays to predict aircraft response. Using CFD to predict wing deformations for flapping wing vehicles presents new and difficult challenges. When air flows over the wing it creates a pressure distribution across the surface of the wing. For conventional rigid wing aircraft, this pressure distribution can be resolved into lift and drag forces that the CFD solver continues to solve for consecutive time steps. For a non-rigid flapping wing, the pressure distribution causes the wing to deform. The deformation of the wing will cause a change in the resulting lift and drag forces. In order to successfully model a non-rigid flapping wing, the CFD solver must be coupled with a structural analysis program. The CFD solver computes the lift and drag forces and sends these values to a FE program to calculate the wing deformation caused by these forces. The deformation is calculated and the new geometry is fed back into the CFD solver. The shape of the structure has changed so the CFD solver must remesh or adapt the aerodynamic grid to fit this new shape. Remeshing the grid is a nontrivial task often requiring complex algorithms and multiple interactions. This is often the most complicated and computationally intensive part of the process as it is done for each iteration. The CFD software then computes new lift and drag forces based on this new geometry and feeds back new lift and drag forces and the cycle repeats as shown in the diagram in Figure 11. The aerodynamic forces need to be known to calculate the structure deformation and the structure shape needs to be known to calculate the aerodynamic force. This process is very computationally intensive and requires a fluid solver as well as a structural solver.

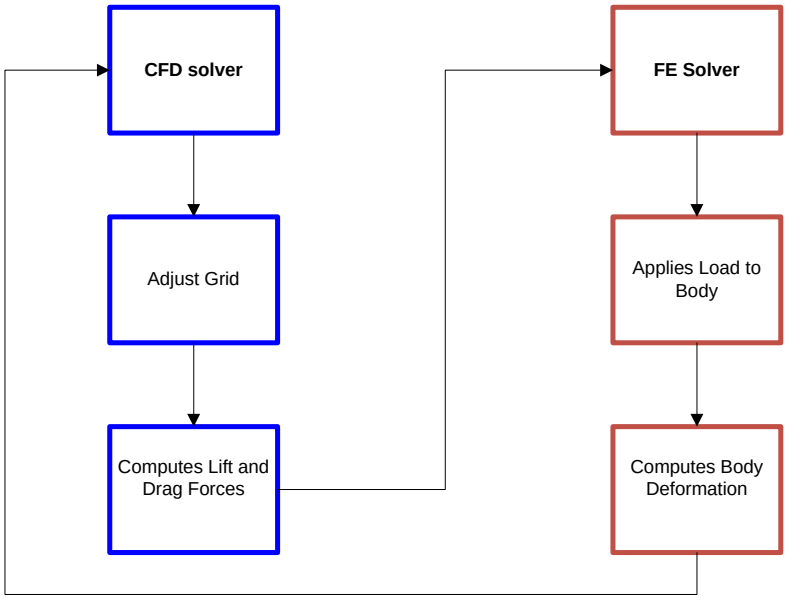

Figure 11. Schematic of workflow process between CFD and coupled FE solver.

Nakata and Liu [27] successfully coupled a FE based computational structural dynamic solver with a CFD based dynamic flight simulator to model insect flapping flight. This fortified Navier-Stokes CFD solver was built in house to specifically manage the complexities associated with insect flight and the associated large deformation of its wings. Nakata and Liu described how the two meshes (the fluid surface grid and structure mesh) must deform together in order to ensure no parts of the load were lost transferring from one program to the next. Furthermore, the fluid grid had to adapt automatically as the structure deformed, requiring a sub-iteration of the two solvers to ensure proper convergence of the interaction between the fluid and structure solver [27]. Although successfully implemented by Nakata and Liu, this approach is very computationally intensive and complicated requiring specific solvers to handle the specific case of flapping wing flight.

Lee, Shin, and Lee used a similar approach by using the lattice Boltzmann method (LBM) and a FE analysis with Euler beam elements to model structural deformations of a flexible flapping plate [28]. The LBM is based on the dynamics of particles used for solving partial differential equations. The LBM essentially uses a fixed mesh to solve fluid structure interaction which is a simpler and more efficient with a sacrifice in accuracy the greater the deformation [28]. Lee and Lee performed a similar analysis by putting a flexible plate normal to free stream at low Reynolds numbers [29]. They also used the LBM and a FE based solver to predict the deformations of the thin flexible plate at a range of different Reynolds numbers.

A myriad of different numerical methods exists to model a flapping wing with the coupling of a fluid and structural solver but they are all computationally intensive. The goal of this research is to validate structure interaction by modeling the deformations of a flapping wing with the aid of photogrammetry. Stereo photogrammetry uses two images taken of the same surface to calculate a three dimensional location [30]. With two properly placed and calibrated cameras, photogrammetry can be used to provide accurate three dimensional point data of a wing as it deforms throughout its stroke. This method is especially appealing to for non-rigid wings because it is not intrusive. Other methods for modeling a structure involve placing identifying markers on the structure in the form of a specific shape, paint, reflective dots, etc. The application of these materials to larger rigid objects is negligible but the care must be taken when using those methods on SUASs. Because of the light weight and flexible nature of the wings, the weight and stiffness of paint alone can be enough to significantly change the flight mechanics.

Several flapping wing studies have already used photogrammetry to achieve three dimensional models of flapping wings. Norris et al. used stroboscopic photography and the software package *PhotoModeler Scanner* with only one camera [5]. The strobe light was triggered at the same frequency as the flapping mechanism to "freeze" the wing at certain points along the flapping stroke. Image quality is the upmost importance when use photogrammetry so they spent a whole month perfecting the set up, lighting, and camera settings. They also highlighted that the dense surface modeling used by the software does not work with all objects but requires a contrasting or mottled surface [5]. Norris et al. used this method on a flapping hawkmoth wing both in a vacuum and in air to compare the inertial response to the aeroelastic response.

DeLeon expanded upon the methods used by Norris et al but instead of relying on dense surface modeling decided to use three dimensional positions of reference points attached to the flapping wing [25]. Reference points were used because DeLeon figured that they allowed for more control than dense surface modeling leading to more direct comparisons with a higher confidence in the results. However the presence of the reference points change the properties of the wings so DeLeon followed the method of Combes and Daniel that the application of the points may not exceed more than two percent of the weight of the wing in order not to significantly alter the natural frequency and structural qualities of the wing [25, 26]. Although this process proved very effective for modeling the flapping wing DeLeon commented that it was an extremely time consuming process requiring manual inputs therefore reducing the amount data able to be processed. This led to the work of Murray to improve upon the photogrammetry data capture process [30].

Murray found that in order to improve upon the process that stereo photogrammetry had to be used instead of the stroboscopic photogrammetry. As stated earlier, stereo photogrammetry uses two images taken simultaneously from cameras at different angles to calculate three dimensional locations in the similar manner that the brain uses the eyes to compute depth perception. Murray was able to automate the calibration and data processing to allow for a much less time consuming process. Murray confirmed that using the Stereo Vision Toolbox produced reliable data and is able to be applied to flapping wing projects [30].

The aeroelastic response of a flapping wing involves the interaction between highly complex aerodynamic forces and the structure. While extensive research efforts have gone into figuring out the aerodynamic side of the response, surprisingly few efforts have been devoted towards validating the structural side. The inertial response of a wing is equally as important as the aerodynamic forces on the wing yet most research never attempts to validate their structural model. Most papers describe their aerodynamic process thoroughly yet hardly mention the structural model they use or present any results that the structural model is valid. For rigid wings the structural calculations can easily be handled by a FE solver and are hardly worth mentioning, yet as research explores the boundaries of flapping wing flight, the wings are becoming more and more flexible. Flexible wings are much more difficult to model and require a second look. Flexible membranes are highly nonlinear and one cannot assume that the structural model can correctly predict the response. The flexibility of wings can vary based on the design and obviously the more rigid the wing the easier to predict the response. This research will focus on a thin, highly flexible membrane with a modulus of elasticity of

approximately 2.5 GPa. Without any stiffening support a membrane of this nature would not be able to support forces normal to the membrane plane. This type of membrane will be very difficult to predict but it is a necessary component in predicting the aeroelastic response as more flexible wings are developed. This research will set out to validate the deformations of a highly flexible wing model in FE.

III. Methodology

3.1 Test Article

The primary test article was a two-wing, commercial-off-the-shelf (COTS) SUAS that can fly indoors and outdoors called the Duck Hunter Extreme henceforth referred to as the test article or duck. It has a mass of 13.5 g, a wingspan of 30 cm and a flap angle of ±15º. A picture of the test article is shown in Figure 12. A remote control can change the flapping frequency to control thrust and the angle of the horizontal tale to control the flight direction. The test article cannot hover and must maintain a forward velocity of 1.75 m/s in order to achieve sustained flight. Using Equation (0.1) the advance ratio of the wing can be calculated to be 0.8 indicating that the test article was well under the advance ratio of 10 and unsteady terms will dominate the quasi-steady terms.

Extensive measurements were taken of the test article wing to achieve an accurate FE model. The dimensions and thickness of two different wings were taken in several locations. The values were averaged for use in the FE model. The wing membrane was composed of several different types of materials. Most of the membrane was composed of a very flexible Mylar, but two strips of a stiffer material run down the chordwise direction of the wing, hence referred to as battens, as shown in Figure 13. Along the leading edge beam, a tape material wrapped around the beam and attached to the membrane on both sides. This tape was the only attachment of the membrane to the beam and it made the section of the membrane adjacent to the leading edge stiffer than the Mylar but less stiff than the battens. It is also important to note that there was a rigid plastic tab located at the rear of the wing that connects the wing to the SUAS body by a pin joint.

The average measurements recorded are listed in Table 2, with their corresponding locations on the wing shown in Figure 13. The battens and tape material were translucent and difficult to see so a corresponding diagram of the wing was constructed with the stiffeners and tape material outlined.

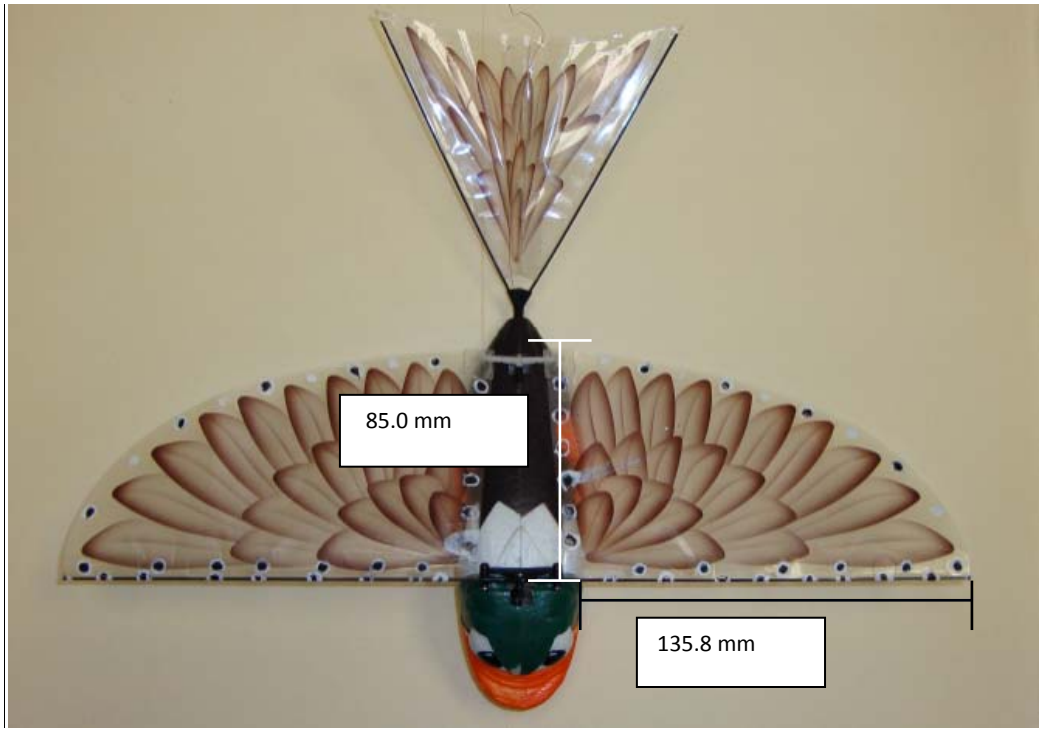

Figure 12. SUAS test article.

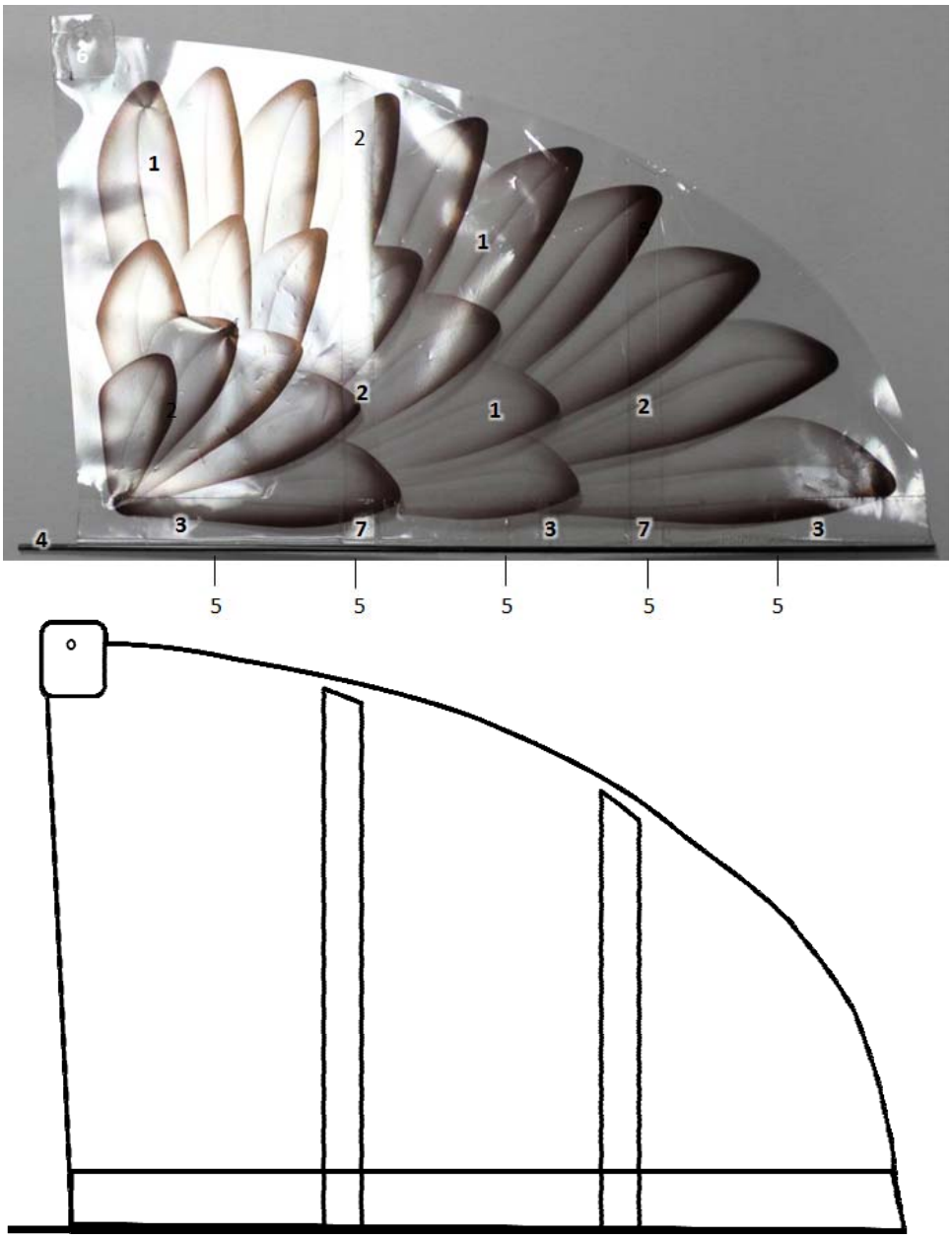

Figure 13. SUAS wing and measure locations and wing outline.

Table 2. Wing Measurements

Wing Location	Part	Average Thickness (mm)
1	Membrane	0.0215
2	Batten + Membrane	0.1426
3	Tape + Membrane	0.1185
4	Bar	0.9737
5	Bar + tape	1.0613
6	Connecter	0.6172
7	Batten + Tape + Membrane	0.2429

The duck achieves flight through a battery driven motor located at the front of the fuselage that flaps the wings. A dissected view of the mechanism can be shown in Figure 14. This motor turned several gears which in turn cranked a bar vertically up and down. This single bar was connected to both the wing joints and drove the flapping motion for both wings. The joining of the bar linkage at the top of the duck had loose fittings allowing the bar to slide during operation. Previous work on this project had shown that this could be modeled as a four bar linkage [31]. While this mechanism was not a true four bar linkage the output to the wings was relatively the same. This flapping mechanism was relatively simple when compared to the complex motions found in natural flyers like the hawkmoth. The stroke plane angle and amplitude were fixed so

changing the flapping frequency was the only available means to modify the forces generated during flight. This mechanism had its pros and cons. The relatively simple nature did not allow for much control during flight, but replicating the flapping mechanism was simpler. Since the focus of this research was on predicting the structural response rather than controlling the vehicle, this made the simple mechanism an appealing choice.

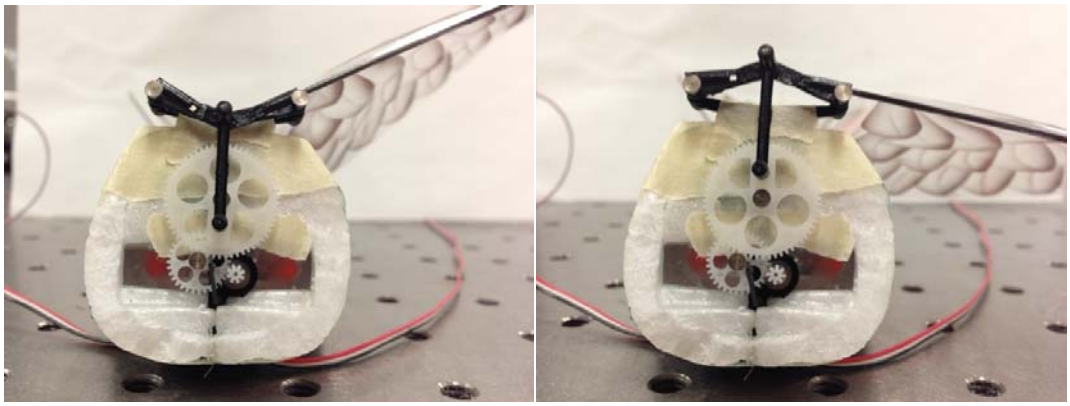

Figure 14. Dissected view of the mechanism that drives flight in the test article. Left shows link at the bottom of the crank which corresponds to the top of the upstroke and right shows the bottom of the down stroke.

Abaqus was chosen as the finite element solver for this study because it excelled at handling highly nonlinear, dynamic problems. This strength was well-suited for this research project because most of the wing was composed of a flexible membrane.

Starting simple and working toward a more complex model, only the leading edge beam was modeled. By starting simple, the model could be easily validated at a low computational cost, then complexity could be added on. This process was easy to build upon and debug when a problem did occur. First, a beam only model was created in

NATSTRAN and Abaqus. These two models were compared against each other because a relatively simple analysis should produce similar results whether from Abaqus or NASTRAN.

3.2 Modal Testing

A scanning laser vibrometer was used to perform an eigenvalue/eigenvector analysis on the leading edge beam of the duck. The beam of the wing was clamped in between two metal plates and mounted to an electrodynamic shaker. The shaker would provide the input, while two lasers were used in this experimental setup to measure the input/output relationship. A reference laser was directed at the plate clamping the beam to the shaker to measure the velocity of the input into the system. A scanning head was also set to scan the length of the beam to measure the output velocity. To help strengthen the laser return signal, small pieces of reflective tape were placed along the length of the beam. The tape was light enough and the beam was stiff enough that any effect on the modal properties was minimal. A pseudorandom input was generated and input into the system through the shaker. Seven averages were recorded for each test with 800 frequency lines over a usable frequency range of 250 Hz (approximately 80% of Nyquist frequency). A rectangular window was applied to the data because the pseudorandom input was generated such that it was periodic at the Nyquist frequency. A frequency response function was generated from the recorded input/output signals using the Polytec vibrometer software and the system eigenvalues and eigenvectors measured were used to validate the model. The test setup is displayed in Figure 15 and a picture of the beam in the clamped configuration is shown in Figure 15.

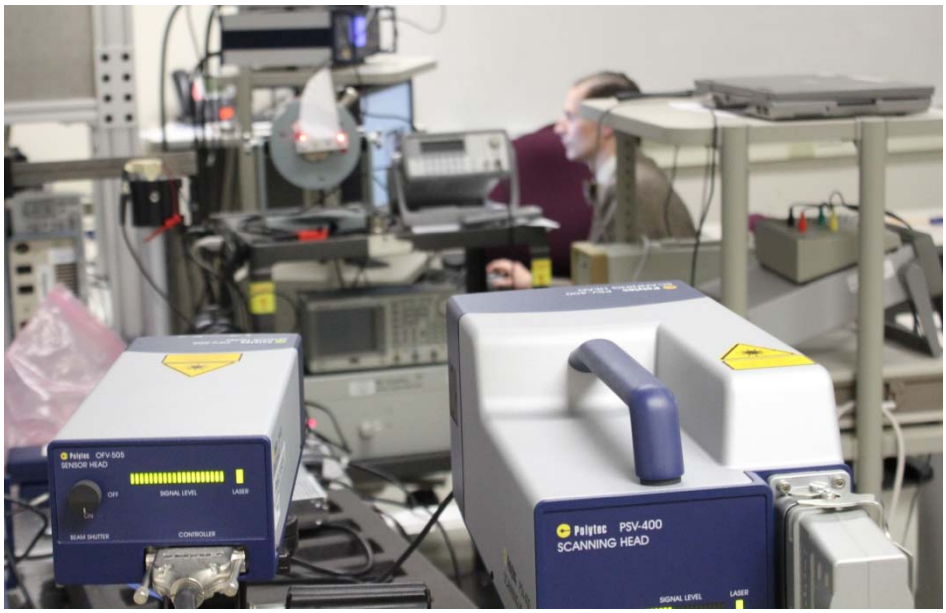

Figure 15. Test setup for the laser vibrometer. The two lasers are located at the bottom of the image with the scanning laser on the right and the reference laser on the left. In the background the wing is shown clamped to the shaker. The same test setup was performed for the leading edge beam.

Figure 16. Leading edge beam of the duck wing shown clamped between two plates. The plates were bolted to an electrodynamic shaker for testing.

The FE model was validated by comparing the first three modes to the measured modes in the laboratory. Any discrepancies between the model and the experimental

results were reconciled via model tuning. The density of the model was verified by weighing the beam and changing the FE model density to match the measured weight. A clamped beam is easy to model so a representative model was constructed in MATLAB. An eigenvalue analysis was run to ensure the modes matched the Abaqus model. Modeling tuning occurred by changing the modulus of elasticity until the first two modes matched the experimental results. A sequential quadratic programming optimization algorithm in MATLAB modified the modulus of elasticity until the first two modes matched. The model had been tuned to the clamped beam, but the housing within the duck that the leading edge beam sits in has some wobble. This boundary condition was a source of error between the model and the physical test article.

To remedy this unknown factor, modal testing was accomplished with the entire test article. The duck was strapped to a plate via zip ties and the plate was bolted to the shaker. The Styrofoam body of the duck did not allow direct mounting to the shaker but the zip ties firmly secured the duck so not to allow the body to slip or wiggle during testing. The bar was mounted in housing on the duck in place of the wing (Figure 17) and the scanning laser vibrometer was used in the same manner as before. This gave a more realistic boundary condition and allowed for insight into how the modes were affected by the compliance in the joint.

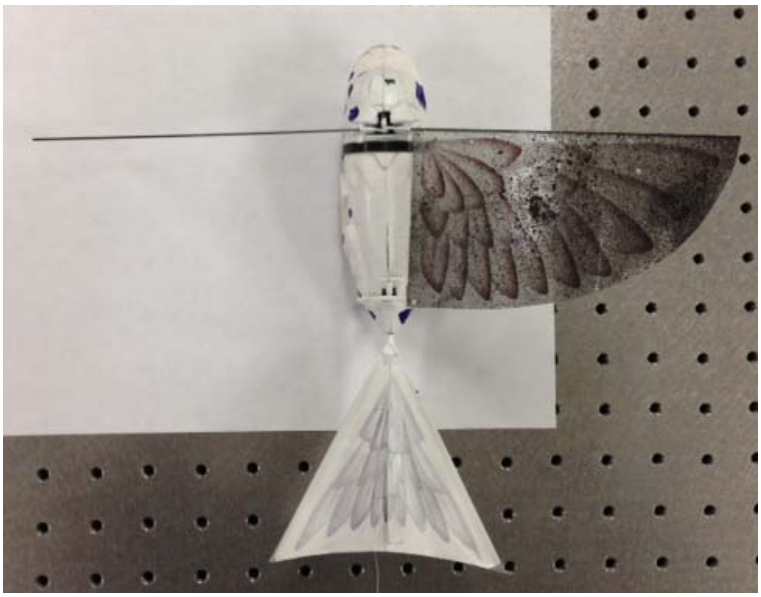

Figure 17. Top view of the test article used for modal testing with the wing membrane removed from the leading edge beam on the left side. This configuration would show different results than the bar in the clamped configuration.

The model was then tuned by modifying the boundary condition. The clamped boundary condition was stiffer than the actual joint. To weaken the attachment point the modulus of elasticity and length of the element attached to the boundary condition was varied until the model matched the first two measured modes. The methodology behind this decision was that the full bar and wing model would be actuated by forcing a rotation at the root of the wing. In the Abaqus solver this can only be accomplished by constraining the degrees of freedom at that point and then applying the forced rotation. By weakening the beam at the attachment point, it would simulate this weak connection and the results could be properly seen in the dynamic analysis as well as the frequency analysis.

Again MATLAB was used to optimize this connection. This optimization gave an accurate bar model with an appropriate boundary condition. With this simple model

validated, the next step was to add the wing membrane to the leading edge bar. As with the bar, a wing model was created in Abaqus and FEMAP. Analyzing these models gave a comparison between the NASTRAN and Abaqus solver.

Two wings were measured in detail using a micrometer for the thickness of the wing membrane, batten, connector, tape, tape/membrane overlap, and the bar thickness. Figure 13 above shows the locations for all the measurements and Table 1 lists the average measurement of each part. Next, material property testing was conducted since the actual materials used for each part was unknown. Several spare wings were dissected into their different components: leading edge beam, wing membrane, batten, and tape. The connector was not tested because it was fairly stiff and its affect on the outcome of the simulation was insignificant. The tape and membrane overlap area was too small to test in the appropriate testing equipment.

To model the membrane portion of the wing more accurately in Abaqus, a picture of the wing was taken from directly above. This image was loaded into Abaqus and the part was crafted by tracing the wing outline and all other features. The leading edge was modeled as a simple beam as a separate part from the rest of the wing. The membrane was sectioned so that each feature of the wing could be properly segregated. The final assembly can be found in Figure 18. More details about the model can be found below.

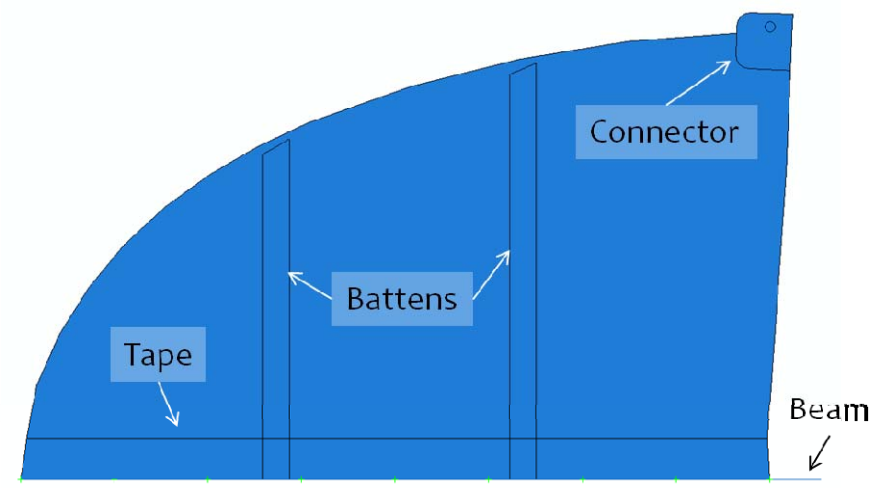

Figure 18. The Abaqus wing model includes several features found on the duck such as the tape, battens, and connector. Note: the leading edge beam runs the whole length of the wing membrane. The wing membrane is connected to the beam by the strip of tape at the leading edge.

With the full model developed, modal analysis was then performed on the entire wing with methodology similar to that used for the bar. The setup for the wing testing was the same as shown in Figure 15 above. The wing had to be coated with Spotcheck for the scanning vibrometer to receive a strong enough return from the laser. Spotcheck is a spray of white developing particles that can be quickly applied. Without this layer of particles, most of the scanning laser would pass through the translucent membrane. This method added some weight to the wing, which was taken into account when model verification occurred, but was a necessary step to accomplish this testing. The extra weight of the Spotcheck most likely made the measured modes lower than those seen during flight. Spotcheck was applied sparingly to reduce the effect of the added weight but it was necessary to achieve a sufficient return from the laser. The wing was tested in a clamped configuration (Figure 19) as well as in the configuration used in flight (Figure

20). The modal modeling was accomplished in Abaqus. As previously stated with the beam, the test article housing had some compliance and was not a perfect clamped boundary condition so the modal tuning was accomplished in the same manner as described for the beam.

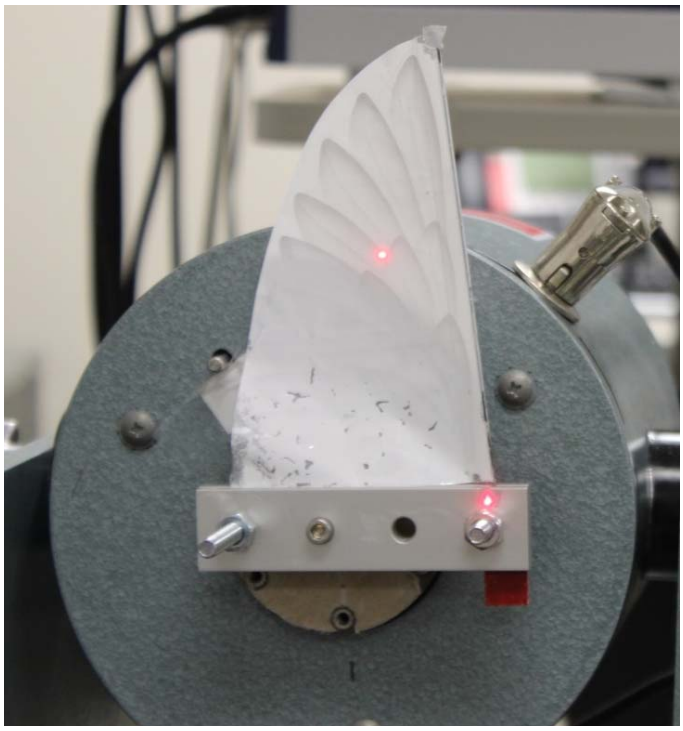

Figure 19. Duck wing attached to shaker in clamped configuration. The wing was painted with Spotcheck to achieve a strong laser return. The reference laser can be seen on the clamp and the scanning laser on a point in the middle of the wing.

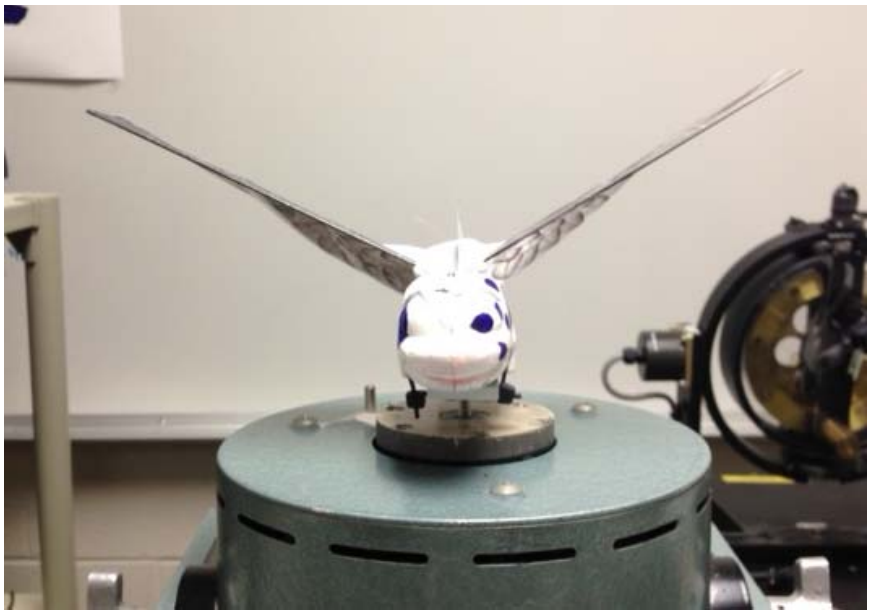

Figure 20. Duck clamped to shaker for modal testing.

3.3 Air and Vacuum Testing

In conjunction with modeling the wing, the test article was also tested in air and vacuum. Predicting the aeroelastic response of the wing is difficult because of the complex interaction between the aerodynamic and inertial forces. As discussed earlier the aerodynamic forces themselves are difficult to understand, let alone model. When they are coupled with the inertial response the two forces become difficult to separate. For a rigid wing the inertial forces are easier to isolate because aerodynamic forces have little effect on the wing shape as it flaps. Hence, the inertial forces can be found by testing the wing in a vacuum since, in the absence of air, the only forces measured will be inertial forces as detailed by [20].

The flexible wing presents more difficulties because the wing will deform in a different manner in a vacuum than under the influence of aerodynamic forces. To test this assumption the wing was tested in a vacuum as well as in air. The vacuum testing

was important because it allowed for a qualitative assessment of the membrane deflection in air. As discussed earlier the FE model does not incorporate aerodynamics so the deflections seen in the model should compare well with deflections measured in a vacuum.

Vacuum testing occurred in a custom vacuum chamber at AFIT that allowed the pressure to range from atmospheric to less than one Torr. This vacuum chamber was ideal because all the sides were translucent, which allowed for easy viewing of the duck from all sides. Three high-speed cameras were setup to capture the wing throughout the flap cycle. This setup would allow for qualitative assessment of the membrane billow and a quantitative assessment through the use of photogrammetry. A picture of the setup can be found in Figure 21. Two of the cameras were setup on either side of the vacuum chamber so that one looked at the side of the duck while the other captured the front of the duck. The third camera was placed directly above the duck. Synchronization between all three cameras was accomplished through a trigger controlled by a MATLAB program.

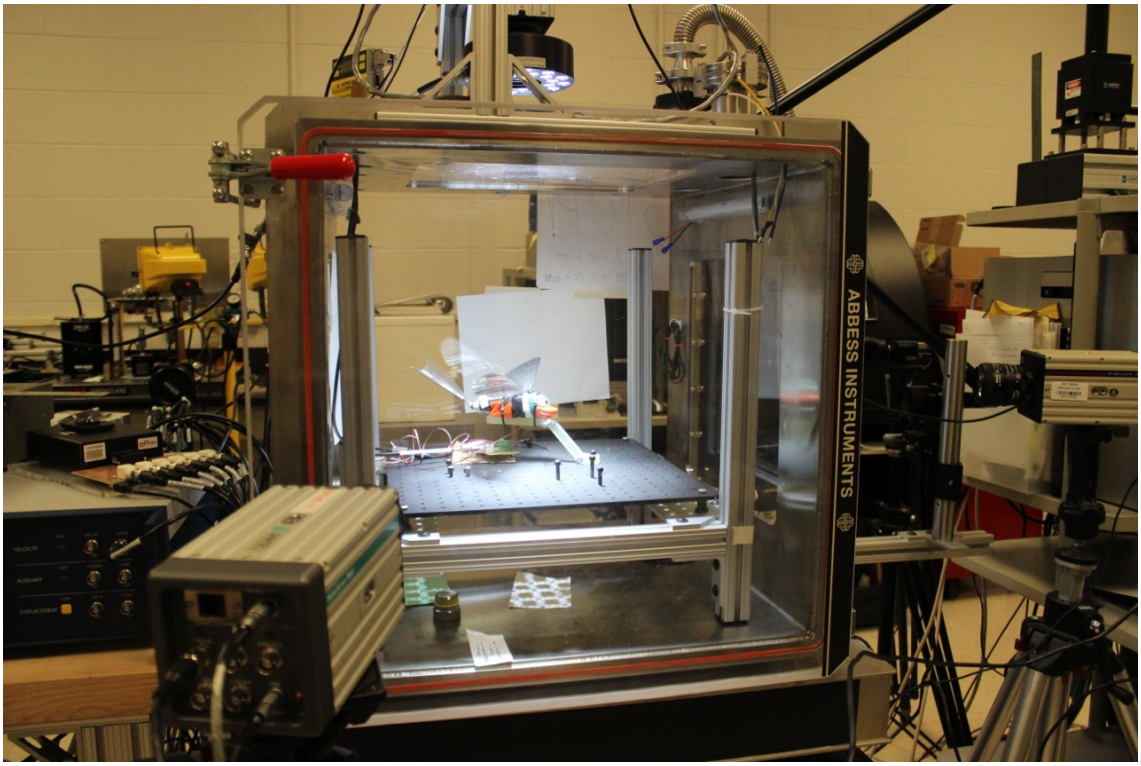

Figure 21. Experimental setup of vacuum testing. The test article was placed in the vacuum chamber and wing stroke was capture by three high speed cameras (right, bottom left, and top of photo).

Under normal operating conditions the duck was powered by a rechargeable lithium-ion battery. Placing this battery in a vacuum could be potentially hazardous. To circumvent this possibility the battery was removed and the duck hooked up to an equivalent DC voltage power source outside the vacuum chamber. With this setup, the duck was safely controlled outside the vacuum chamber with the use of the remote control. The high-speed images would give a qualitative analysis of the membrane while photogrammetry could provide a 3D model of the wing deflection as a function of time. Air testing occurred in two different manners. One occurred while the duck was in the vacuum chamber under atmospheric conditions—hooked up to the DC power supply. A

second test occurred with another test article flapping with the commercially supplied battery. The difference in these two tests would reveal any difference in the two different power supplies.

3.4 Structural Model

As stated earlier the primary development of the structural model was performed in Abaqus. The final model was composed of two parts: the leading edge beam and the wing membrane. The final material properties determined through testing can be found in Table 3. These material properties represent the base model in Abaqus. A multitude of different models were run changing various parameters to see their effect on the output. This was an effort to match the physical deformations seen. Membrane elements and plate elements were both used in the various models and the beam was always modeled with beam elements. Since membrane elements only resist in place forces, they offered a lower computational cost with the risk of poor accuracy. The plate elements provide more degrees of freedom at a longer compute time. Various combinations of these were tried to optimize the ratio between accuracy and computational intensity.

Table 3. FE Model Properties

FE Spec	Beam	Membrane	Batten	Connector
Modulus of Elasticity (GPa)	85.9	2.47	5	50
Poisson's Ratio	0.05	0.489	0.489	0.05
Density (kg/m^3)	1584	917	917	917
Element Type	Beam	Membrane	Shell	Shell

The leading edge beam and the wing membrane were connected in Abaqus through a tie constraint along the nodes of the beam allowing the assembly to act as one part. The only load acting on the structure was gravity. A pinned boundary condition was created at the inner circle on the connector to simulate the connection to the test article body. Since the wing on the test article was actuated by a four bar mechanism described above a forced rotation was placed along the part of the leading edge beam jutting out from the wing membrane. Many other methods were attempted to achieve the proper flapping motion (force at the root, moment input, etc.) but a forced rotation was the only method that produced repeatable and reliable results. Because of the complexities associated with dynamic simulations two different meshes were created. One was a coarse mesh used for most of the analysis because it allowed for a reasonable visualization of the results at a lower compute time. If more exact data was needed or once a model was

verified a finer mesh would be used. Figure 22 and Figure 23 below show an example of a coarse mesh and fine mesh used in the analysis.

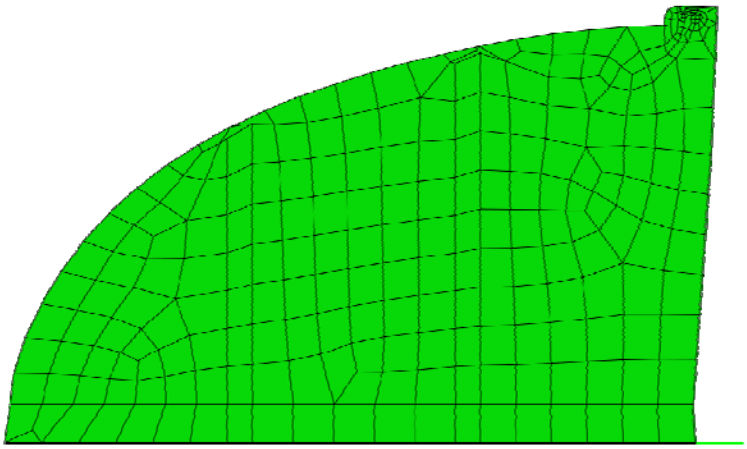

Figure 22. An example of a coarse mesh used for most analysis.

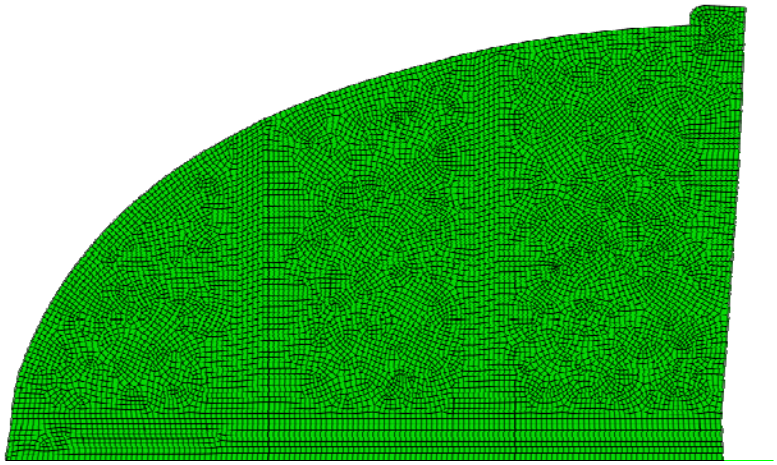

Figure 23. An example of a finer meshed used for in-depth analysis.

The dynamic nature of the flapping motion made the structural problem difficult to solve. Abaqus has two different solvers for dynamic simulations: implicit and explicit. In an implicit dynamic analysis the entire set of nonlinear equilibrium equations must be solved at each time increment. The implicit analysis could take a long time but the

equations are solved at each time step making this method unconditionally stable. For example there is no limit on the size of the time increment for an implicit analysis. The explicit analysis does not solve the nonlinear equations but rather used known quantities at previous time steps to estimate the displacements and velocities at a new time increment. This method was generally less computationally intensive but the time step is conditionally stable. There exists a limit on the size of the time step before the solution becomes unstable. Abaqus defines this limit as the time it takes a stress wave to cross the smallest element length in the model. The smaller the element the shorter the time step can be taken. Another downside of the Abaqus explicit solver was that fewer element types are supported for this analysis. However, beam, plate, and membrane elements were all supported so that both the implicit and explicit solvers could be tested against each other.

IV. Results

4.1 Modeling Goal

The purpose of this research was to correctly model the structural response of a flapping wing of the proposed test article. To that end, before modeling was started it was beneficial to test the actual model in air so that the wing kinematics could be observed. Before quantitative data was taken, high speed images of the wing gave a frame of reference for the modeling that would occur later. The results from the model were qualitatively compared against the images to provide a gauge to judge if the model was generally predicting the motion or if something was not correct. This comparison saved time up front because it allowed for a quick comparison to the test article. Even though the FE results did not model air and therefore should not match the wing in air, it was expected that the kinematics of the wing to be similar. It was theorized that while the vacuum results would probably show greater deflections, the overall movement of the wing would be the same.

The high speed cameras were used to capture images of the flapping wing as it was clamped to a test stand. The series of images in Figure 24 show the motions of the wing throughout the flap cycle. At the beginning of the down stroke, the wing beam began to move down while most of the membrane movement was still in the direction of the preceding stroke. The wing membrane underwent large deformations during the stroke with the most prominent during stroke reversal. During the down stroke the beam again led membrane until the beam was about level then the aft part of the membrane surpassed beam. When the beam began the upstroke, most of the membrane was still moving down

resulting in a larger deformation. At the end of the upstroke, the beam arrived at the top just before the aft part of the membrane.

(a) 3% of Stroke, front view (left), side view (right)

(b) 29% of Stroke

(c) 50% of Stroke

(d) 75% of Stroke

(e) 3% of Stroke

Figure 24. The flap cycle synchronized to percent of the stroke period [31].

Figure 25 shows a trace of the tip displacement during multiple strokes. Birds and insects with complex flapping kinematics can have unique wing tip traces as shown in Figure 26[24]. The test articles wingtip path was relatively simple but interestingly enough, the wingtip path most closely resembled a fruit fly (two wings) from the diagram below whose cruising speed is 3 m/s (the test article's cruising speed is 1.75 m/s). The wingtip trace for the test article's wing was consistent over multiple flap cycles and simple, which was another reason this test article makes a good choice for FE modeling. The features observed during this testing, specifically the leading of the beam or membrane during different phases of the stroke, wingtip path, and consistent deflections during each flap cycle, were used as qualitative gauges of accuracy throughout the modeling process.

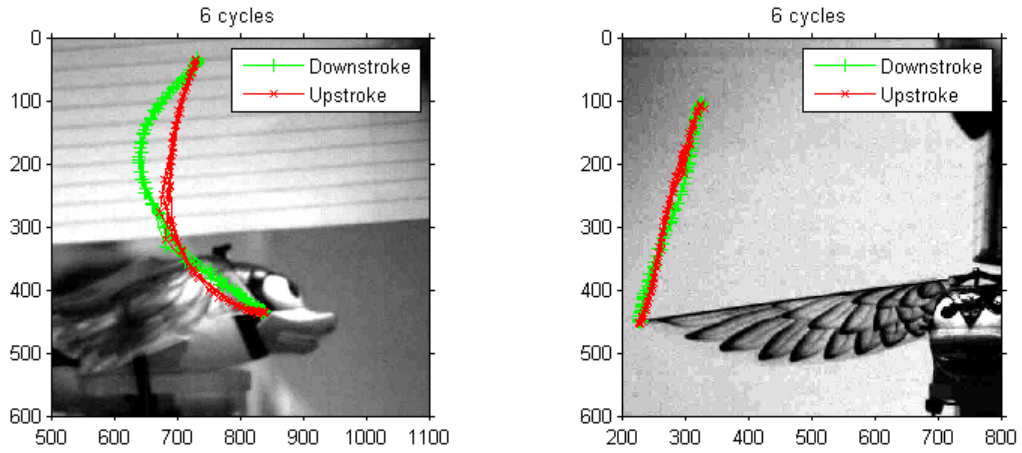

(a) Side View (b) Front View

Figure 25. The path of the tip can be consistently measured from the images [31].

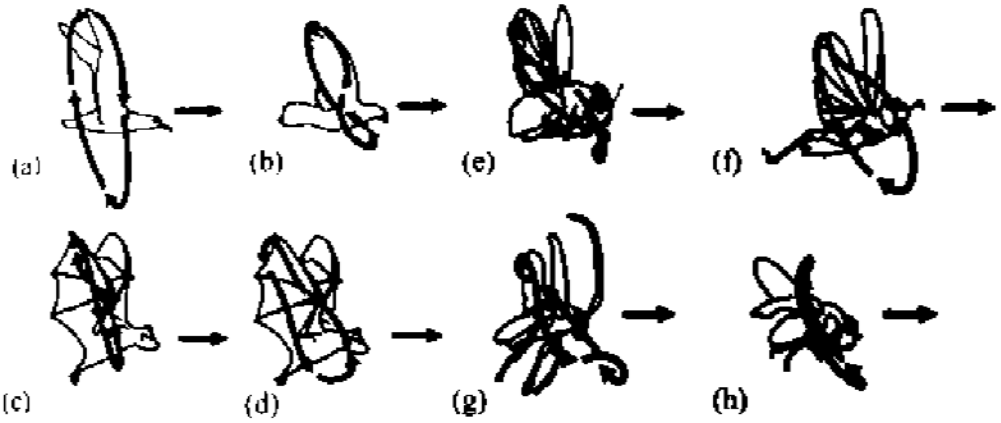

Figure 26. Wingtip trace for (a) albatross fast gait, (b) pigeon slow gait, (c) horseshoe bat fast gait, (d) horseshoe bat slow gait, (e) blowfly, (f) locust, (g) June beetle, (h) fruit fly [24]. The test article most closely resembles the fruit fly wingtip trace.

4.2 FE Solver

Starting with the least complex system, the dynamics of the leading edge beam were modeled in NASTRAN and Abaqus. While NASTRAN is a proven finite element solver it was questionable how well it would handle the dynamic and highly nonlinear interactions of a wing membrane. Abaqus on the other hand, is known for handling dynamic problems, but was a relatively newer program. Modeling only the beam was a first step towards modeling the entire wing but it was also gave early insight as to which solver would better handle the nonlinear dynamic analysis. These early models were developed with the material properties used in the previous work on the duck [31] because material testing had not yet been accomplished. One parameter that will be used constantly throughout the course of this paper to compare different models is the tip deflection over time. The tip deflection is simply a trace of the tip of the end of the

leading edge beam during the flapping cycle as shown in Figure 25. It was theorized that if a model could reproduce the tip displacement over time for the test article, then the rest of the beam would match closely. Tip deflection gave a quantifiable parameter that could easily be obtained in FE models and was measurable in the laboratory.

Figure 27 below shows the tip deflection versus time for the various models. All models were started at the bottom of the stroke because the velocity at this point would be zero and this would allow for a quicker damping out of transients than if started during midstroke. For a frame of reference, the rigid body motion of the beam has been plotting on the graph. This series would be the tip deflection of the leading edge beam if it were to stay perfectly rigid without any deflection throughout the flapping cycle. The NASTRAN methods both reached a steady state around 0.3 seconds and both showed very similar deformations. However, the steady state achieved was not purely sinusoidal. Higher order modes seemed to be present so that, after steady state was achieved, every other down stroke was larger than the average amplitude.

This analysis did not shed any light into the accuracy of one method over the next because of the absence of experimental results for comparison. Both methods predicted approximately a 110 mm max deflection (max to min peak) at some point during the flap cycle while the rigid body calculations only showed a deflection amplitude of 70 mm. Roughly 30 mm of deflection was caused by bending of the beam at stroke reversal but there was also the existence of two peaks at the height of the upstroke. The Abaqus explicit and implicit solvers both predict almost identical results at the beginning of the stroke; yet over time the implicit solver grew with each period until it seemed that the

solution was growing unbounded. This finding suggested that the implicit analysis was unstable so this method was investigated further.

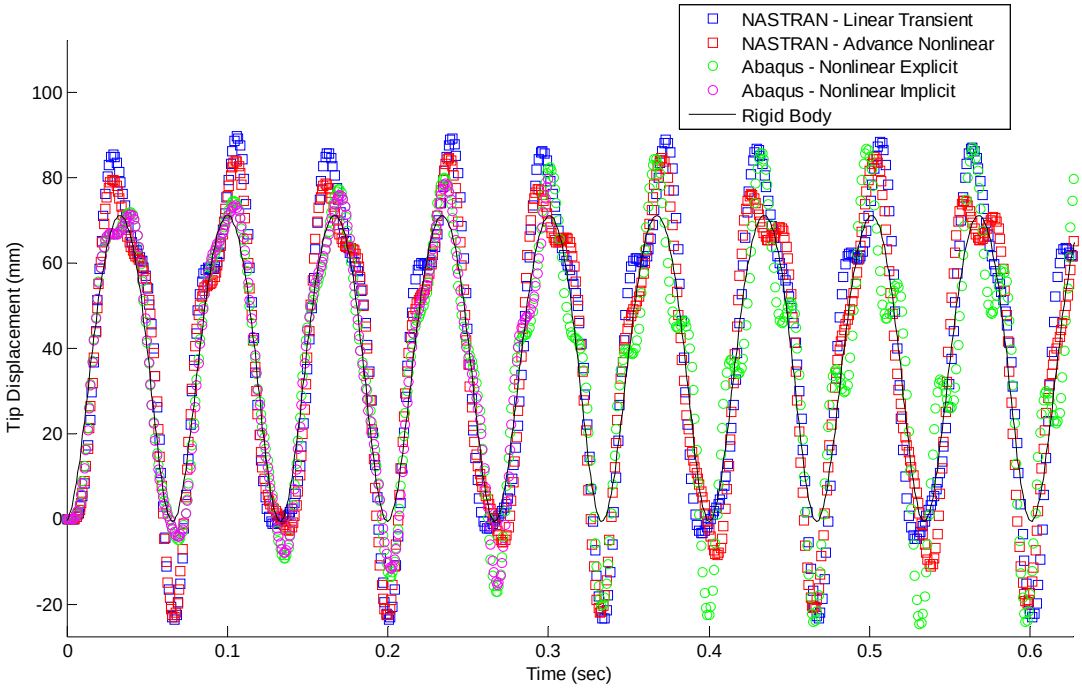

Figure 27. Tip displacement over time comparison between NASTRAN and Abaqus of the leading edge beam only.

While the implicit solver seemed to perform well 0.6 seconds into the analysis, after this point the amplitude began to grow with each stroke until it seemed the solution was growing unstable. This trend was disconcerting because although the implicit solver was supposed to be more computationally intensive, it was supposed to be the more stable of the two solvers. The same model was run reducing the step size from 0.001 to 0.0001 to see the effect on the solution. Changing the step size had a drastic effect on the solution as seen in Figure 28. While the solution was relatively the same through 0.4 seconds, the implicit analysis with a larger time step increased over time especially on the bottom of

the down stroke. This gave less confidence in the implicit solver, because it seemed that the solver could not obtain convergence with that large of a time step. Coupled with the fact that the implicit solver took much longer to run at a time step of 0.0001, the explicit analysis was chosen as the solver of choice because the addition of the wing membrane would only increase the complexity and analysis time drastically, and for this scenario the explicit solver seemed to handle the nonlinearities better than the implicit solver did.

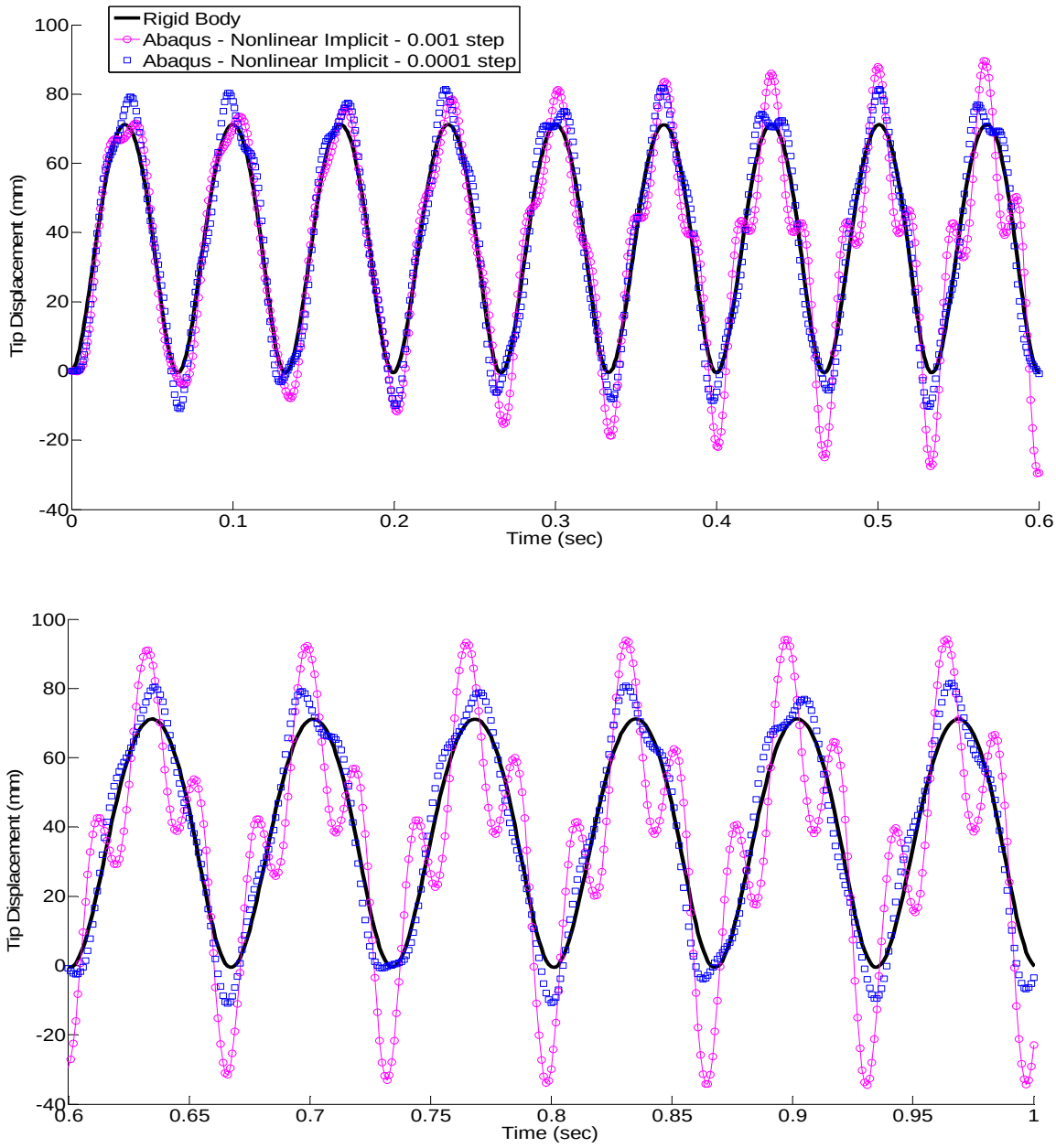

Figure 28. Comparison of implicit solvers.

Investigation of the best solver to use began with incorporating the full wing into the NASTRAN solver. The same geometry in the model developed by Alerding [31] was imported into FEMAP. The beam and wing model in FEMAP is shown in Figure 29.

The model was adequately meshed and analysis was performed using the NASTRAN linear transient and nonlinear solvers. Beam elements were used to mesh the beam and plate elements that comprised the membrane. Figure 30 shows the membrane deflection predicted by these analyses. The membrane deflections were completely unreasonable, characterized by a high number of ripples deflecting unrealistically large amplitudes. The membranes looked as if they exhibited an extremely low stiffness. Several attempts were made to remedy these results in the model but the only way to force the results to qualitatively match reality was to arbitrarily add bending stiffness to the membrane. It was determined that the NASTRAN solver could not handle the highly nonlinear aspects of the wing membrane so Abaqus was chosen as the FE solver.

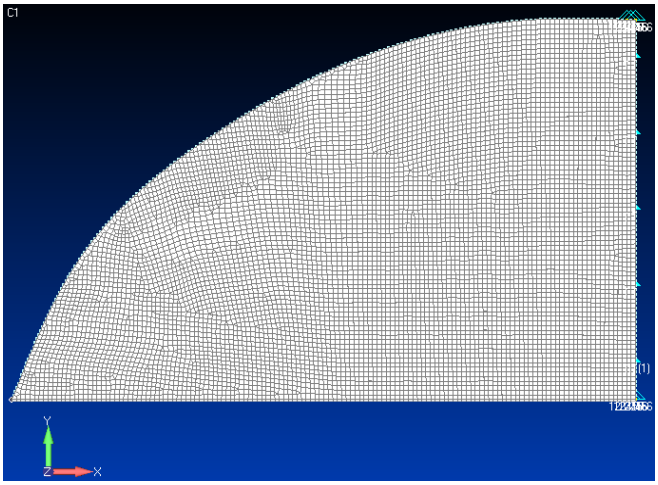

Figure 29. Wing modeled and meshed in FEMAP for comparison of the NASTRAN with the Abaqus solver.

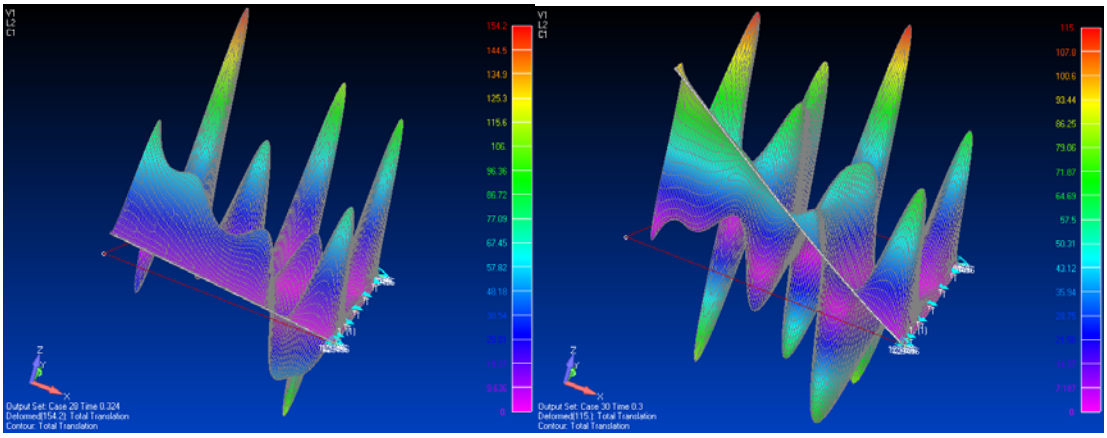

Figure 30. Membrane mesh deformations are unrealistic and fail to match physical model. Left: NASTRAN linear transient solver. Right: NASTRAN advance nonlinear solver.

4.3 Material Testing

Material testing on the wing produced some mixed results. Standard tensile testing was performed on the membrane, battens, and tape. The wing membrane gave repeatable results with the average modulus of elasticity at 2.47 GPa. This find also corroborates well with the work of Gogulapati [32] who tested a similar wing membrane material and found a modulus of elasticity was 2.72 GPa. The tape results were unreliable due to the adhesive between the layers. The tape made this material behave as a composite with a very weak adhesive. During testing the material would stretch and then part of the adhesive would give, then the material would stretch more before more adhesive would give. The adhesive skewed the stress strain curves so in the linear region it appeared that the tape and membrane layer had an average modulus of elasticity of 0.839. This was deemed unrealistically low. For the final model the membrane modulus of elasticity was used for the tape area.

The batten material was much stiffer than the membrane. As a result the load cell on the testing apparatus was maxed out (40 N) before the material failed. Unfortunately the next load cell size up would not have been able to accurately measure the small loads associated with this material. For the model a conservative estimate of 5 GPa—approximately twice the membrane modulus—was used. For reasons stated above the load cell could not measure the relatively stiff carbon fiber beam. As a work around the beam was divided into several sections and tested in a three point bending configuration shown below in Figure 31. This three point bending gave repeatable results and a modulus of elasticity of 88.1 GPa was found for the leading edge beam. The same test setup used for the leading edge beam was also used to test the battens in an attempt to find the material properties. Unfortunately, the battens did not exhibit enough bending stiffness so the forces generated were below the noise threshold for the sensors. As part of the material testing, the leading edge beam was weighed and found to have a density of 1584 kg/m^3. The density of the material was updated in the Abaqus model to reflect these material property changes.

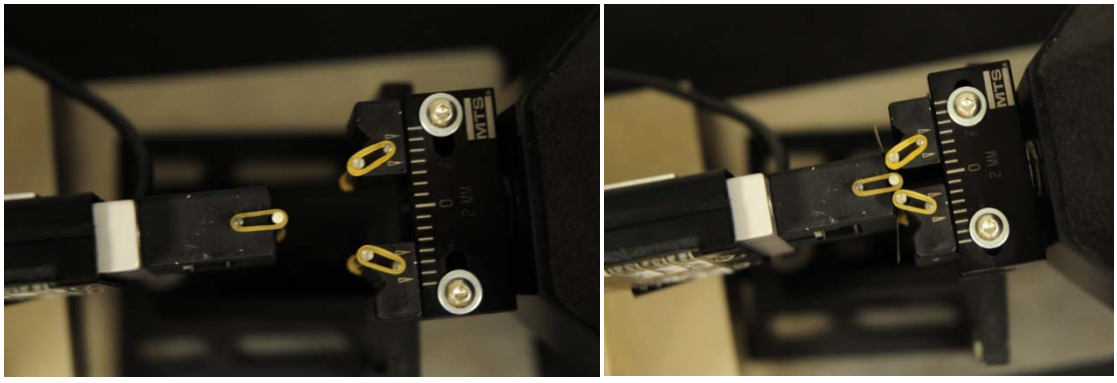

Figure 31. Three point testing configuration for material testing. On the right the apparatus is in the open configuration. On the left the material (batten in this picture) is bent.

4.4 Laser Vibrometer

Model tuning via modal testing, as outlined in Chapter 3, proved very insightful. The frequency response functions (FRFs) and coherence for the leading edge beam in the clamped configuration are shown below in Figure 32. The coherence was excellent over the range of interested frequencies. The first three modes are shown in Table 4. The Abaqus bar only model in a perfectly clamped configuration gave similar results but there was still a 1-3% error in each mode. To tune the model, a MATLAB FE code was developed and ran to show that they matched the Abaqus results. As discussed in Chapter 3 an interior-point algorithm was used for all optimization routines. The modulus of elasticity was modified to match the first mode in the beam. The results of the optimization are shown in Table 4. The model was tuned within 1% of the physical beam and the modulus of elasticity was decreased by 2.5% to achieve this. The model was tuned to match the first mode because this mode occurred nearest the flight flapping frequency of 15 Hz. Note that while the first mode matches by design the second and third modes still exhibit some error. The two plates the bar was sandwiched between was not a perfect clamp so some error was expected.

The leading edge beam was also tested in the housing on the duck to compare how closely it resembles a clamped boundary condition. The FRF and coherence for the in-flight configuration are shown below in Figure 32. While the coherence was still excellent, the FRF looks significantly different. The FRF of the perfectly clamped beam looked a lot cleaner than the beam in the duck housing. The peaks of the magnitude plots have been reduced significantly signifying that the housing in the test article introduced damping into the system. The beam was allowed room to wiggle and energy in the

system was lost in this manner. The looseness of the clamp also reduced the frequency of the first three modes. By analyzing the eigenvectors and looking for the first three beam bending modes the first two frequencies of the beam were found and shown in Table 4. The third mode was so damped on the FRF that the actual frequency of occurrence could not be determined. The first two modes dropped by 23% and 9% respectively. This drop in the modes signifies that the duck housing was more compliant than an ideal clamp.

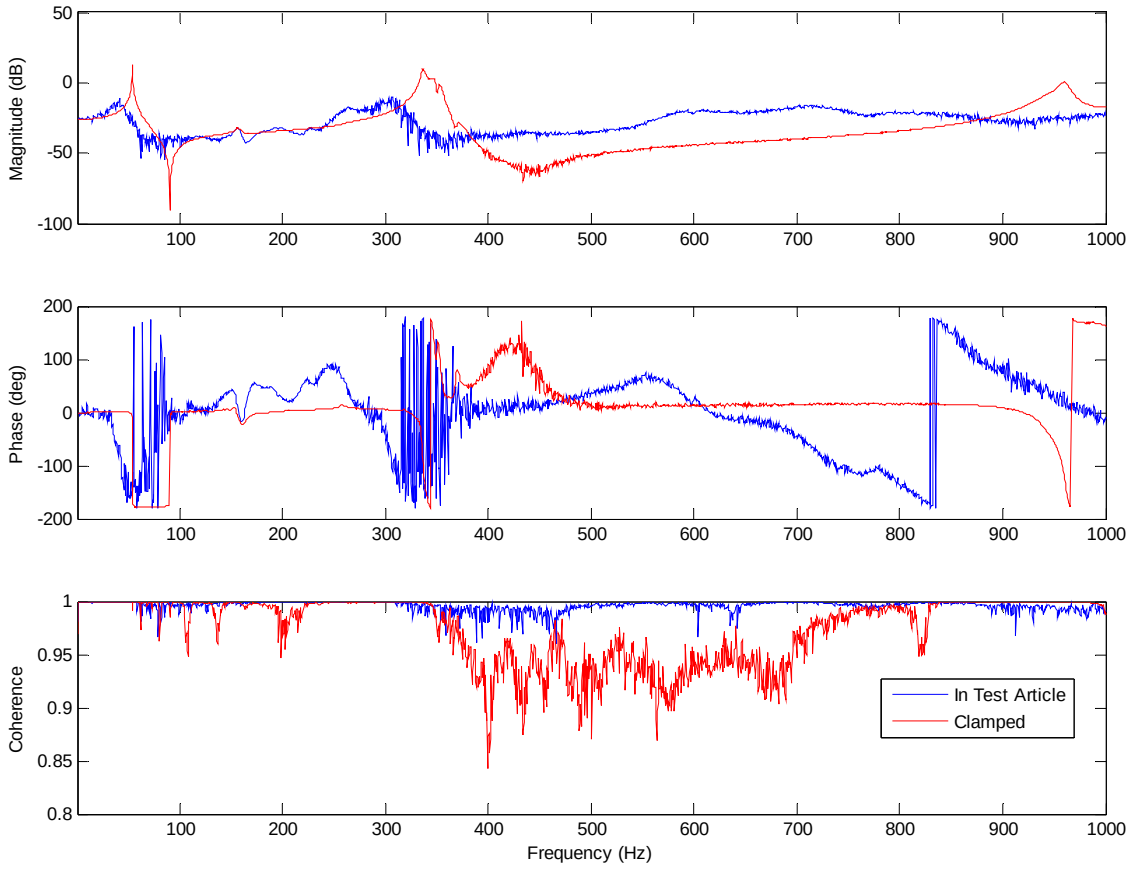

Figure 32. Comparison of the measured frequency response functions of the beam in the test article and clamped configurations.

Table 4. Comparison of measured modes for the leading edge beam in a clamped configuration and in the test article. Frequencies are in Hz.

Beam Configuration	Mode 1	Mode 2	Mode 3	Modulus of Elasticity (GPa)
Clamped	54.38	336.9	960	-
Abaqus Model	55.01	345.0	965.9	88.1
MATLAB Clamped Model (untuned)	55.07	345.1	966.3	88.1
MATLAB Clamped Model (tuned)	54.38	340.8	954.2	85.9
Experiment in Test Article	41.88	306.3	-	-
MATLAB Loose Clamp	41.88	279.6	809.9	85.9

To account for this “wiggle room” in the physical article, another optimization routine was developed to weaken the joint. The clamped position was moved toward the duck body or fuselage, effectively lengthening the free end of the beam ever so slightly. An element was created equal to the length of the distance the pivot point was moved. This element was weakened by changing the length, modulus of elasticity, and the radius of the element. This element provided a weak link that attached the rest of the bar to the clamp in order to mimic the actual housing the beam sat in. The results of the optimization are shown in Table 5. Since the original length of the beam from the clamped end was 135.8, this optimization method only lengthened the beam by 3.8% which had a small but negligible effect on the overall simulation. The advantage of this method was its ease of implementation inside of Abaqus.

Table 5. Comparison of optimized FE model versus experimental results of beam in loose housing.

	Mode 1	Mode 2	Mode 3
In Test Article	41.88	306.3	-
MATLAB Loose Clamp	41.88	279.6	809.9
Optimization Parameters			
	Length (mm)	Modulus (GPa)	Radius (mm)
Weakened Beam Element	5.14	27.1	.453
Normal Beam Element	-	85.9	.487

Modal testing was also performed on the wing to assess the change in the FRF by adding the wing to the beam. Figure 33 shows the FRF of the entire wing—that is all the FRFs from each test point have been averaged to create this one plot. This graph gives the overall effect of the membrane on the beam. As expected the membrane provided damping to the beam so that the first two modes occured at 11.6 and 36.9 Hz. The beam in a clamped configuration had the first mode out at 54 Hz and now the entire wing has two modes below the first beam-bending mode. The overall FRF presents no way to distinguish if these two modes are membrane or beam driven modes. As such the FRFs of six distinct points on the wing were graphed against each other in Figure 34. These six locations were the beam tip, batten, tape in the middle of the wing, a membrane location in the middle of the wing, a membrane location near the root of the beam, and a membrane location near the aft edge of the wing. The exact locations of these points are shown pictorially in Figure 35.

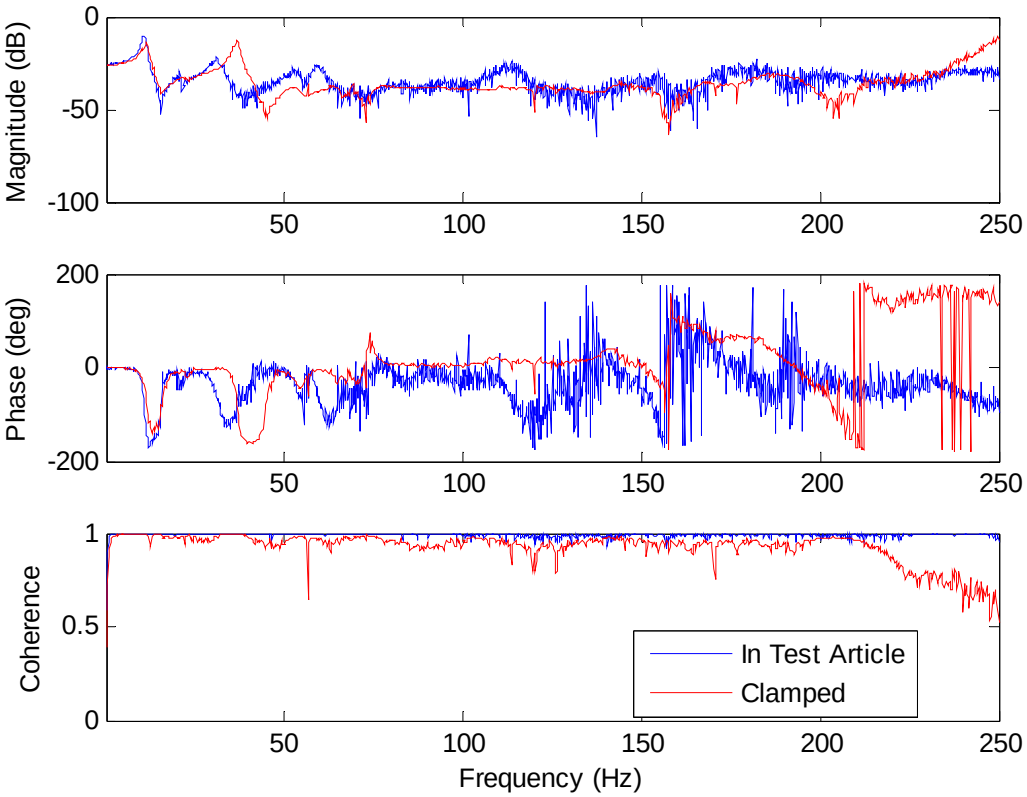

Figure 33. Overal FRF of wing in clamped configuration and in the test article.

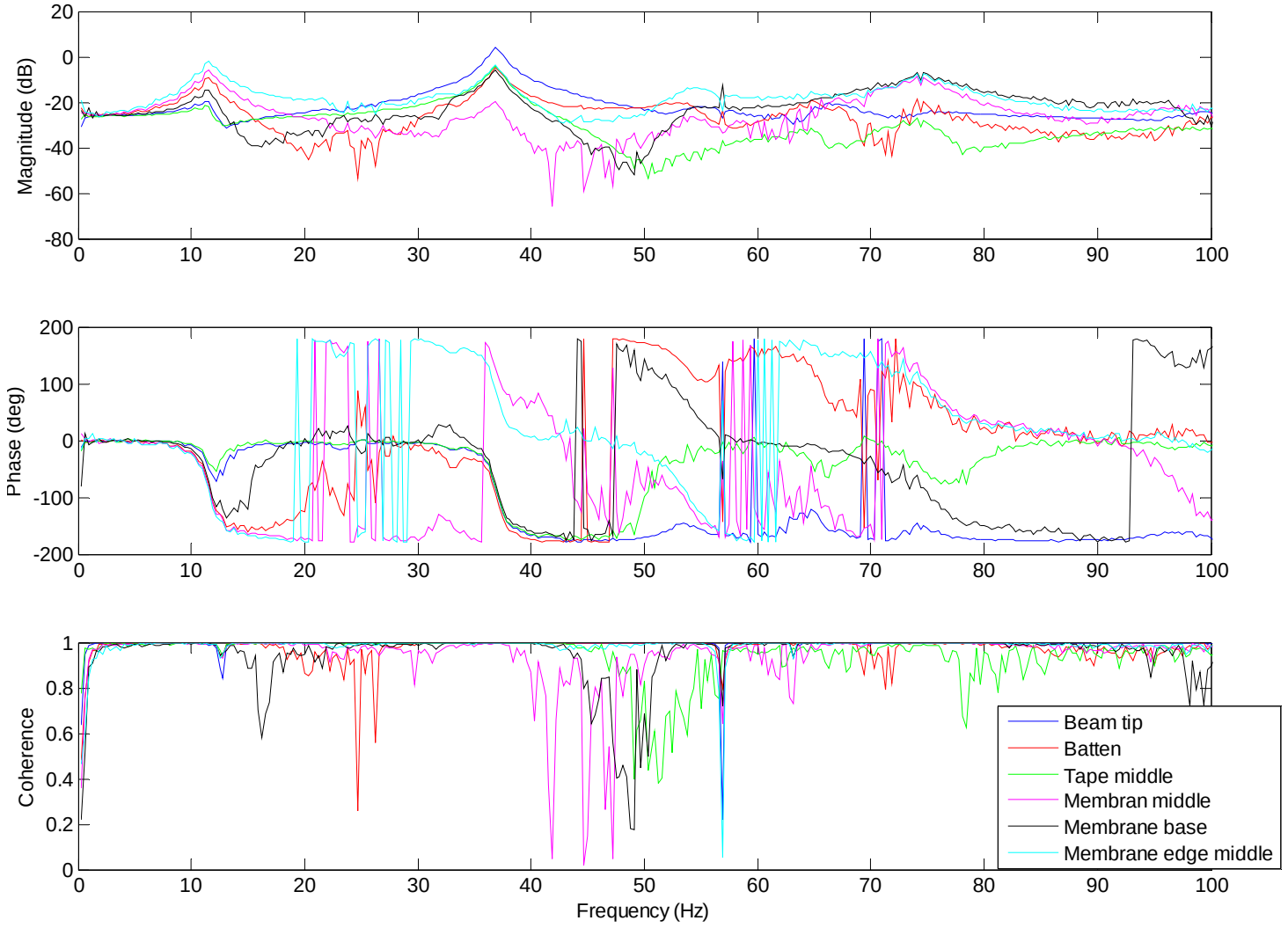

Figure 34. FRF and coherence for wing in clamped configuration at six different points.

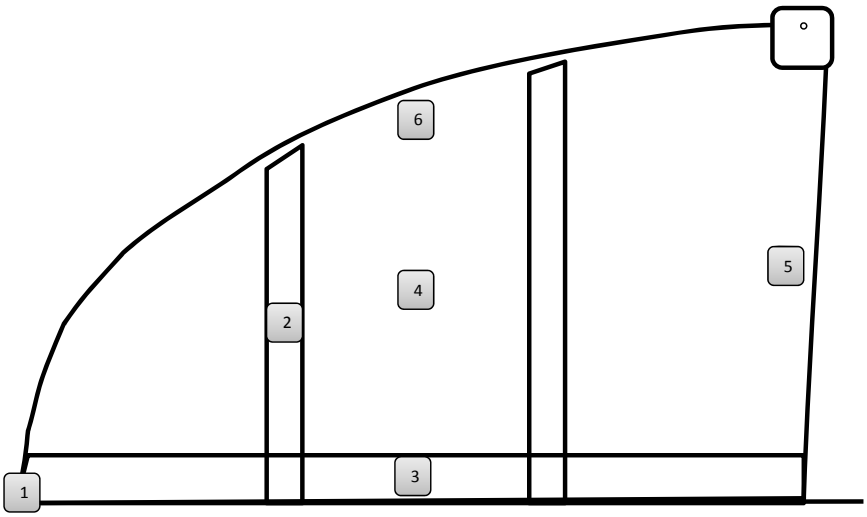

Figure 35. Locations of selected FRF plots numbered to correspond with order of appearance in the legend.

The strongest FRFs at the first mode were the membrane, edge of the membrane, and batten. This suggested that the first mode of the wing was actually driven by the membrane and not the beam. Contrary, at the second mode, the beam FRF was the highest of all the parts so this mode was driven by the beam dynamics. Without the membrane, the clamped beam bending mode occurred at 54.4 Hz but with the addition of the membrane this mode has been reduced by 32% to 36.9 Hz. Also, while the coherence of the beam was generally near one over the range of tested frequencies, the coherence of the membrane FRFs dropped below acceptable values over certain frequency ranges. The coherence was acceptable around the frequencies of the first two modes but the coherence of the membrane dropped below 0.8 for several frequency bands especially in the higher frequencies. Since coherence is a measure of the linearity between the input and output, either the membrane did not behave in a linear manner at certain frequencies or the data recorded at some points were poor. It was probably a combination of both

explanations. The coherence was better at some locations versus others but the wing was painted to give a good return to the laser and even the points with a worse coherence still had frequency ranges with very good coherence. Perhaps the membrane did not behave as linear as the stiffer materials like the beam. While the change in coherence further shows the difficulties in modeling membranes, the coherence was good around the frequencies of the first two modes. To validate the effect of the membrane and beam on the first two modes the mode shapes of the first two wing modes were investigate further.

The first two mode shapes of the wing measured in the lab are displayed in Figure 36. The first mode at 11.6 Hz was characterized by high membrane deflections especially in the region highlighted by the red in the first picture. This section of the membrane was farthest from the clamped boundary condition at the root and the attachment at the leading edge. This membrane deflection drove the first mode and caused the beam to deflect but the beam remained mostly rigid. More beam deflection and bending was seen in the second mode. Here the maximum velocity occurred out at the tip of the beam and membrane. The section of the membrane previously characterized by high deflections in the first mode deflected a minute amount in the second mode. These findings confirmed that the membrane drove the first mode and the beam drove the second mode. The beam shape resembled a first bending mode. Interestingly enough, the duck flaps at 15 Hz in air which is closer to the membrane driven mode rather than the first beam driven mode. Previous research studies have shown that it is most efficient to flap near the resonance frequency [7] however most studies have been performed on smaller flexible wings or larger more rigid wings where the first mode is a beam bending mode. Since no studies have involved the use of highly flexible membrane, either the flapping frequency of

highly flexible membrane is closer to the first bending mode or this design was simply not optimized to flap at the most efficient flapping frequency. The latter reason was probably true because this COTS SUAS exhibits poor flying qualities, yet there could exist a correlation between this membrane mode and flapping efficiency but without more experimental data it is impossible to know if a first membrane mode is more common to flexible wings or simply unique to this test article.

Since the flapping frequency occurred near the first membrane mode, it would be expected that the flapping shape would look similar to the first mode. Air and vacuum testing described below indeed shows that the wing at the top and bottom of the stroke closely resembles the top and bottom pictures in left column of Figure 36. However, this laser vibrometer test was performed with the wing in a clamped configuration. Beam modal testing showed there was a difference between the clamped configuration and in the test article. To study the effect of the boundary condition on the wing FRF, the wing was tested attached to the test article—the same configuration as it would experience in flight.

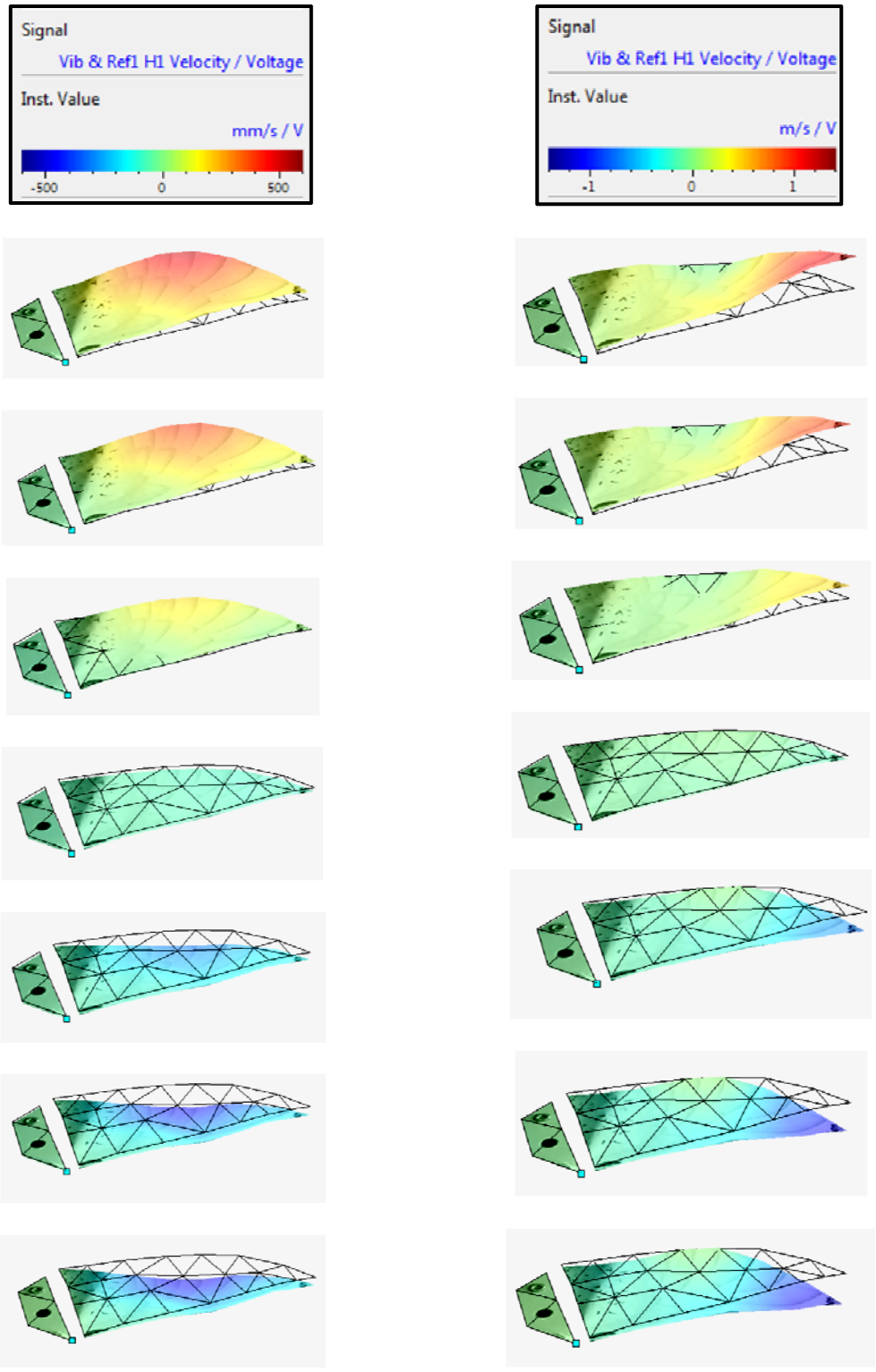

Figure 36. Mode shape for clamped wing at 11.6 Hz (left) and 36.9 Hz (right)

The same six points graphed in Figure 34 above are compared to their equivalent points on the wing attached to the test article in Figure 37. The phase and coherence of these points can be found in the Appendix. As with the beam, the FRFs from the wing on the duck were less clean than their clamped counterparts. However, looking at the test point on the beam, the max peak was dampened and reduced in frequency but the overall magnitude in the system was relatively similar. The first mode stayed relatively unaffected for most parts of the wing. Beyond this first mode the FRF was altered in different ways depending on the part. The loose clamp introduced damping into the system but since it left the first mode relatively unchanged the mode shape was expected to be similar to the clamped testing. The loose nature of the test article clamp shows that it was designed to operate in the 15 Hz region. Were the test article to be driven at a flapping frequency of 50 Hz or higher the wing would most likely interact with the housing in a negative way. Also the housing in the duck has seemed to significantly alter the FRFs of the membrane more than the beam.

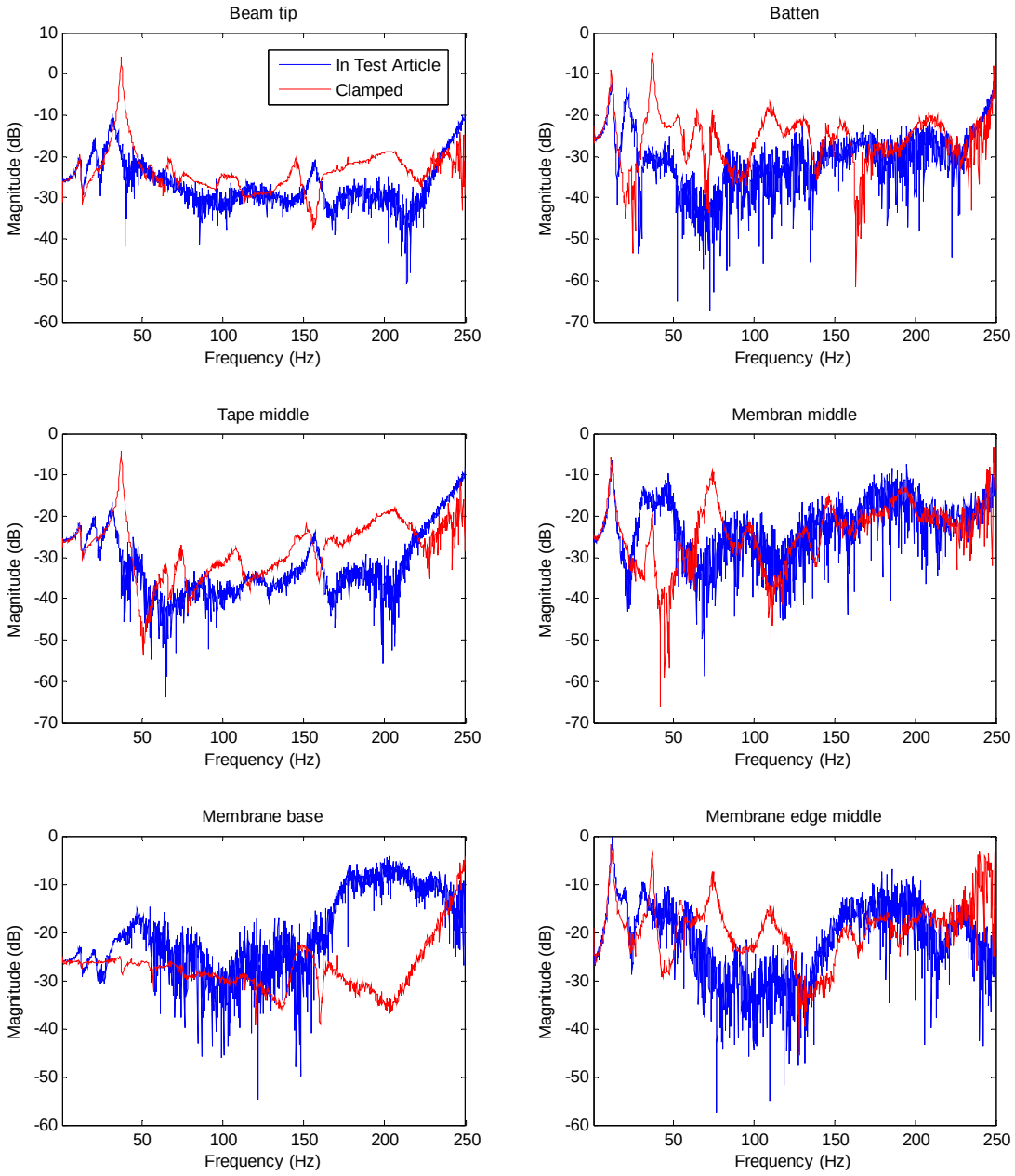

Figure 37. Comparison between the clamped and in flight configurations for six different points on the wing.

The beam FRF changed slightly because, although the boundary condition changed, the beam was still a stiff material. On the other hand, the other boundary condition that changed from the clamped configuration to that in the test article was the connector piece on the back of the membrane. In the clamped configuration, the connector was clamped between the same two plates the beam was clamped between so that there was no slack in the membrane. When the wing was attached to the duck, the connector was angled slightly below the beam attachment point. This created a slight camber in the wing membrane as seen in Figure 38. This camber put the wing in a different state of tension compared to the clamped configuration and showed that the membrane was depended on the initial tension applied to the membrane. This initial tension made the membrane difficult to model in Abaqus.

Figure 38. Trace of the camber of the outside of the wing.

The entire duck article was also subjected to laser vibrometer testing. This testing gave greater insight into the overall modes of the entire system. The overall test article FRF compared to just the wing in the test article can be found in Appendix. The main difference between the clamped wing and the entire test article was the addition of another mode at 15.6 Hz. This mode was cause by the tail and characterized by a flapping motion seen in Figure 40. The first mode in Figure 39 was the same as the

membrane mode described above and likewise the mode shape displayed in Figure 41 was the same as the second mode in the clamped wing configuration. A summary of first three wing mode frequencies for the three configurations can be found in Table 6.

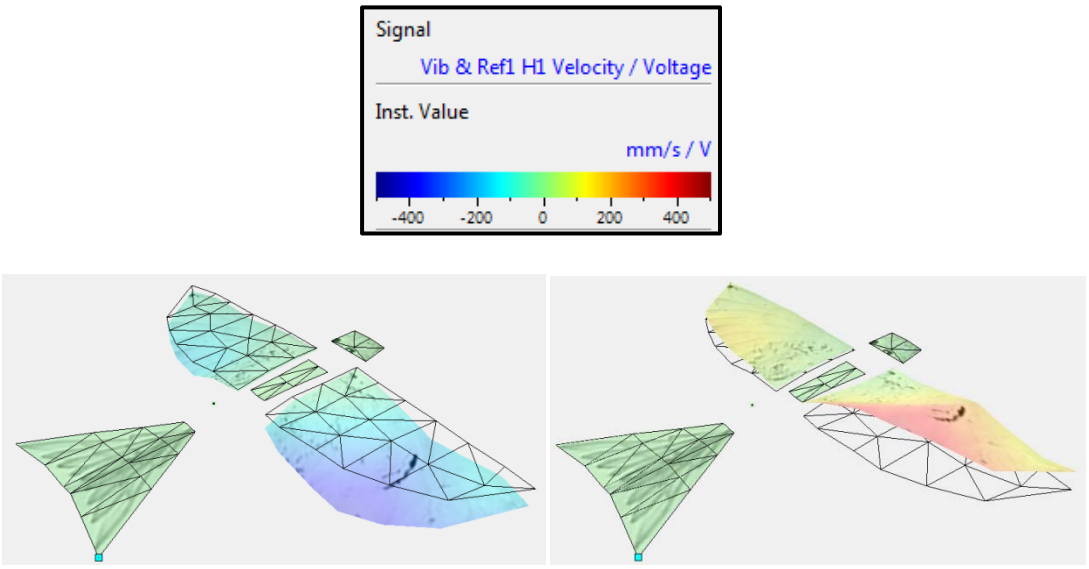

Figure 39. Mode shape at 10.63 Hz.

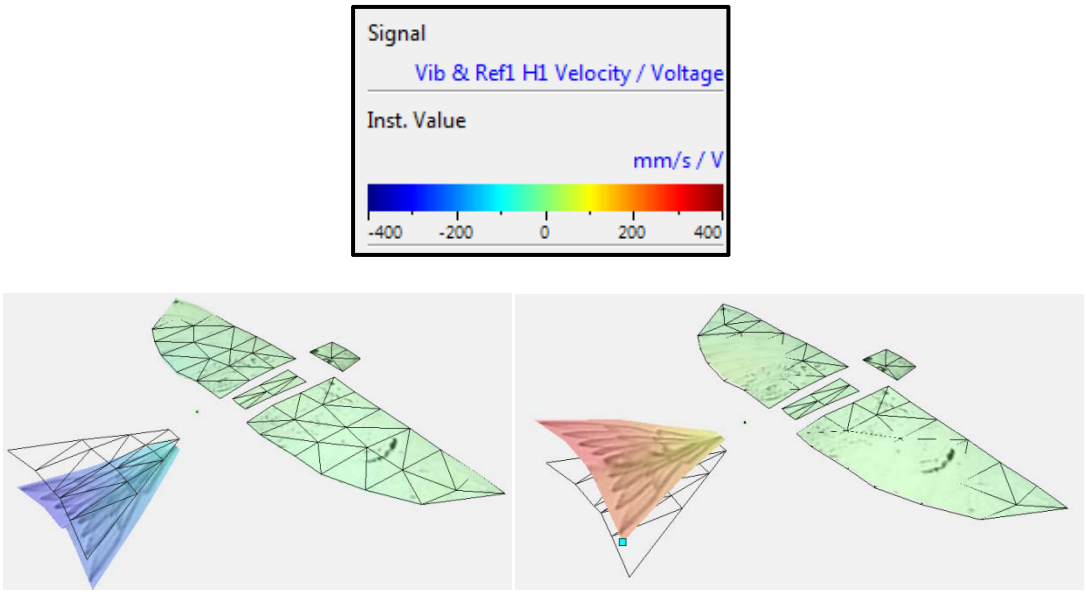

Figure 40. Mode shape at 15.63 Hz.

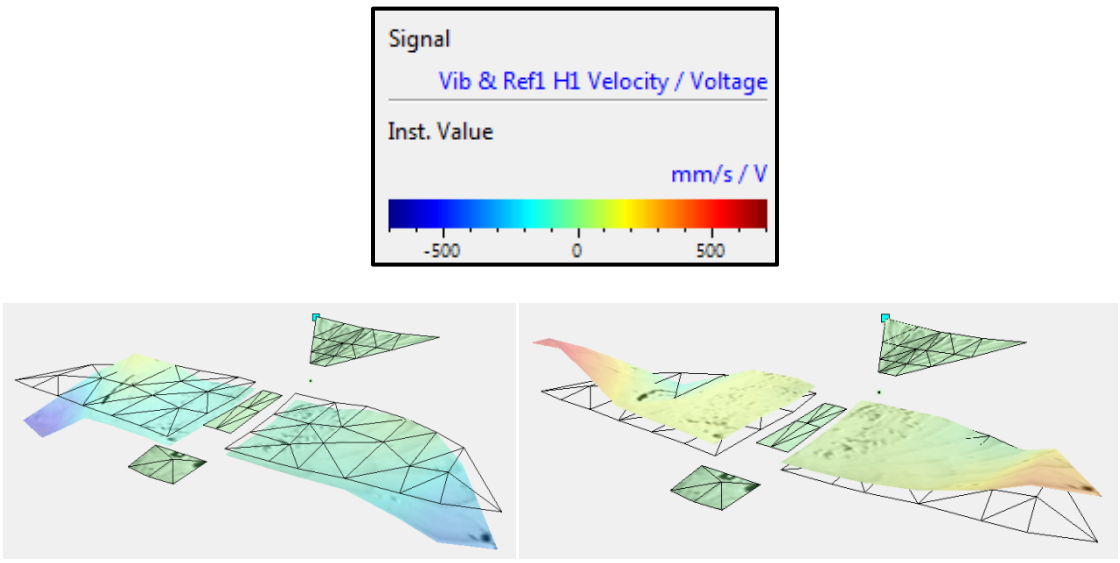

Figure 41. Mode shape at 33.28 Hz.

Table 6. Summary of laser vibrometer testing for the wing.

	Frequencies (Hz)		
	Mode 1	Mode 2	Mode 3
Wing Clamped	11.56	36.88	-
Wing In Duck	10.94	31.25	-
Entire Duck	10.63	15.63	33.28

4.5 Vacuum Testing

Model tuning gave some validation that the FE model matched the test article but this did not guarantee that the FE analysis would produce the same dynamic results as the wing flapping in vacuum. The vacuum test setup described above was the main crux and comparison tool used to validate the dynamic simulations. When the duck was hooked up to the DC power supply located outside the vacuum chamber the flapping frequency of the duck would drop from 15 to 12.5 Hz even though the manufacturer specified 3.7

mV were supplied to the duck. This small change in frequency did not matter in the end because ultimately the FE model could be modeled to reflect any excitation. Vacuum testing took place from 763 Torr all the way down to 1.33 Torr. The low pressure of the vacuum chamber provided an environment that proved to be an excellent comparison against the FE model as opposed to other vacuum tests described in chapter two that either utilized a vacuum chamber with poor view of the test article or did not have access to a true vacuum chamber and had to replicate the effects using other methods such as replacing the air with helium.

The flapping frequency at a range of pressures was evaluated to determine the effect of the vacuum chamber on the duck. Figure 42 below shows that as pressure decreases the flapping frequency increases in an exponential manner. An exponential curve, $y = 4.59e^{-0.0053x} + 12.4$, fit the data the best and shows that at the lower pressures the flapping frequency was more sensitive to changes in pressure. The trend shows the importance of being able to test the duck in a proper vacuum chamber. As the air in the chamber was removed the flapping frequency increased for a constant excitation voltage because less damping was experienced by the wing. Since the wing was more sensitive in the lower pressure region, a difference of 30 Torr corresponded to a flapping frequency reduction of approximately 1 Hz. Therefore, in order to get a proper comparison between vacuum data and a FE model, a relatively small change in air pressure could cause significantly different behavior in the wing membrane.

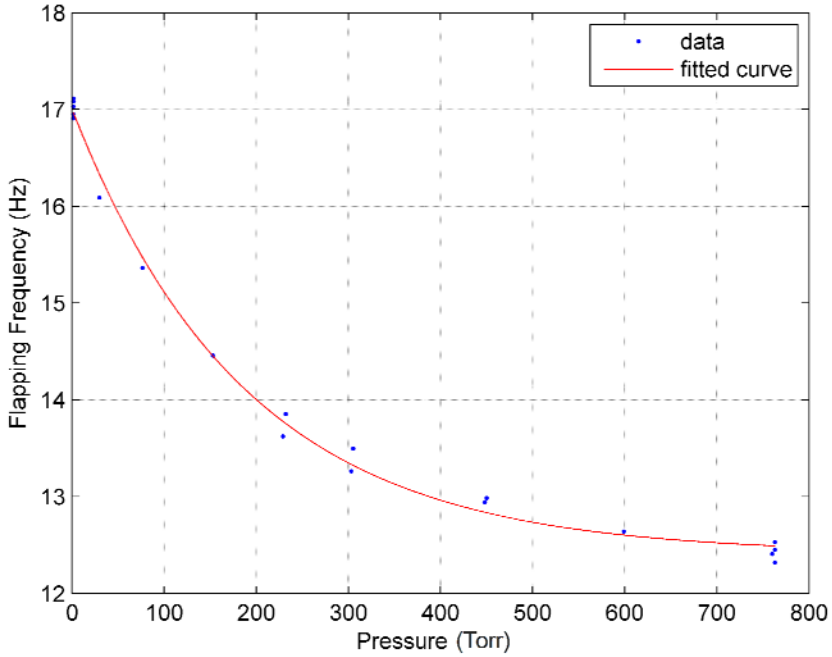

Figure 42. As the pressure decreases the flapping frequency of the test article increases as voltage is held constant.

One area of interest in the vacuum test was the qualitative difference between the wing behavior in air versus vacuum. At a casual glance the behavior of the flapping motion did not appear significantly different: the flapping motion stayed constant and no irregularities were noticed. Careful inspection of the high speed footage revealed the true differences between was responses at the different pressures. Figure 43 and Figure 44 below highlight the difference between the flapping strokes at atmospheric pressure (760 Torr) and the lowest pressure test (1.33 Torr). The membrane deflections in the vacuum where much more pronounced than in air as was expected. Because of the lack of damping in the absence of air and the presence of larger membrane deflections, the leading edge beam deflected farther at the top and bottom of the stroke and the curvature

of the beam was more pronounced. This extra deflection was largely due to the membrane. In air the leading edge of the wing pulled the membrane through the stroke and at the end of each stroke the momentum of the membrane caught up to the motion of the beam so that the beam and aft part of the membrane arrived at the bottom of the stroke at roughly the same time. In vacuum, however, the momentum of the membrane was not slowed by aerodynamic forces and as a result when the beam came to the bottom of the stroke the membrane still had extra momentum and pulled the beam even farther at the top and bottom of the stroke. This observed membrane behavior was a key feature in the qualitative assessment of the FE model.

A
I
R

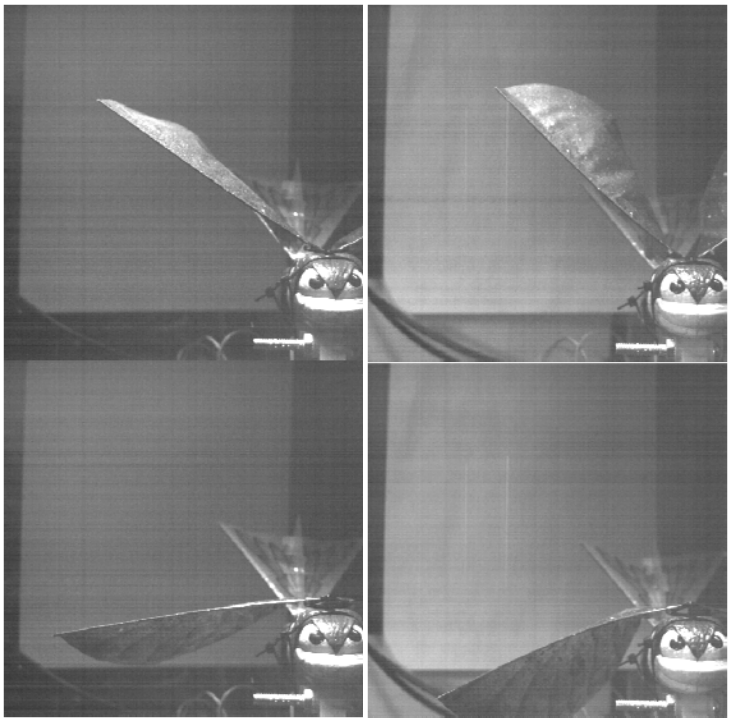

V
A
C
U
U
M

Figure 43. High speed footage captured during vacuum testing. The two pictures on the left were taken at atmospheric conditions (760 Torr). The two pictures on the right were taken at 1.33 Torr. The top two pictures were at the top of the stroke while the bottom two pictures were the bottom of the stroke.

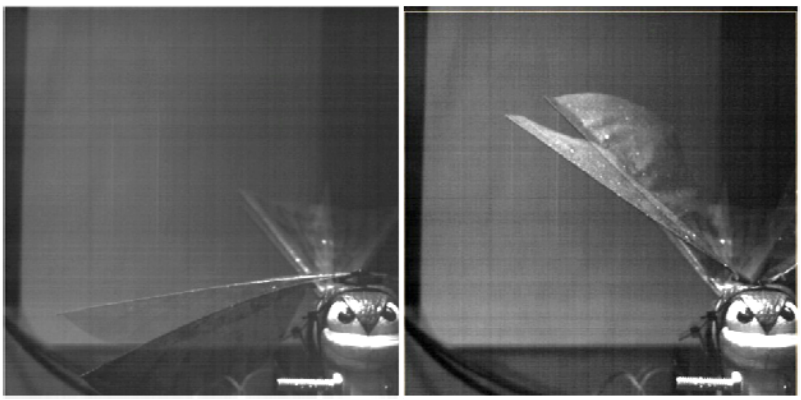

Figure 44. Same four images as above figure overlaid on top of each other. The beam and membrane deflections of the near vacuum pressure deflect more than the atmospheric tests.

4.6 FE Model

Modeling the wing in Abaqus proved to be a difficult task. While FE solvers can excel at handling stiff lightly damped structures the flexible nature of the membrane brought many computational hardships with it. The high flexibility of the membrane caused the FE solver to predict modes approximately every 5 Hz. With this many modes it made the task of model tuning nearly impossible because many more modes were predicted and none of the predicted modes matched the experimental mode shapes. The response of the wing membrane was also sensitive to the input and material properties. Because of all these reason, validating the membrane was a very intricate procedure and tip deflection and a qualitative assessment of the deformations were used as primary methods of assessing the analysis.

Many models were run in Abaqus to find the parameters that produce the best dynamic explicit results. For modal analysis shell elements were used for all wing parts (excluding the beam) as the membrane elements proved to be problematic for an

eigenvalue analysis. For the dynamic simulations several iterations were run with different permutations of shell and membrane elements. As more parts were converted to shell elements the computational cost rose. Eventually, the final configuration was found with batten and connector elements as shells and tape and membrane as membrane elements as detailed in Table 3. This configuration was the happy medium between accuracy and computational cost. When shell elements were used for the membrane portion of the wing, the computational cost rose significantly and the membrane behaved artificially stiff during the simulation. All simulations were run using Abaqus 6.11 on Linux operating system. It was found that changing the damping values had negligible effects on the simulation unless they increased by several orders of magnitude.

As discussed earlier, the wing was flapped in Abaqus by forcing the rotation on the beam. This forced boundary condition gave the advantage that the rotation could be explicitly controlled. The downside to this method of rotation was that it did not accurately capture how the wing was actuated. During the vacuum testing it was shown that at a constant voltage the flapping frequency increased as the pressure in the chamber decreased. With virtually no aerodynamic forces acting on the wing there was less resistance and the flapping frequency increased. By forcing the rotation at the root, the FE solver would not be able to repeat this behavior. In order to replicate the vacuum experiments the flapping frequency would have to be increased to 17 Hz from the 15 Hz that had been prescribed in all previous work done on this project. Figure 45 shows an early comparison of the full wing versus the Abaqus explicit bar only model at 15 Hz flapping frequency.

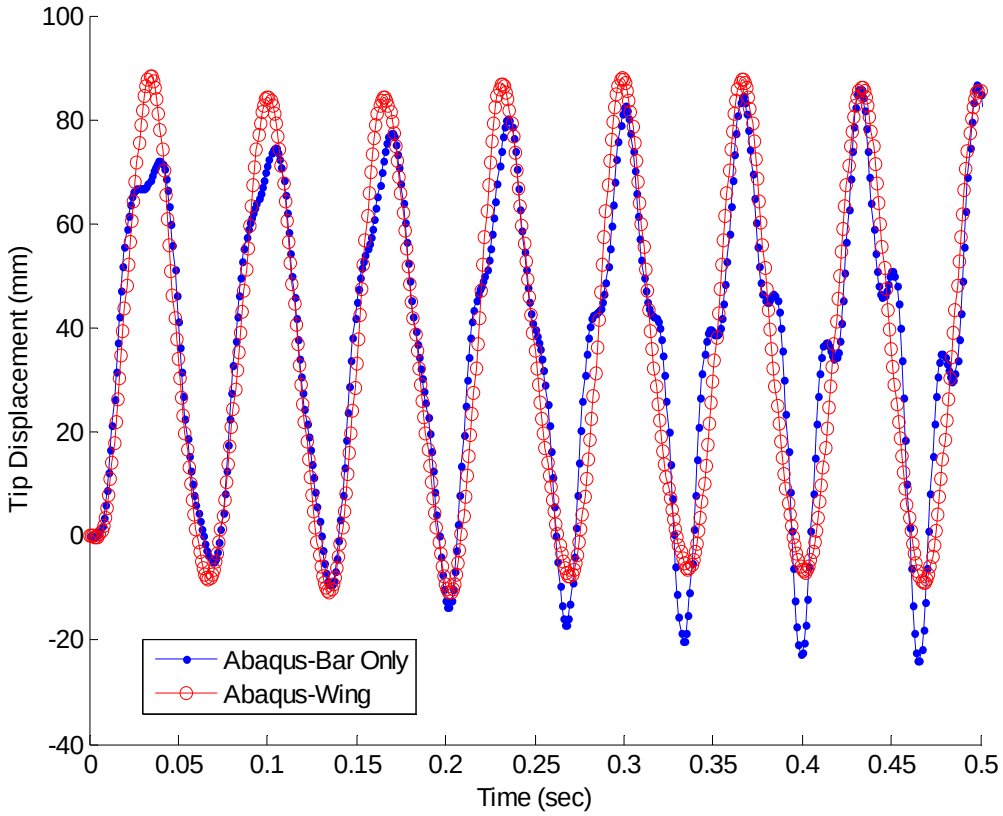

Figure 45. Early comparison of the tip deflection versus time of the Abaqus bar only model to the full wing model flapping at 15 Hz.

One of the most apparent differences is the damping of the transients. The bar only model exhibited high frequency modes on top of the 15 Hz flapping frequency as well as a very low transient increasing in amplitude near the end of the 0.5 second time window. The addition of the wing membrane damped out these high frequency transients. A low frequency transient was still observed in the wing model but the amplitude of such was negligible. The average amplitudes between the two models where similar but it was expected that the wing model would have greater deformations due to the addition of the membrane alone. In the vacuum testing, the inertia of the membrane was observed

creating greater deflections during stroke reversal but this was not seen in the FE element model. To further compare the wing model to the vacuum testing, the tip deflection was compared to the vacuum test as shown in Figure 46.

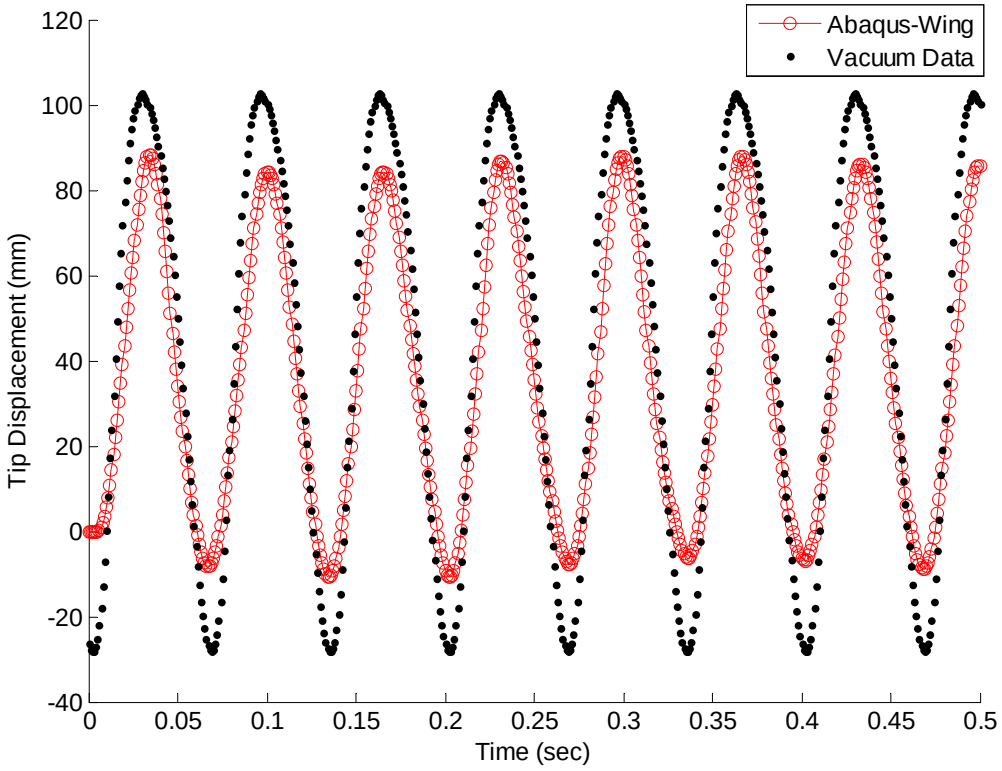

Figure 46. Comparison of tip deflection of the FE model versus vacuum data conformed to 15 Hz.

It is important to note that the time vector of the vacuum data has been conformed to 15 Hz by multiplying it by $\frac{15}{17}$ to compare it against the FE model. The actual flapping frequency of the vacuum data was at 17 Hz. For now, it is apparent from the above figure that the FE solver under predicted values observed in the vacuum chamber. The actual tip deflection was 130 mm but the FE analysis only predicted approximately a 95

mm deflection—a difference of 27%. This would not be an acceptable difference for modeling purposes. To rectify this difference, the forced flapping rotation in the FE model was reinvestigated. Previously models of the wing used the four bar linkage Simulink simulation which outputted a stroke amplitude of 30°. Physical measurements of the test article showed that the actual stroke amplitude was 36.4°. This six degree difference at the root could account for a large difference at the tip. The simulation was rerun with this new stroke amplitude and the results are shown below in Figure 47.

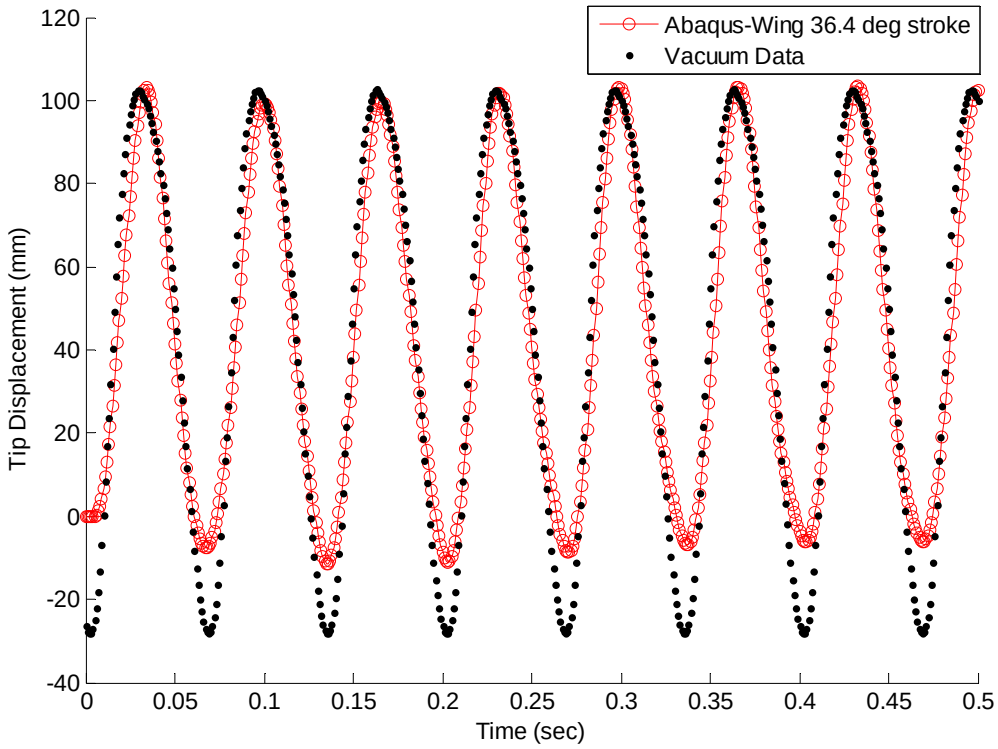

Figure 47. Tip deflection comparison with FE model at a 36.4 degree stroke amplitude with vacuum data conformed to 15 Hz.

The six degree increase in stroke amplitude has recovered approximately 12% of the amplitude but with a tip deflection amplitude of 110 mm the FE analysis was still off by

15%. In all these comparisons the time vector of the vacuum data has been conformed to 15 Hz, so the forced rotation in the FE model was increased to 17 Hz to match the actual frequency seen during the vacuum tests. With this change the new tip deflection is shown below in Figure 48. The average amplitude increased to 120 mm corresponding to a 8% difference. This model matched the vacuum data much better but it did introduce more transients in the beginning. The tip deflection just represents one physical point in the entire simulation and does not convey how the membrane acts.

The membrane deflections will be compared qualitatively using the high-speed images from vacuum testing. Figure 49 shows a comparison of the down and upstroke of between the FE results and experimental results. The most obvious difference between the two on the down stroke is the membrane deflection. The membrane in the experimental testing deflected far more than the FE model at both the top and the bottom of the stroke. Not only was the membrane deflection smaller but the membrane dynamics behaved a little differently than the experimental results. In the vacuum testing results the membrane can be seen to be lagging behind the leading edge beam until the wing rotates just below horizontal. The FE program predicted the membrane leading the beam well before crossing this threshold and in fact the membrane led more than the beam during the down stroke.

The upstroke shows similar trends. The FE membrane deflections were less than observed except during the end of the stroke. At the top of the stroke the membrane deflections looked very similar and the point in the stroke where the membrane crossed the leading edge beam was similar to the observed results. The upstroke on the test article happened faster than that of the FE predictions. This was evident by the uneven

spacing of the wing positions of the vacuum data. In fact, the FE element stroke looked symmetrical—the down stroke and upstroke were almost identical. This was not the case with the vacuum results. The membrane deflections were different in the upstroke and down stroke and the moment the membrane crossed the beam occurred at different phases during the up and down stroke. The difference in the flapping motions is apparent in Figure 50.

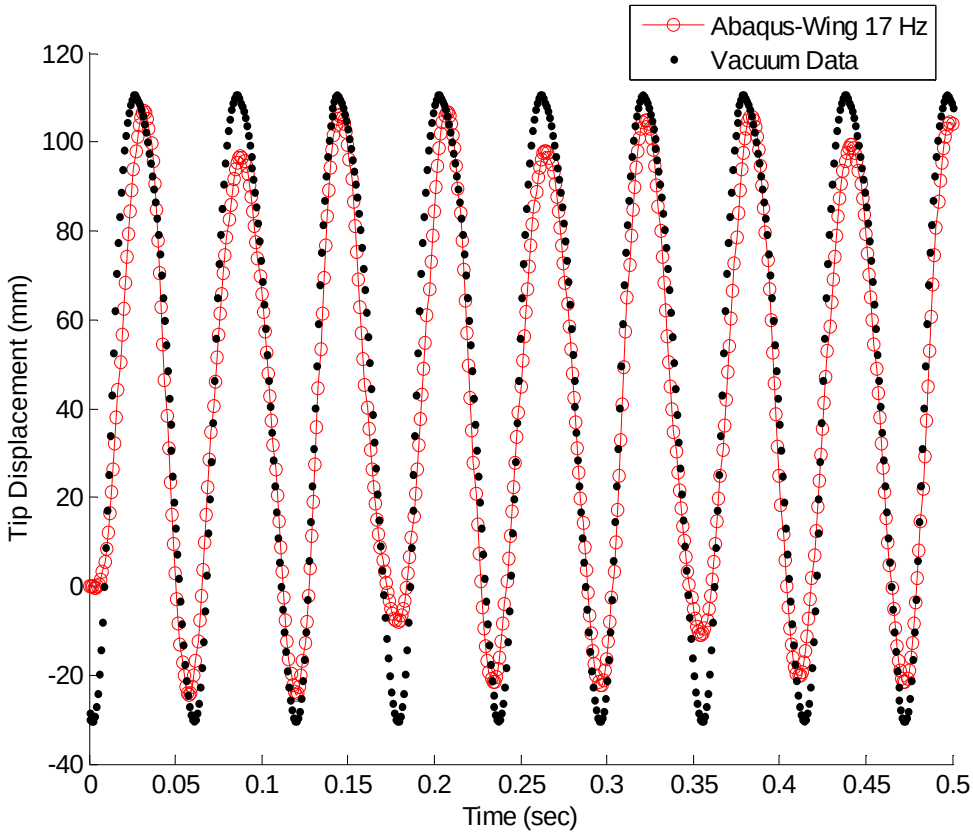

Figure 48. Tip deflection comparison with FE model run at 17 Hz.

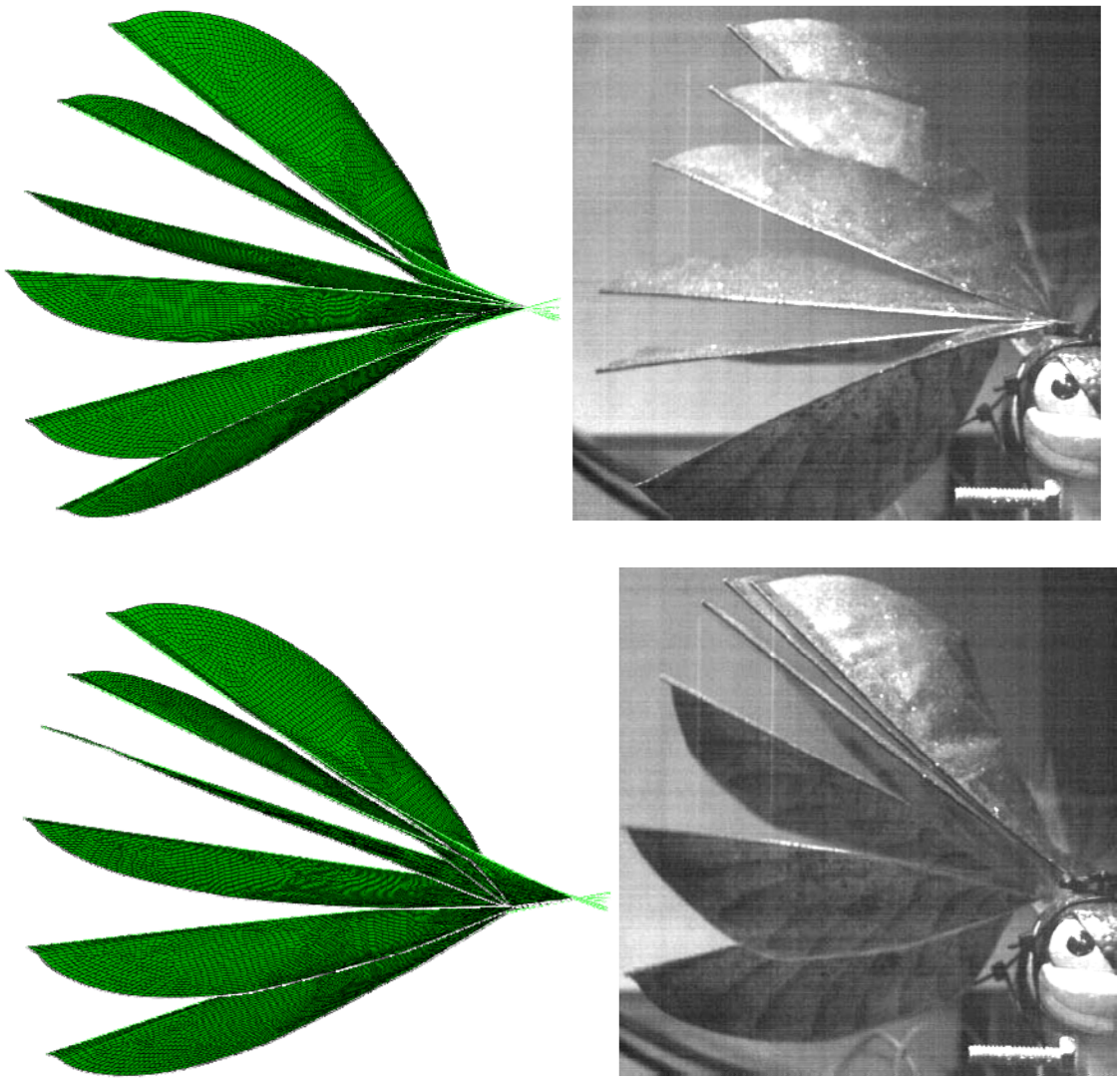

Figure 49. Comparison of FE simulation versus vacuum testing. Top row shows the down stroke, bottom row shows the upstroke.

Figure 49 shows the tip deflection from eight flap cycles plotted on top of one another. The FE data was taken from 0.5-1 seconds after the run began to mitigate the effect of transients. The vacuum data represents the average steady state values measured in the lab. The blue line represents the shape of the input signal going into the FE simulation. The amplitude and bias of the input signal have been altered to match the

scale of the graph so the y-axis values corresponding to the blue line are not meaningful, but what is meaningful is the shape of the input. The input signal was not a pure sinusoid—close but not a sinusoid.

The FE data was relatively repeatable and would converge toward a steady state solution if run for a long enough simulation time. The apparent difference in the same 17 Hz stroke comes from the upstroke. The Abaqus results overall look symmetric and sinusoidal. The input signal is shown for a frame of reference and not to suggest that the tip deflection should follow the input signal because it should not. The tip of a pure rigid body should display the same signal shape as the input but because of the deflections of the beam the actual dip path will deviate. The important takeaway is that the input to the FE element program was not purely sinusoidal but the output at the tip was more sinusoidal. This differs greatly from the tip deflection of the vacuum data. The upstroke occurs faster than the down stroke causing a skewed sinusoid. This feature was not observed in the FE simulation and was probably mostly likely due to an oversimplification in the input mechanisms into the FE simulation.

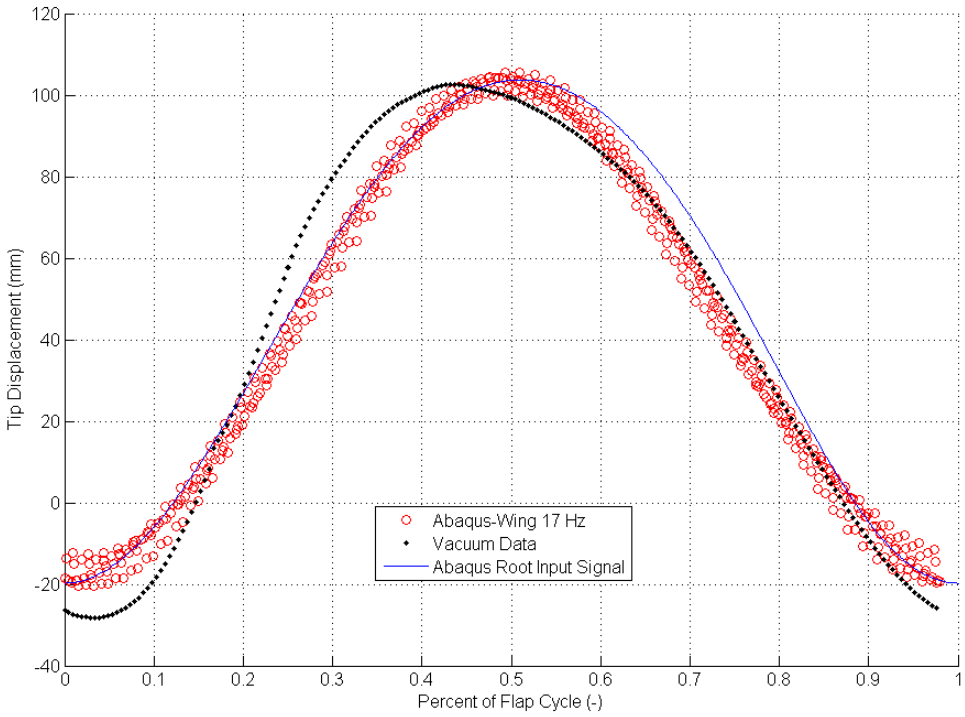

Figure 50. Tip deflection from eight flap cycles. The FE data comes from after 0.5 seconds into the run. The vacuum data is an average of the steady state values.

The FE model with the weakened joint described earlier was run in Abaqus. While the method worked for tuning the model, it failed to produce a workable model for the dynamic simulation. The weakened joint was simply too weak to withstand the forces imparted by the rotation of the wing. As a result, the joint deformed excessively producing unusable data. Tuning the model with the clamped data proved to be the more accurate and reliable method. Had the weakened joint worked properly, it should have captured a small portion of the behavior of the physical model.

V. Conclusions and Future Work

5.1 Overview

Modeling the flapping wing motion remains an area of ongoing study because of the importance to aircraft designers. With an understanding of the inertial and aerodynamic forces aircraft designers could optimize SUAS designs to meet the rising demand for smaller operational vehicles. Most research has been aimed at figuring out the low Reynolds number and unsteady aerodynamic effects that characterized flapping wing flight. Less research has focused on validating structural models of flapping wings. As wings become more flexible, the structural response becomes more nonlinear and more effort must be focused on structural validation.

A FE model of a flapping wing from a COTS SUAS was made and compared against the actual test article. Model tuning brought the first beam bending of the leading edge beam of the wing to within 1% of the test article. Wing modal tuning was not accomplished due to the myriad of modes predicted in the FE element solver. The FE solver had difficulties with the large flexible membrane area and none of the predicted modes matched the measured. Wing modal testing showed that the addition of the membrane to the beam decreased frequency the first beam bending mode by 32%. The first wing mode was found to be driven by the membrane and not the beam. This mode was closest to the flapping frequency and the mode shape resembled the flapping motion of the test article. The tip deflection amplitude was predicted to within 8% of vacuum data. Overall predicted membrane deflections were lower than those observed in the vacuum chamber.

5.2 Significance of Research

This research ventured into an area of flapping wing studies that has been relatively untouched. No significant research has delved into the structural aspect of a billowing flapping wing. With no prior examples to base the work upon, this research encountered many unforeseen complexities involved with highly flexible structures. The complex nature of the membrane dynamics required precise modeling of the problem. Everything from the dimensions, material properties, and input signals were had significant influence on the results.

While the modulus of elasticity and density were both important parameters controlling how the membrane deflected, the membrane density had the most significant impact on the membrane kinematics. A small change to the membrane density changed the transient response and tip deflection. Increasing the density increased the mass of the membrane which not only decreased the modes at which the membrane was excited at but the added mass made the membrane more dominate in the beam membrane relationship in regards to flapping. When the membrane had more mass it could cause greater tip deflections because it had more influence over the lighter beam. However, the mass and stiffness had a coupling effect. If the membrane excitation was not in sync with the beam then a heavier membrane could cause less tip deflection because the membrane motion would oppose the beam motion. In this manner, the density and modulus of elasticity were two important sensitive parameters toward exacting the FE response.

Through modal testing, the effect of the addition of a membrane to a leading edge spar was seen. Not only did the membrane decrease the beam natural frequency by 32% but the first membrane mode was closest to the actual flapping frequency. It was shown

that modeling a loose joint by weakening the material properties worked for modal analysis but proved useless for dynamic simulation.

5.3 Future Work

While the general flapping nature predicted by the FE program looked to be fundamentally the same motion as produced by the test article, the differences in flapping kinematics could be improved upon. Reasons for different membrane kinematics could have resulted from the approximations made in the FE solver. Membrane elements where used for the Mylar membrane portion instead of plates. It was found that shell elements worked well for the stiffer parts of the wing but if used for the highly flexible membrane then the shell elements made it unnaturally stiff. The density of the membrane could be increased or the modulus of elasticity decreased in an attempt to get more deflection out of the membrane but these values are difficult to tune because the dynamic simulations can be computationally intensive.

Another culprit could potentially be the forced rotation at the root. It was shown above how just a small change in the stroke amplitude or the flapping frequency increased the tip deflection. The previous four bar Simulink simulation was used as an input for every test case. While the output of the simulation was not a pure sinusoidal signal the FE flapping motions look more sinusoidal than the test article data. The four bar linkage could have overly simplified the input. A small change in the input had significant changes in the tip deflections as explained in Chapter 4. The same was probably true of the membrane kinematics. Figuring out the actual input to the wing warrants further investigation by taking measured data rather than relying on simulations.

Another possible cause of the difference in wing kinematics and tip deflection could have been the location of the input. For all the models, the input location was assumed to be where the membrane met the leading edge beam (the same location as previous studies). A closer look at the wing in the housing revealed a slight gap (less than 2 mm) between the wing attachment point and the pivot point. While not a significant distance, this gap would cause a longer rotation arm and could account for some difference in tip deflection as well as the wing kinematics.

The low stiffness of the membrane made the model difficult to tune. Focusing solely on modal tuning of a flexible membrane model would greatly benefit the flapping wing field. Modal testing allowed the tuning of the leading edge beam but the membrane was not able to be tuned. The FE solver predicted too many mode shapes—none of which matched the experimental results. Finding a way to tune the membrane would give more confidence in the dynamic simulation. The tension on the membrane plays a large part in this model tuning. To what degree is unknown but the lack of tension on the membrane in the FE model could have made a difference in the modal analysis.

Initial intentions were to supplement the FE model with aerodynamic forces in an attempt to realize an aeroelastic model that did not rely on CFD. Abaqus allows for a subroutine to define a force field that changes with each subroutine. A combination of BET, empirical methods, and unsteady models could be implemented into the user subroutine to add aerodynamic loading to the structure. While an initial shell of the code needed to implement the above method was developed, time constraints hindered full development. Future efforts could easily leverage the existing framework to add a complete aerodynamic model to the system.

While mimicking flapping wing motions in a FE solver is possible, it is not a trivial task. The wing membrane was sensitive to small changes in density, input conditions, and modulus of elasticity. Although running a dynamic simulation was not as computationally intensive as coupling a CFD and FE solver together, the task took long enough to make running different permutations difficult. It is recommended that any future work on this project leverage the use of the network of clustered processors. This would reduce the computation time and greatly speed up the process.

5.4 Summary

The foundation for modeling a highly flexible flapping wing was established. The flapping motion and dynamic simulation can be complex so precise modeling of the flapping mechanism and wing geometry is extremely important. Everything from geometric measurements, material properties, boundary conditions, and activation plays an essential part toward predicting the exact behavior. The flexible membrane proved to be the most difficult part to model in the wing. While incorporating the more subtle aspects of the problem into the model would help to better results, membrane modal analysis and dynamic response will still prove difficult. Future efforts should focus more on correctly modeling the membrane portion. More advance analysis techniques within Abaqus should be investigate because the standard membrane and shell elements have difficulties predicting the nonlinearity of the wing membrane. Future efforts should focus on improving membrane modal testing, updating the established model to incorporate the more subtle aspects of the problem, and add aerodynamic forces into the model through a user subroutine.

Appendix

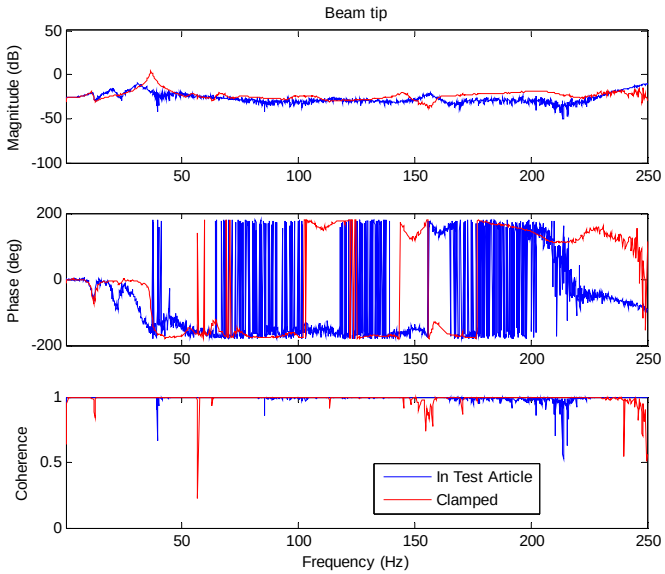

Figure A- 1. Frequency response function comparison of wing in clamped configuration and in the test article at the tip of the beam.

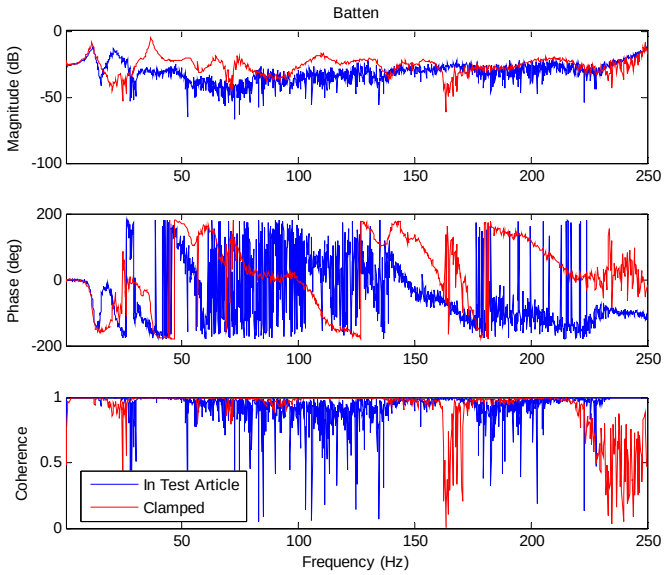

Figure A- 2. Frequency response function comparison of wing in clamped configuration and in the test article at the batten.

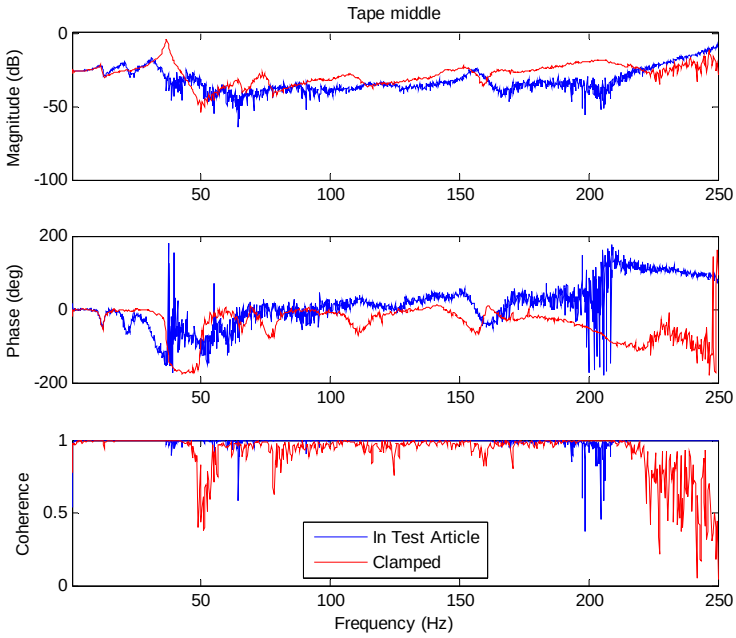

Figure A- 3. Frequency response function comparison of wing in clamped configuration and in the test article at the middle of the tape area.

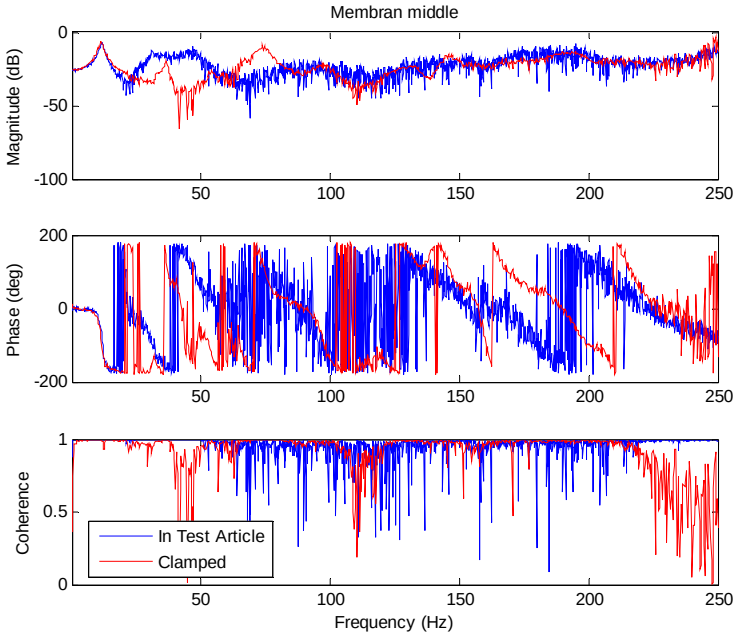

Figure A- 4. Frequency response function comparison of wing in clamped configuration and in the test article at the middle of the membrane.

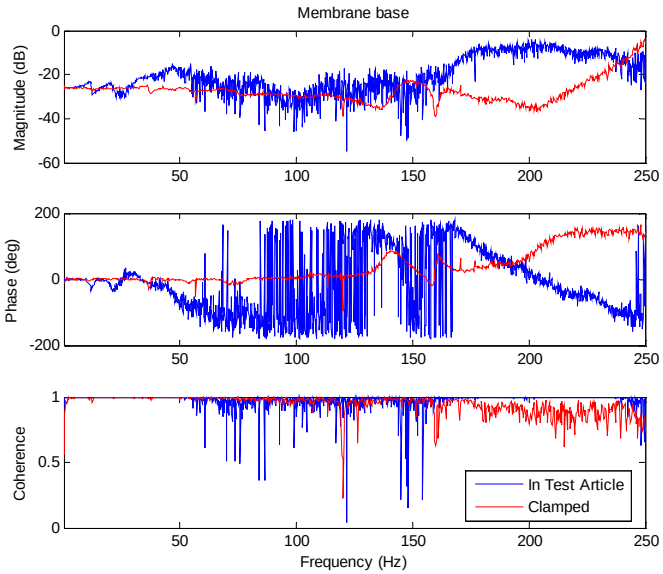

Figure A- 5. Frequency response function comparison of wing in clamped configuration and in the test article at the membrane near the base of the wing.

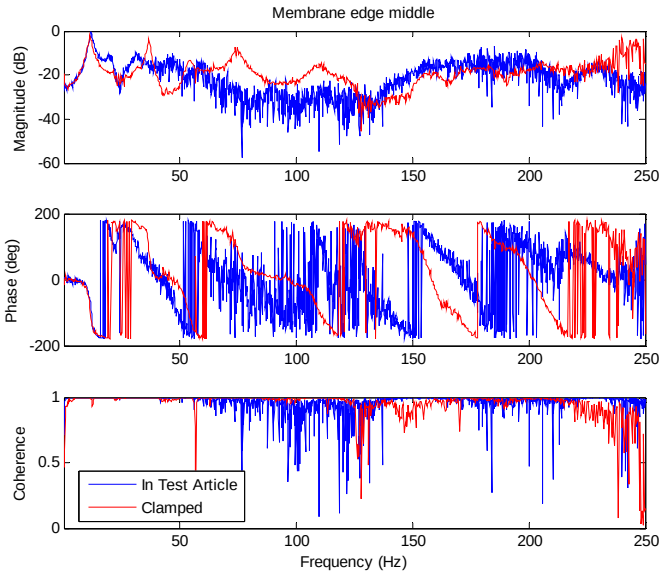

Figure A- 6. Frequency response function comparison of wing in clamped configuration and in the test article at the edge of the membrane.

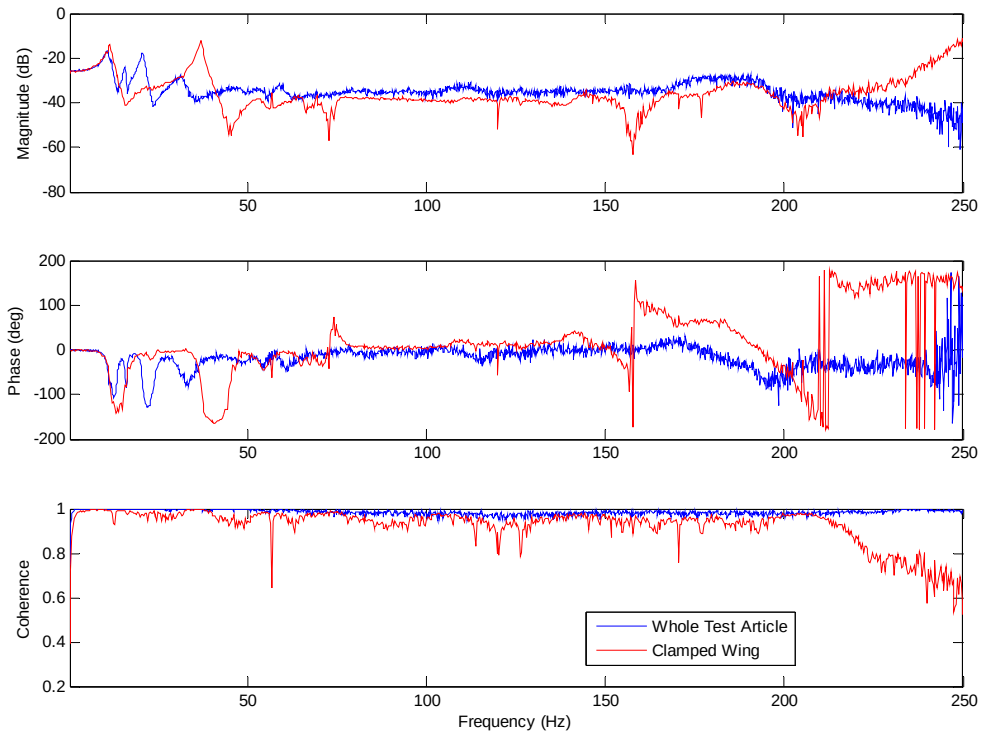

Figure A- 7. Wing averaged frequency response function comparison between clamped configuration and whole test article.

Bibliography

[1] N. Sladek, *Flapping Wing Micro Air Vehicle Wing Manufacture and Force Testing,* Wright-Patterson AFB, OH: Master's thesis, Air Force Institute of Technology, March 2011, AFIT/GA/ENY/11-M14.

[2] Office of the Secretary of Defense, *UAS Roadmap 2005,* 2005.

[3] W. R. Davis, B. B. Kosicki, D. M. Boroson and D. F. Kostishack, "Micro Air Vehicles for Optical Surveillance," *The Lincoln Laboratory Journal,* vol. 9, 1996.

[4] T. J. Mueller, Fixed and Flapping Wing Aerodynamics for Micro Air Vehicle Applications, Lexington: American Institute of Aeronautics and Astronautics, Inc., 2001.

[5] A. Norris, A. Palazotto and R. Cobb, "Structural Dynamic Characterization of an Insect Wing: Torward the Development of Bug Sized Flapping Wing Micro Air Vehicles," *American Institute of Aeronautics and AStronautics,* 2006, AIAA-2010-2790.

[6] R. Mandangopal, A. K. Zaeem and S. K. Agrawal, "Biologically Inspired Design of Small Flapping Wing Air Vehciles Using Four-Bar Mechanisms and Quasi-steady Aerodynamics," *Journal of Mechanic al Design,* vol. 127, pp. 809-816, 2005.

[7] M. L. Anderson, *Design and Control of Flapping Wing Micro Air Vehicles,* Wright-Patterson AFB, OH: Master's thesis, Air Force Institute of Technology, March 2012, AFIT/DS/ENY/11-12.

[8] R. Dudley, The Biomechanics of Insect Flight, Princeton: Princeton University Press, 2000.

[9] C. P. Ellington, "The Novel Aerodynamics of Insect Flight: Applications to Micro-Air Vehicles," *The Journal of Experimental Biology,* vol. 202, pp. 3439-3448, 1999.

[10] S. A. Ansari, R. Zbikowski and K. Knowles, "Aerodynamic Modelling of Insect-like Flapping Flight for Micro Air Vehicles," *Progress in Aerospace Sciences,* vol. 42, pp. 129-172, 2006.

[11] S. P. Sane, "The Aerodynamics of Insect Flight," *The Journal of Experimental Biology,* vol. 206, pp. 4191-4208, 2003.

[12] M. Sun and J. Tang, "Unsteady aerodynamic force generation by a model fruit fly wing in flapping motion," *Journal of Experimental Biology,* vol. 205, pp. 55-70, 2002.

[13] S. Sunada and C. P. Ellington, "Approximate Added-Mass Method for Estimating Induced Power for Flapping Flight," *AIAA Journal,* vol. 38, no. 8, pp. 1313-1321, 2000.

[14] M. F. M. Osborne, "Aerodynamics of Flapping Flight with Application to Insects," *Journal of Experimental Biology,* vol. 28, pp. 221-245, 1951.

[15] J. A. Walker and M. W. Westneat, "Mechanical Performance of Aquatic Rowing and Flying," *Proc R Soc London,* pp. 1875-1881, 2000.

[16] W. Johnson, Helicopter Theory, Princeton: Princeton University Press, 1980.

[17] X. Yan, S. Zhu, Z. Su and H. Zhang, "Added Mass Effect and an Extended Unsteady Blade Element Mode of Insect Hovering," *Journal of Bionic Engineering,* vol. 8, pp. 387-394, 2011.

[18] T. Vanneste, J. B. Paquet, S. Grondel and E. Cattan, "Design of a Lift-Optimized Flapping-Wing using a Finite Element Aeroelastic Framework of Insect Flight," in *Structural Dynamics and Materials Conference*, Honolulu, AIAA 2012-1635.

[19] S. P. Sane and M. H. Dickinson, "The Aerodynamic Effects of Wing Rotation and a Revised Quasi-Steady Model of Flapping Flight," *The Journal of Experimental Biology,* vol. 205, pp. 1087-1096, 2002.

[20] P. Seshadri, M. Benedict and I. Chopra, "Towards a Fundamental Understanding of Low Reynolds Number Flapping Wing Aerodynamics," in *Structural Dynamics and Materials Conference*, Honolulu, AIAA 2012-1639.

[21] W. Thielicke, A. B. Kesel and E. J. Stamhuis, "Reliable Force Predictions for a Flapping-wing Micro Air Vehicle: A "Vortex-lift' Approach," *International Journal of Micro Air Vehicles,* vol. 3, no. 4, pp. 201-215, 2011.

[22] J. Wu, A. Vakili and J. Wu, "Review of the Physics of Enhancing Vortex Lift by Unsteady Excitation," *Progress in Aerospace Sciences,* vol. 28, pp. 73-131, 1991.

[23] E. C. Polhamus, "A Concept of the Vortex Lift of Sharp-edge Delta Wings Based on a Leading-edge Suction Analogy," National Aeronautics and Space Administration, December 1966, 1966.

[24] W. Shyy, Y. Lian, J. Tang, D. Viieru and H. Liu, Aerodynamics of Low Reynolds Number Flyers, New York: Cambridge University Press, 2008.

[25] N. DeLeon, "Manufacturing and Evaluation of a Biologically Inspired Engineered MAV Wing compared to the Manduca Sexta Wing under Simulated Flapping Conditions," Master's

thesis, Air Force Institute of Technology, Wright-Patterson AFB, OH, March 2011, AFIT/GAE/ENY/11-M07.

[26] S. Combes and T. Daniel, "Into thin air: contributions of aerodynamic and inertial-elastic forces to wing bending in the hawkmoth Manduca sexta," *Journal of Experimental Biology,* vol. 206, pp. 2996-3006, 2003.

[27] T. Nakata and H. Liu, "A fluid-structure interaction model of insect flight with flexible wings," *Journal of Computational Physics,* vol. 231, pp. 1822-1847, 2012.

[28] J. Lee, J. Shin and S. Lee, "Fluid-structure interaction of flapping flexible plate in quiscent fluid," *Computers and Fluids,* vol. 57, pp. 124-137, 2012.

[29] J. Lee and S. Lee, "Fluid-structure interaction analysis on a flexible plate normal to a free stream at low Reynolds numbers," *Journal of Fluids and Structures,* vol. 29, pp. 18-34, 2012.

[30] J. Murray, "Development of Photographic Dynamic Measurements Applicable to Evaluation of Flapping Wing Micro Air Vehicles," Master's thesis, Air Force Institute of Technology, Wright-Patterson AFB, OH, March 2011, AFIT/GAE/ENY/11-D02.

[31] A. Jennings, J. E. Alerding and J. Black, "Flapping Wing Force and Deformation Analysis," in *Structural Dynamics and Materials Conference*, Honolulu, AIAA 2012-1637.

[32] A. Gogulapti, "Nonlinear Approximate Aeroelastic Analysis of Flapping Wings in Hover and Forward Flight," University of Michigan Dissertation, 2011.

[33] A. R. Ennos, "Inertial and Aerodynamic Torques on the Wings of Diptera in Flight," *Journal of Experimental Biology,* vol. 142, pp. 87-95, 1980.

[34] F. Lehmann and M. H. Dickinson, "The Changes in Power Requirements and Muscle Efficiency During Elevated Force Production in the Fruit Fly Drosophila Melanogaster," *The Journal of Experimental Biology,* vol. 200, pp. 1133-1143, 1997.

[35] J. Wakeling and C. Ellington, "Dragonfly Flight III. Lift and Power Requirements," *Journal of Experimental Biology,* vol. 200, pp. 583-600, 1997.

[36] S. P. Sane and M. H. Dickinson, "The Control of Flight Force by a Flapping Wing: Lift and Drag Production," *The Journal of Experimental Biology,* vol. 204, pp. 2607-2626, 2001.

REPORT DOCUMENTATION PAGE

Form Approved
OMB No. 074-0188

1. REPORT DATE *(DD-MM-YYYY)*	2. REPORT TYPE	3. DATES COVERED *(From – To)*
21-03-2013	Master's Thesis	Oct 2011 – Mar 2013

4. TITLE AND SUBTITLE
Finite Element Analysis of a Highly Flexible Flapping Wing

5a. CONTRACT NUMBER

5b. GRANT NUMBER

5c. PROGRAM ELEMENT NUMBER

6. AUTHOR(S)
Mason, Justin K., First Lieutenant, USAF

5d. PROJECT NUMBER

5e. TASK NUMBER

5f. WORK UNIT NUMBER

7. PERFORMING ORGANIZATION NAMES(S) AND ADDRESS(S)
Air Force Institute of Technology
Graduate School of Engineering and Management (AFIT/EN)
2950 Hobson Way, Building 640
WPAFB OH 45433

8. PERFORMING ORGANIZATION REPORT NUMBER
AFIT-ENY-13-M-22

9. SPONSORING/MONITORING AGENCY NAME(S) AND ADDRESS(ES)
Intentionally Left Blank

10. SPONSOR/MONITOR'S ACRONYM(S)

11. SPONSOR/MONITOR'S REPORT NUMBER(S)

12. DISTRIBUTION/AVAILABILITY STATEMENT
DISTRIBUTION STATEMENT A: APPROVED FOR PUBLIC RELEASE; DISTRIBUTION UNLIMITED

13. SUPPLEMENTARY NOTES

14. ABSTRACT

Small unmanned aerial systems are being designed to emulate the flapping kinematics of insects and birds which show superior control in slow speed regimes compared to fixed wing or rotorcraft aircraft. The flight of flapping wing vehicles is characterized by aeroelastic effects. Most research has been dedicated towards understanding the aerodynamic side of the aeroelastic response with minimal effort spent towards validating the structural response. A finite element model of a wing from a commercial flapping wing vehicle was created to validate the structural response. Vacuum testing allowed the isolation of the inertial response for a direct comparison to the finite element model. Wing tip displacement amplitude was matched to within 8%. The membrane kinematics of the finite element model were similar to the vacuum test article but overall membrane deflections predicted by the finite element solver were less than observed deflections seen in the vacuum. This research shows that significant focus must be placed on validating the structural side of a flexible structure in order to correctly model the complete aeroelastic response.

15. SUBJECT TERMS
Finite element, MAV, flapping wing, aeroelastic, vacuum

16. SECURITY CLASSIFICATION OF:			17. LIMITATION OF ABSTRACT	18. NUMBER OF PAGES	19a. NAME OF RESPONSIBLE PERSON
a. REPORT	b. ABSTRACT	c. THIS PAGE			Black, Jonathan T, Ph.D
U	U	U	UU	121	19b. TELEPHONE NUMBER *(Include area code)* (937) 785-3636, x 4578 (jonathan.black@afit.edu)

Standard Form 298 (Rev. 8-98)
Prescribed by ANSI Std. Z39-18